PolyPublie
Polytechnique Montréal

POLYTECHNIQUE MONTRÉAL
UNIVERSITÉ D'INGÉNIERIE

Titre: Title: Hypoxic-Core Spheroids on a Chip

Auteur: Author: Elena Refet

Date: 2025

Type: Mémoire ou thèse / Dissertation or Thesis

Référence: Citation: Refet, E. (2025). Hypoxic-Core Spheroids on a Chip [Thèse de doctorat, Polytechnique Montréal]. PolyPublie. https://publications.polymtl.ca/65811/

Document en libre accès dans PolyPublie
Open Access document in PolyPublie

URL de PolyPublie: PolyPublie URL: https://publications.polymtl.ca/65811/

Directeurs de recherche: Advisors: Thomas Gervais, & Philip Wong

Programme: Program: Génie biomédical

Ce fichier a été téléchargé à partir de PolyPublie, le dépôt institutionnel de Polytechnique Montréal
This file has been downloaded from PolyPublie, the institutional repository of Polytechnique Montréal

https://publications.polymtl.ca

POLYTECHNIQUE MONTRÉAL

affiliée à l'Université de Montréal

Hypoxic-Core Spheroids on a Chip

ELENA REFET

Institut de génie biomédical

Thèse présentée en vue de l'obtention du diplôme de *Philosophiæ Doctor*

Génie biomédical

Mai 2025

© Elena Refet, 2025.

POLYTECHNIQUE MONTRÉAL

affiliée à l'Université de Montréal

Cette thèse intitulée :

Hypoxic-Core Spheroids on a Chip

présentée par **Elena REFET**

en vue de l'obtention du diplôme de *Philosophiæ Doctor*

a été dûment acceptée par le jury d'examen constitué de :

Gregory DE CRESCENZO, président
Thomas GERVAIS, membre et directeur de recherche
Philip WONG, membre et codirecteur de recherche
Géraldine MERLE, membre
Robert BRISTOW, membre externe

DEDICATION

To Science and Knowledge, here is my little brick

ACKNOWLEDGEMENTS

Thomas and Phil, thank you for trusting me with this project and thank you for allowing me the freedom I needed to thrive during my Ph.D. I learned a lot from both of you, and hopefully one day I will be able to transmit that as well, in my own lab. Greg, thank you for remembering me, for giving me my first job as a teaching assistant and for listening to what I needed to share when I needed to share it.

Audrey and Ouafa, a gigantic thank you for your support, your knowledge, your teaching, your challenging of my ideas, and your multiple free therapy sessions in the microscopy room. You helped me a lot to forge the researcher I am today. Our tea spilling alongside Rodin and Alyia were more important than you think and helped me "survive" the Ph.D.

I also want to thank all of Thomas' and Phil's group for sharing both tea and knowledge. Thank you, Etienne, for always asking extremely interesting questions: I hope that one day we will be able to work together. Thank you, Maryam, for your many "I have a question", for showing interest in what I am doing and also for sharing interesting ideas of what we both could do.

An enormous thanks to Catherine and Aymeric from whom I learn a lot. Thank you for our multiple brunches, lunches and dinners, thank you for listening to my rant and thank you for being here. Cathou, I would not be here without you, you helped me push myself to become the woman I am today.

Of course, an enormous thank you to my family for your blind support. Thank you for always showing interest in what I am doing even when I know you are lost in what I am saying. To my parents, thank you for the long hours on the phone listening to all my stories. I would not be here without you both (literally and figuratively).

Rodin, I think writing all the "thank you" might be as long as the thesis. Thank you for being in my life, for your trustworthy support, for making me stronger, for challenging my ideas and for always thinking of the convoluted questions reviewer 2 might ask. I think that together we will be able to get that Ig Nobel, the only award that is worth to get! Nobel prize is so last season…

And thank you for coming with me to the CRCHUM on a lot of Saturdays and Sundays, and for our early breakfasts and late dinners on the 10th floor.

RÉSUMÉ

L'hypoxie tumorale est définie comme une pression partielle d'oxygène [pO2] inférieure à sa valeur physiologique. Résultant naturellement du taux de prolifération incontrôlé et de la vascularisation progressivement erratique des tumeurs solides, l'hypoxie déclenche dans les cellules cancéreuses un ensemble d'adaptations métaboliques et cellulaires servant principalement à survivre aux conditions hypoxiques, acides et pauvres en nutriments. Outre les caractéristiques physico-chimiques intrinsèques du microenvironnement hypoxique, ces adaptations contribuent à augmenter la capacité d'invasion et de métastase de la tumeur, ainsi qu'à une résistance accrue à la plupart des traitements anticancéreux (chimiothérapie, radiothérapie, immunothérapie). De fait, l'hypoxie tumorale est généralement associée à une aggravation du pronostic des patients.

Malgré l'importance clinique de l'hypoxie, les chercheurs font face à un manque apparent d'outils et de méthodologies ergonomiques permettant de simuler correctement le microenvironnement hypoxique dans des modèles *in vitro* ou *in vivo*. Quel que soit le modèle tumoral *in vitro* utilisé (monocouche 2D ou sphéroïde 3D), la plupart des études sur l'hypoxie ont recours à l'induction chimique ou à des environnements à oxygène contrôlé. Ceci ne permet ni de reproduire correctement la structure tridimensionnelle multicouche des tumeurs solides, ni l'interaction entre des cellules présentant différents niveaux d'oxygénation et différents phénotypes. De plus, ces dispositifs expérimentaux sont peu pratiques et parfois incompatibles avec le traitement et l'analyse appropriés des échantillons hypoxiques. Bien que les modèles *in vivo* reproduisent l'architecture, le microenvironnement et les mécanismes d'hypoxie des tumeurs *in vivo*, ils présentent certains inconvénients. Le contenu hypoxique des tumeurs *in vivo* est difficilement prévisible et quantifiable, et les exigences expérimentales pour les tumeurs hypoxiques de grande taille peuvent entrer en conflit direct avec les autorités réglementaires. Ces contraintes, associées à leur coût et à leur faible rendement, rendent les modèles animaux inadaptés à l'étude préclinique de l'hypoxie.

Au cours des deux dernières décennies, les technologies microfluidiques ont bénéficié à la recherche sur le cancer en permettant la génération, la culture, le traitement et la bioanalyse à haut débit de modèles tumoraux cliniquement pertinents dans des dispositifs compacts et polyvalents. Dans notre laboratoire, des dispositifs microfluidiques pour la génération et la culture de modèles tumoraux tridimensionnels (sphéroïdes ou tissus *ex vivo* microdisséqués) ont été développés et appliqués à l'étude de l'efficacité de combinaisons radiothérapie/chimiothérapie. Cependant, les avantages apparents de la microfluidique ne semblaient pas encore avoir été appliqués à la recherche sur l'hypoxie.

L'objectif de ma thèse était donc de concevoir et de valider un dispositif microfluidique ergonomique et polyvalent pour la culture, le traitement et l'analyse de sphéroïdes tumoraux présentant naturellement une hypoxie pertinente cliniquement. Mon objectif principal était d'ainsi fournir enfin à la communauté de recherche translationnelle sur le cancer un outil efficace pour étudier l'hypoxie et ses effets aux niveaux fondamental et préclinique.

J'ai d'abord conçu un dispositif microfluidique permettant de cultiver jusqu'à 240 sphéroïdes de grande taille (> 750 µm de diamètre), avec comme critères de conception additionnels la polyvalence, la compacité et la facilité d'utilisation. En utilisant les sarcomes des tissus mous (STS) comme étude de cas pour les tumeurs solides hypoxiques, j'ai évalué l'expression et la localisation spatiale de protéines hypoxiques de référence dans mes sphéroïdes. Ce dispositif et les modèles tumoraux qu'il contient ont ensuite été appliqués à des tests thérapeutiques, sous forme d'associations sur puce du promédicament hypoxique tirapazamine (TPZ) et de radiothérapie externe (EBRT). Les résultats de ces travaux, publiés dans mon premier article (chapitre 4), démontrent la présence reproductible d'un coeur hypoxique au sein de mes larges sphéroïdes de STS sur puce, absent des sphéroïdes plus petits provenant des mêmes lignées cellulaires et la dépendance à l'oxygène de l'efficacité de l'association TPZ/EBRT.

Malgré la présence stable d'un coeur hypoxique induit par diffusion et les effets directs de l'hypoxie sur l'efficacité de TPZ, la pertinence clinique de mes sphéroïdes à coeur hypoxique (HyCo) n'était pas encore suffisamment prouvée. Il me fallait donc démontrer que les sphéroïdes HyCo étaient non seulement hypoxiques en leur cœur, mais présentaient également les caractéristiques de l'hypoxie telle que rencontrée en clinique. Toujours à l'aide de lignées cellulaires de STS, j'ai comparé les profils d'expression génique de mes sphéroïdes HyCo à ceux de petits sphéroïdes normoxiques et à la littérature sur l'hypoxie tumorale. J'ai également évalué la résistance des sphéroïdes HyCo à l'EBRT et à la chimiothérapie cisplatine, et leur potentiel d'invasion dans le Matrigel. Enfin, j'ai présenté les applications de mes sphéroïdes HyCo pour tester quatre thérapies ciblées, sélectionnées sur la base de données de séquençage et utilisant le potentiel d'invasion comme critère d'évaluation principal. Les résultats de ces travaux sont présentés dans mon deuxième article (chapitre 5) et démontrent que les sphéroïdes HyCo reproduisent les caractéristiques clés de l'hypoxie : expression génique spécifique à l'hypoxie, radio/chimiorésistance, et invasivité et agressivité accrues. De plus, les sphéroïdes HyCo sur puce peuvent facilement être appliqués aux tests et au développement de traitements basés sur les données de séquençage.

Dans l'ensemble, mon dispositif et mon modèle de sphéroïde HyCo récemment validés sont particulièrement qualifiés pour l'étude fondamentale et préclinique de l'hypoxie tumorale et de ses effets sur le phénotype cellulaire et la réponse au traitement. En combinant ergonomie, polyvalence et pertinence clinique, les sphéroïdes HyCo sur puce peuvent être appliqués à divers axes de recherche translationnels en cancérologie, avec une relative aisance.

ABSTRACT

Tumor hypoxia is defined as an oxygen partial pressure [pO_2] lower than physiological. Naturally resulting from the unchecked proliferation rate and progressively erratic vasculature of solid tumors, hypoxia triggers in cancer cells a set of metabolic and cellular adaptations mainly designed to survive the acidic and nutrient-scarce hypoxic conditions. Along with intrinsic physico-chemical characteristics of the hypoxic microenvironment, these adaptations contribute to increased tumor invasion and metastasis, resistance to most anti-cancer treatment (e.g., chemotherapy, radiotherapy, immunotherapy), and have therefore been typically associated with worsened patient outcomes.

Despite the clinical relevance of hypoxia, there is an apparent lack of user-friendly tools and methodologies to properly emulate the hypoxic microenvironment in either *in vitro* or *in vivo* models. Regardless of the *in vitro* tumor model used (2D monolayer or 3D spheroid), most studies on hypoxia resort to chemical induction or oxygen-controlled environments, failing to adequately mimic the multi-layered three-dimensional structure of solid tumors and the interplay between cells of various oxygenation and phenotypic status. In addition, these experimental setups are impractical and at times incompatible with proper treatment and analysis of hypoxic samples. Although *in vivo* models do recapitulate the architecture, microenvironment and mechanisms of *in vivo* tumors, they are not without disadvantages. The hypoxic content of *in vivo* tumors is poorly predictable and hard to quantify, and experimental requirements for large hypoxic tumors can come into direct conflict with regulatory bodies. Coupled with their expensive and time-consuming nature, this makes animal models ill-suited for pre-clinical study of hypoxia.

Over the past two decades, microfluidic technologies have benefited cancer research by enabling high-throughput generation, culture, treatment and bioanalysis of clinically-relevant tumor models in compact and versatile devices. In our lab, microfluidic devices for the generation and culture of three-dimensional tumor models (spheroids or micro-dissected *ex vivo* tissues) have been developed and applied to the testing of radiotherapy/chemotherapy. However, the apparent advantages of microfluidics have yet to translate into hypoxia research.

The aim of my thesis was to engineer and validate a user-friendly and versatile microfluidic device for the culture, treatment and subsequent analysis of tumor spheroids naturally exhibiting clinically-relevant hypoxia.

By doing so, my overarching goal was to finally provide the translational cancer research community with a user-friendly tool to study hypoxia and its effects at the fundamental and preclinical levels.

I first designed a microfluidic device for the culture of up to 240 large spheroids (> 750 µm in diameter), with versatility, compacity and user-friendliness as additional design inputs. Using soft tissue sarcomas (STSs) as a case study for hypoxic solid tumors, I assessed the expression and spatial localization of gold-standard hypoxic proteins within my spheroids. Then, this device and tumor models therein were applied to treatment testing, in the form of on-chip combinations of the hypoxia prodrug Tirapazamine (TPZ) and external beam radiotherapy (EBRT). The results of this work were published in my first article (Chapter 4), and demonstrate the reproducible presence of a hypoxic-core within my large on-chip STSs spheroids, absent from smaller spheroids of the same cell lines, along with the oxygen-dependent efficacy of TPZ/EBRT combination.

Despite the stable presence of a diffusion-driven hypoxic-core and the demonstrable effects of hypoxia on TPZ efficacy, the clinical relevance of my hypoxic-core (dubbed HyCo) spheroids was not sufficiently proven yet. As such, I needed to showcase that HyCo spheroids not only were hypoxic in their core but exhibited the hallmarks of clinical hypoxia. Still using STSs cell lines, I compared the gene expression profiles of my HyCo spheroids to that of small normoxic ones and to the literature on tumor hypoxia. I also assessed that HyCo spheroids were resistant to both EBRT and chemotherapy, in the form of cisplatin, and displayed increased Matrigel invasion potential. Finally, I showcased applications of my HyCo spheroids to the testing of 4 targeted therapies, selected based on sequencing data and using invasion potential as my main endpoint. The results of this work are presented in my second article (Chapter 5), and demonstrate that HyCo spheroids indeed recapitulate key hallmarks of hypoxia: hypoxia-specific gene expression, radio/chemoresistance and increased invasiveness and aggressivity. Furthermore, on-chip HyCo spheroids can easily be applied to data-driven treatment testing and development.

Overall, my device and newly-validated HyCo spheroid models are uniquely qualified for fundamental and pre-clinical study of tumor hypoxia and its downstream effects on cell phenotype and treatment response. By combining user-friendliness, versatility and clinical-relevance, on-chip HyCo spheroids can be applied to a variety of research avenues of translational cancer research, with relative ease.

TABLE OF CONTENTS

LIST OF TABLES

LIST OF FIGURES

LIST OF SYMBOLS AND ABBREVIATIONS

2D	2 Dimensions
3D	3 Dimensions
ABC	ATP Binding Cassette
ABCB1	ATP Binding Cassette Subfamily B Member 1
ABCC1	ATP Binding Cassette Subfamily C Member 1
ABCG2	ATP Binding Cassette Subfamily G Member 2
AMPK	AMP-Activated Protein Kinase
ARNT	Aryl Hydrocarbon Receptor Nuclear Translocator
ATF4	Activating Transcription Factor 4
ATF6	Activating Transcription Factor 6
Bcl-2	B-cell Leukemia 2
BiP	Binding Immunoglobin Protein
BNIP3	BCL2 Interacting Protein 3
BNIP3L	BCL2 Interacting Protein 3 Like
CAD	Computer-Assisted Design
CAIX	Carbonic Anhydrase IX
ccRCC	Clear Cell Renal Cell Carcinoma
CD73	Ecto-5'-Nucleotidase
CHOP	CCAAT/enhancer Binding Homologous Protein
CO_2	Carbon Dioxide
CT	Chemotherapy
CXCL12	C-X-C Motif Chemokine 12
DCA	dichloroacetate

EBRT	External Beam Radiotherapy
eIF2	eukaryotic Initiation Factor 2
EMA	European Medicines Agency
ER	Endoplasmic Reticulum
ERAD	Endoplasmic Reticulum-Associated protein Degradation
fMRI	functional Magnetic Resonance Imaging
FDA	Food and Drug Administration
G3PP	Glycerol-3 Phosphate Phosphatase
GADD34	Growth Arrest and DNA Damage Inducible Protein
GRP78	Glucose-Regulated Protein 78
HAP	Hypoxia Activated Prodrug
HCO_3^-	Bicarbonate Anion
HIFs	Hypoxia Inducible Factors
HR	Homologous Recombination
IF	Immunofluorescence
IHC	Immunohistochemistry
IRE1α	Inositol-Requiring Enzyme 1α
JNK1	c-Jun N-terminal Kinase 1
LDH	Lactate Dehydrogenase
LOX	Lysyl Oxidase
MCM	Minichromosome Maintenance complex
MDR1	Multidrug Resistance 1
mTOR	Mammalian Target of Rapamycin
p21	G1-checkpoint CDK inhibitors A - CDKN1A

p27	G1-checkpoint CDK inhibitors B - CDKN1B
PBMC	Peripheral Blood Mononuclear Cell
PDMS	Polydimethylsiloxane
PERK	RNA-like Endoplasmic Reticulum Kinase
PET	Positron Emission Tomography
PGK1	Phosphoglycerate Kinase 1
PHD	Proline-Hydroxylase
pO_2	Oxygen Partial Pressure
pVHL	Von Hippel-Lindau Protein
RNAseq	RNA sequencing
ROS	Reactive Oxygen Species
RT	Radiotherapy
RTqPCR	Reverse Transcriptase quantitative Polymerase Chain Reaction
NER	Nucleotide Excision Repair
NHEJ	Non-homologous End Joining
SLC2A1	Solute Carrier Family 2 Member 1
STS	Soft Tissue Sarcoma
TME	Tumor Microenvironment
TPZ	Tirapazamine
UPR	Unfolded Protein Response
UV	Ultraviolet
VEGFA	Vascular Endothelial Growth Factor A
VIM	Vimentin
XBP1	X-box Binding Protein 1

CHAPTER 1 INTRODUCTION

Tumor hypoxia is characterized by an oxygen partial pressure [pO_2] lower than physiological, and is known to be a major contributor of treatment resistance, tumor aggressivity, metastasis progression, overall associated with poor patient outcome (Figure 1-1) [1], [2], [3], [4].

The presence of hypoxic regions inside solid tumors is the result of the high metabolic and proliferative rates of tumor cells and of poor or damaged vasculature [1]. Under hypoxia, tumor cells must adapt their metabolism to survive extreme condition of low oxygen, high acidity and poor nutrient concentration, all of which are a part of the hypoxia response pathway [1], [5]. In turn, those hypoxic cells will drive the neighboring normoxic cells to be more proliferative, resulting in increased tumor growth and invasion [6], [7]. This establishes a vicious circle of hypoxia as the tumor keeps growing, resulting in more depletion of oxygen, further driving a more aggressive phenotype. Furthermore, hypoxic regions are more resistant to anti-cancer treatment [8], [9]. Indeed, radiotherapy (RT) efficacy depends on generation of free radicals (hydrogen or hydroxyl radicals) that require oxygen to permanently fix DNA damages [2].

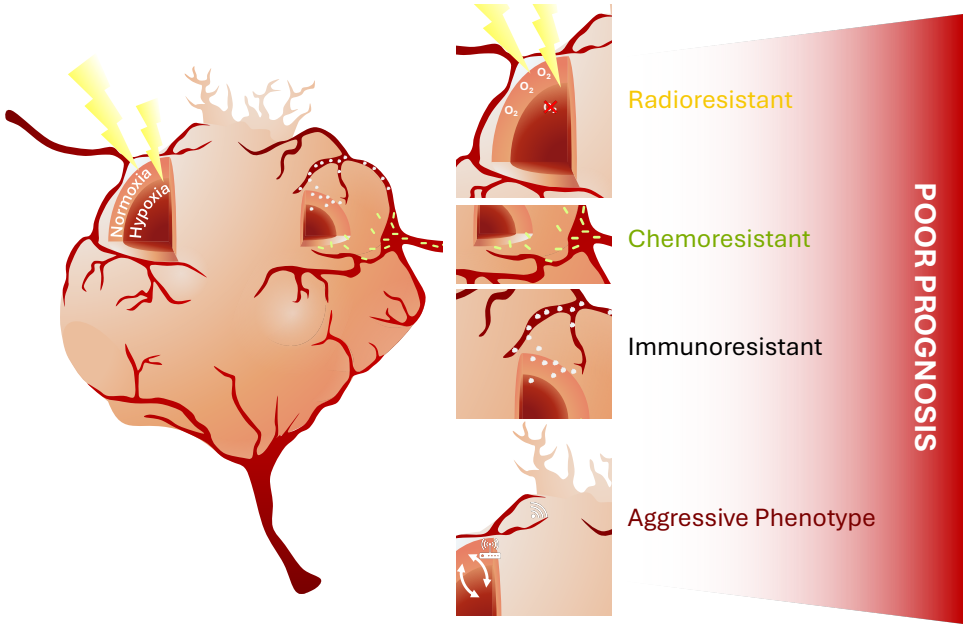

Figure 1-1 Hypoxia: A known contributor of treatement resistance and tumor aggressivity, associated with poor patient outcome

Similarly, chemotherapy (CT) is less efficient in hypoxic regions, as the drug often fails to penetrate deep enough due to the poor and damaged vasculature and as the highly acidic microenvironment can alter drug conformation and efficacy [10]. Additionally, hypoxia increases drug efflux and expression of genes involved in chemoresistance [11]. Like for CT, hypoxia drives an immunosuppressive phenotype making immunotherapy less efficient [1]. Immune cells cannot easily penetrate deep enough to invade the hypoxic regions, and the few cells that managed to do so are inactivated due to the acidity of the tumor microenvironment (TME) [12].

Soft tissue sarcomas (STSs), a rare type of cancer originating from mesenchymal cells, account for 1% of all cancers in adults and for 20 % of pediatric cancers [13]. STSs are known to form large and dense tumors and are prone to have extensive hypoxic regions. Treatment protocols of STS patients depend on clinical stratification but usually consist of preoperative RT to reduce tumor size, improve surgical outcome and preserve patient function [14], [15]. CT can be added to the patient treatment regimen for stages II and above, but with variable efficacy [16]. Despite efficient local control of the disease through surgery and neoadjuvant RT, metastasis remains the main cause of death for patients with STS [17]. Indeed, depending on the stage of the cancer, the 5-year relative survival rate varies from 81 % to only 16 % for patient with metastatic diseases [18]. Of note, around 50 % of STS patients will develop metastatic diseases, partly due to high hypoxia content (~ 45 %) [14], [18], [19], [20]. Overall, the poor patient survival rate can easily be explained by the hypoxic nature of STSs that makes them more resistant to treatment, more aggressive and more metastatic [19]. Although described here for STSs, these findings can be generalized to other cancer types such as glioblastomas, head and neck carcinomas or cervix and pancreatic adenocarcinomas, all of which are aggressive cancers with poor prognosis [20], [21], [22], [23], [24].

As such, studying hypoxia at the fundamental and translational level, particularly in the context of STSs, would be of major interest for treatment development and could hopefully in the future improve patient survival [19], [25], [26], [27], [28].

Of note, while impact of tumor oxygenation on treatment efficacy has been known since 1953, there are still few clinically available hypoxia-related treatments [20], [29], [30]. Despite showing promising results *in vitro* and in early phases of clinical trials, hypoxia-activated prodrugs (HAPs) such as tirapazamine (TPZ, SR-4233) or evofosfamide (TH-302) have either failed to prove their efficacy or induced severe adverse effects [30]. TPZ, discovered and developed by Brown and Lee in 1986, is one of the first compound to specifically target hypoxic cells [31]. Activation of TPZ, enabled by local absence of O_2, results in production of free radical species and subsequent topoisomerase II-mediated induction of double-strand DNA breaks [32]. By acting as a complementary cytotoxin and selectively killing hypoxic cells, the most resistant cells in tumors, TPZ could enhance the antitumor effects of RT or CT [32]. However, as stated above, TPZ failed to translate into clinical studies due to its non-negligeable adverse effects without higher local tumor control or better overall survival [32]. However, this failure could be partly attributed to poor patient stratification for hypoxia. Indeed, despite extensive study, assessing the presence of hypoxia remains a challenge as no pan-cancer or STS-specific biomarkers are available for clinical trials [19].

As previously mentioned, few drugs in development take hypoxia into account, mainly due to the lack of relevant biomarkers and user-friendly translational tumor models on which one can study hypoxia and its effects on treatment response [19], [33], [34], [35]. In fact, there is also an apparent lack of user-friendly tools allowing the study of tumor hypoxia in a controlled manner [35], [36]. Currently, *in vitro* study of hypoxia involves complex experimental setups to control oxygen levels or the use of chemicals acting as oxygen scavenger or interacting with the hypoxia-response pathway [37], [38]. Both approaches are used to artificially induce hypoxia in both 2-dimensional (2D) or 3-dimensional (3D) cell culture (e.g., spheroids). The most commonly-used experimental setups are either hypoxic chambers or oxygen-controlled incubators [38]. However, these methods do not allow long-term culture, experiments or treatment without reoxygenation of the samples, as tissues must invariably be reoxygenated when taken out of the incubator for medium change [35], [38]. Hypoxic gloveboxes partially resolve those issues but are expensive, do not allow RT treatment and require large volumes of nitrogen gas. Additionally, in all three setups, oxygen level is controlled by injecting nitrogen, thereby acidifying culture media and creating uncontrolled biases in experiments [39]. Similarly, chemical induction can also create uncontrolled bias by interacting with other metabolic pathways or affecting treatment response [1], [40].

Finally, none of these *in vitro* methods capture the whole picture of clinical hypoxia, among which the complex interplay between hypoxic and normoxic cells within the same sample [35], [41], [42]. On the other hand, *in vivo* tumor models can naturally exhibit hypoxia, arising from the same mechanisms as in patients (i.e., erratic vasculature, high proliferation rate).

However, the tumor must be large to be sufficiently hypoxic, which in mice corresponds to volumes close to the maximum limit accepted the ethics committees. Therefore, the duration of the experiments is limited by regulatory bodies and not by the requirements of the experiments themselves [43]. Moreover, *in vivo* quantification of hypoxia is usually assessed *postmortem* by immunofluorescence (IF) or immunohistochemistry (IHC) labelling of tissue sections [44]. Live detection of hypoxia in mice is possible but requires complex imaging techniques such as Positron Emission Tomography (PET), functional Magnetic Resonance Imaging (fMRI) or needle-type O_2 electrodes [44]. These techniques are not necessarily available in all research facilities, can be extremely expensive and require trained and qualified personnel to ensure accurate data acquisition. Overall, working with animal models to study hypoxia can be ill-adapted for the first steps of preclinical studies.

However, 3D *in vitro* models, among which tumor spheroids, have the potential to address this problem [45]. Indeed, in spheroids larger than ~ 450 µm of diameter, the oxygen gradient is steep enough for cells at the core to fall below the 10 mmHg hypoxic threshold [4], [46], [46], [47]. Although numerous techniques to form spheroids are available, such as hanging drops, spinning flask or ultra-low-attachment 96-well plates, these methods are not user-friendly and ill-adapted to high-throughput production of size-controlled spheroids [41], [45], [48]. As the latter is essential for experimental reproducibility and control of hypoxic content, this constitutes a major drawback to broad adoption of 3D spheroids to study hypoxia [49], [50].

For the past two decades, the advent of microfluidic technologies has enabled high-throughput generation of size-controlled spheroids which can be directly treated on-chip with RT, CT or drugs combination [51]. Microfluidic 3D culture chips consist of a small device mainly made of biocompatible polymers such as polydimethylsiloxane (PDMS) [52]. These chips are usually comprised of two parts, a bottom “wells” layer housing the spheroids and a top “channel” layer communicating with the wells [52].

Previous work from our lab demonstrated our ability to form spheroids within a couple of days and then subject them to RT-CT combinations [53]. One particularity of the designs developed in our lab is that our chips are not perfused, instead relying on daily culture medium change. This feature makes them extremely user-friendly [33], [53], [54], [55]. Moreover, thanks to the advent and democratization of microfabrication techniques, provided by computer-assisted micromilling and 3D printing, chip design can be tuned to fit specific research hypothesis and experimental requirements[56], [57].

Thus, the purpose of my PhD project is to design a microfluidic chip allowing the generation of tumor spheroids that naturally express a hypoxic core, characterize their multi-layered structure, validate hallmarks of clinical hypoxia and study its impact on treatment efficacy. My overarching goal is to provide a user-friendly tool to study hypoxia at the fundamental and preclinical level for translational cancer research.

CHAPTER 2 LITERATURE REVIEW

2.1 Hypoxia, Definition and its Impact in Cancer

Hypoxia is defined as intra-tissue oxygen partial pressure (pO_2) lower than physiological level. As physiological pO_2 varies between 3 % (24 mmHg) and 7 % (56 mmHg) across tissues, a range of pO_2 defined as "hypoxic" exists (Figure 2-1) [1], [2], [10], [20], [58].

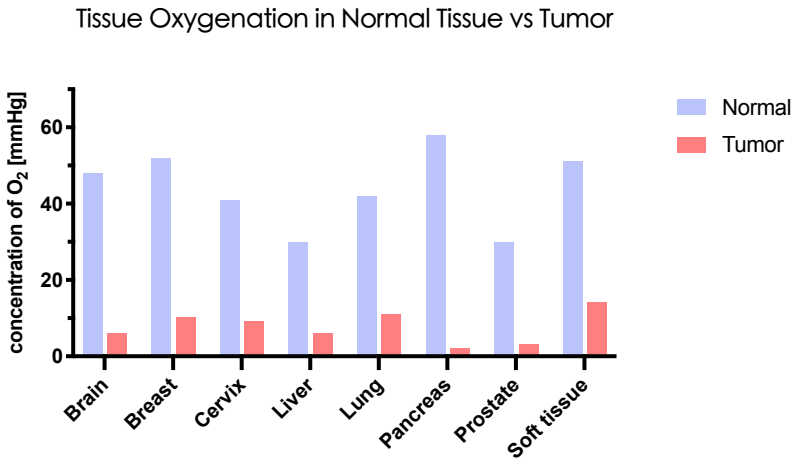

Figure 2-1 Tumor pO2 measurements from published clinical studies documenting the hypoxic state of various solid tumors [36], [59]. Note: Data from Vaupel et al. [59]

Furthermore, different dynamics of hypoxia exist, from intermediate to chronic (diffusion-limited), acute (perfusion-limited) and even transient [20]. Hypoxia can occur during exercise or in developing embryos but is also found across multiple diseases such as atherosclerosis, mountain sickness, anemia, stroke, heart disease or cancer, with the latter being the focus of my Ph.D. [60], [61].

Indeed, hypoxia is considered a hallmark of cancer and is found in 90 % of solid tumors regardless of their size, stage, grade or histology [20]. Presence of hypoxia and of its effects in cancer was first identified in 1953 by Thomlinson and Gray, [3], [4] the latter being the British physicist in whose honor the unit of radioactive energy deposition in tissue is named . Since then, 70 years of fundamental, preclinical and clinical studies have demonstrated that hypoxia is a major contributor to treatment resistance, tumor aggressivity, metastasis progression and is overall associated with poor patient prognosis [62], [63].

This culminated in 2019 with the Nobel Prize of Physiology and Medicine being awarded to William Kaelin, Peter Ratcliffe, and Gregg Semenza for their work on how human and animal cells sense and adapt to oxygen supply [63], [64].

Hypoxia in solid tumors arises from their rapid cellular expansion and abnormal and erratic blood vessel formation, which contribute to a deteriorated and deteriorating diffusion of oxygen [1]. As such, lack of oxygen inside solid tumors has generally been observed to start occurring between 100 μm to 200 μm away from a blood vessel, which results in multiple hypoxic niches inside of solid tumors [1].

Key regulatory pathways, genes and their downstream targets involved in cellular adaptation to hypoxia can be classified as hypoxia-response pathways [65], [66], [67]. Initiation of hypoxia-response pathways, adaptation of cancer cells to hypoxia and impact of hypoxia in cancer treatment will be discussed in the following sections.

2.1.1.1 Initiation of Hypoxia-Response Pathways

Evidently, oxygen (O_2) is essential for any aerobic organism, including humans, to produce energy thanks to the mitochondrial respiratory chain. Mitochondria is, after all, the powerhouse of the cell. Briefly, O_2, as the final electron acceptor in the electron transport chain, bonds to a proton (H^+) and forms H_2O. This process triggers the formation of a proton gradient with a higher concentration of H^+ in the mitochondrial intermembrane space and a lower concentration in the mitochondrial matrix. Through chemiosmosis, the stored H^+ act as a source of energy used by the ATP synthase to produce adenosine triphosphate (ATP) by oxidative phosphorylation of adenosine diphosphate (ADP) (Figure 2-2).

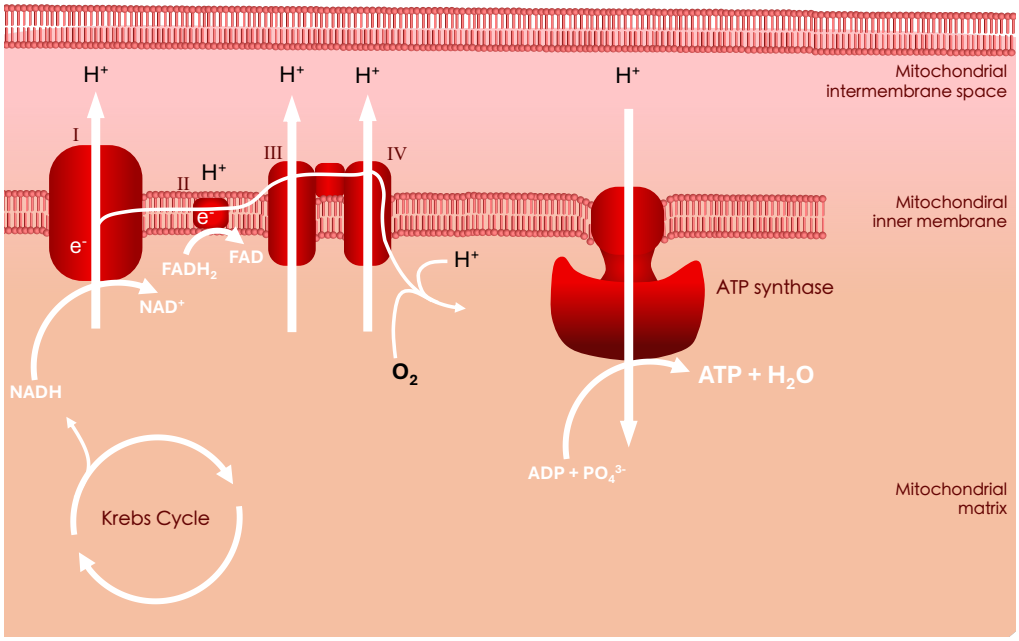

Figure 2-2 The Role of Oxygen in ATP Production during Oxidative Phosphorylation.

Adapted from Berg et al. 2002. [54]

The electron transport chain is composed of membrane-embedded proteins organized in four large complexes (I-IV) found in the inner mitochondrial membrane. During cellular respiration, NADH molecules, produced by the Krebs cycle, transfer their electrons to complex I and are reduced to NAD^+. The energy released by electrons moving through complex I by a succession of reductive and oxidative reactions is then used to pump protons (H^+) from the matrix into the intermembrane space. Then, electrons are transferred to O_2 which bonds to H^+ to form H_2O. This process results in the apparition of a proton gradient, with a higher concentration of H^+ in this intermembrane space and a lower concentration in the matrix. As shown on fig 2.1, the H^+ stored by the gradient acts as a form of energy, a process called chemiosmosis, used by the ATP synthase to produce ATP. Adapted from Berg et al. 2002. [68]

As oxidative phosphorylation is an O_2-dependent chemical reaction, drastic metabolic adaptation can be expected in oxygen-deprived cells. Indeed, in hypoxia, multiple metabolic and genetic modifications occur in order to compensate the energy imbalance and maintain tissue function. This compensation is regulated by numerous genes belonging to hypoxia-response pathways, the transcription of which is governed by hypoxia-inducible factors (HIFs), mTOR and the unfolded protein response (UPR). Interestingly, these pathways are activated at different levels of oxygenation. For example, the HIFs response pathway begins to be activated at $O_2 < 10$ % with high activation at 0.5 % [69], [70]. The UPR-PERK response pathway appears to be more important in the regulation of cellular stress under extreme hypoxia, i.e., $O_2 < 0.02$ % [71], [72]. Finally, the mTOR response pathway is prominent under moderate hypoxia exposure of $O_2 < 1$ % [73].

2.1.1.2 Hypoxia-Response Pathways, the role of HIFs

HIFs are the main factors that mediate the transcription of more than 100 downstream genes in response to hypoxia [34], [66]. The HIF family contains 4 genes HIF1A, HIF2A (also referred to as EPAS1), HIF3A and Aryl Hydrocarbon Receptor Nuclear Translocator (ARNT) coding for HIF-1α, HIF-2α, HIF-3α and HIF-1β respectively, each HIF-α subunit are oxygen-sensitive and can heterodimerize with the constitutively-expressed β subunit [34], [66], [74]. Under normal physiologic conditions, all HIF-α subunit proteins are continuously produced but undergo ubiquitination and consecutive degradation by the proteasome through hydroxylation of prolyl residues. Of note, HIF-1α is ubiquitously-expressed while HIF-2α and HIF-3α are only expressed in specific tissues [75]. HIF-2α is found in vascular endothelium, liver parenchyma, lung type II pneumocytes and kidney epithelial cells while HIF-3α is found in the thymus, cerebellar Purkinje cells and the corneal epithelium of the eye [75]. Degradation of the HIF-α subunit consists of hydroxylation of 2 proline sites by the oxygen-dependent proline-hydroxylase family (PHDs) among which, PHD1, PHD2 and PHD3 [34], [76], [77]. Upon hydroxylation, HIF-α is recognized and marked for proteasomal degradation by the Von Hippel-Lindau protein (pVHL) complex.

As oxygen is a necessary substrate for PHD activity and subsequent HIF-α degradation, PHD activity is diminished under hypoxia – this is also true for Ph.D students – allowing HIF-α stabilization [76]. Under hypoxic conditions, other molecular pathways can lead to HIF-α stabilization such as ROS-mediated PHD inhibition or mTORC1 inhibition [74], [76]. Indeed, there is an increase in ROS production under hypoxic condition, mainly due to dysfunctional mitochondrial respiration [8], [78]. Hypoxia also inhibits mTORC1, a complex containing the mammalian target of rapamycin (mTOR), through HIF1-dependent transcription of DNA damage-inducible transcript 4 (DDIT4), BNIP3 and AMP-activated protein kinase (AMPK) [8]. This results in a positive feedback loop between mTOR and HIF1 by the hypophosphorylation of eukaryotic translation initiation factor 4E binding protein 1 (eIF4EBP1) favoring cap-independent translation of multiple transcripts among which HIF1A [8], [34], [78]. Finally, once HIF-α are stabilized, they are translocated into the nucleus and form a heterodimer with HIF-1β. The HIF-α/HIF-1β complex binds on Hypoxic Responsive Elements (HREs) region of the DNA, within target gene promoters, to drive the expression of HIFs targets [8], [62]. On a side note, it has been documented that HIF-1α can be stabilized under normoxia by newly-discovered pVHL regulator, but these pathways remain unclear [66]. (Figure 2-3)

HIF1A and HIF2A and their associated proteins are the most characterized, while HIF3A was the last to be identified [79], [80]. While HIF-1α and HIF-2α share some redundant functions and regulate many similar hypoxia-induced genes, they also mediate a distinct set of genes [81]. Indeed, HIF1A transcription regulates metabolic reprogramming whereas HIF2A plays a role in angiogenic extracellular signaling regulation and other extracellular matrix remodeling factors [82]. HIF3A has been identified as a negative mediator of the other HIFs genes, although recent studies have pointed out its role as an oxygen-dependent transcription factor, activating its own specific subset of genes under hypoxia [80], [83].

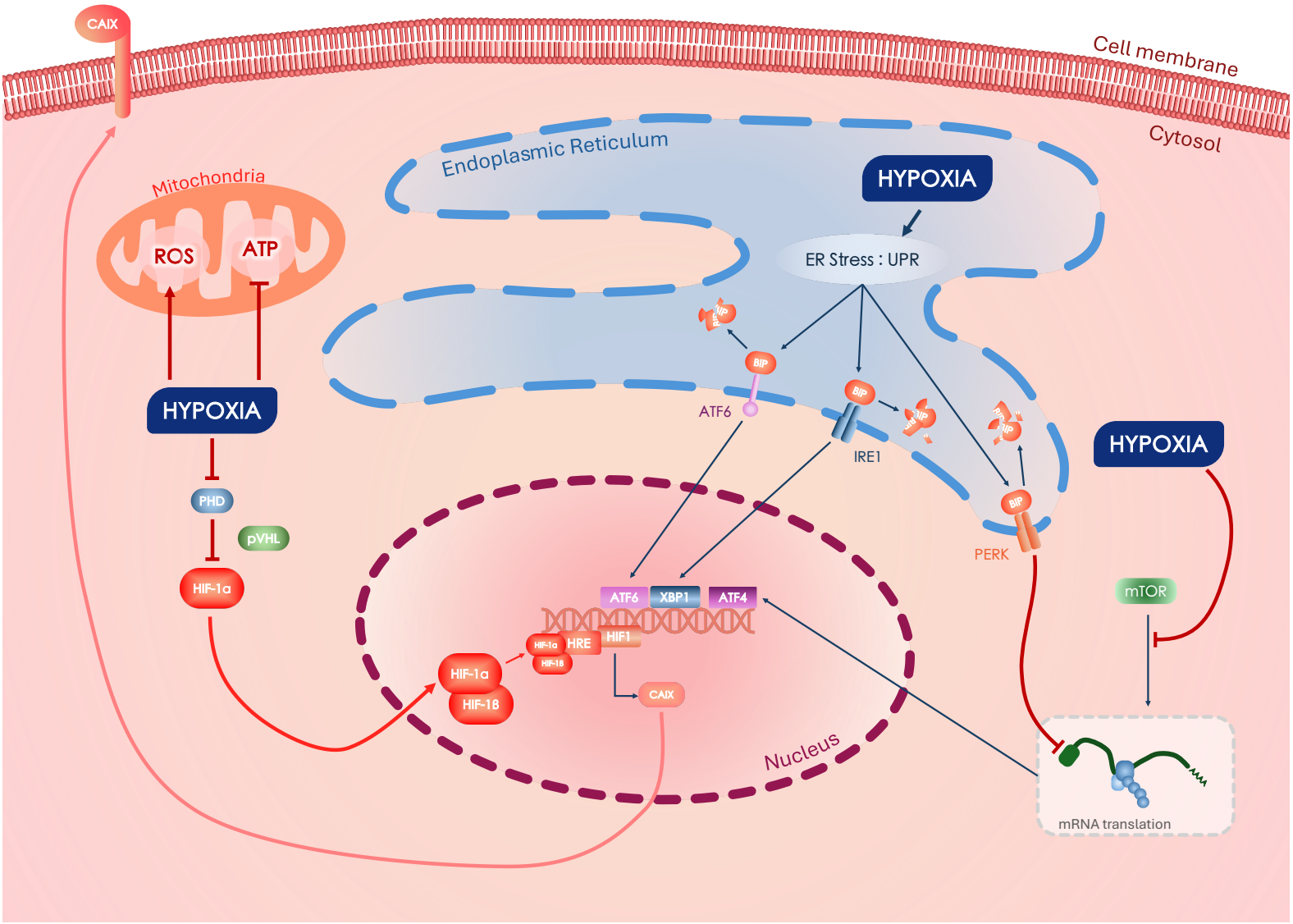

Figure 2-3 Oxygen Response Pathways : HIFs, UPR and mTOR. Adapted from Wouters and Koritzinsky [1]

2.1.1.3 Hypoxia-Response Pathways, the Role of mTOR and of the Unfolded Protein Responses

Other than stabilization of HIFs, cellular adaptation to hypoxia is also governed by mTOR and the (unfolded protein response) UPR. (Figure 2-3)

mTOR, a part of mTOR complex 1 (mTORC1), is a key regulator of cell survival and cell proliferation the activation of which under energy-replete stimulates protein translation [65], [84]. Thus, mTOR activity being directly linked to cell energy, its activity is inhibited under hypoxia [8], [65], [84]. More precisely, hypoxia inhibits mTORC1 through an HIF1-independent pathway involving AMPK-dependent activation of tuberous sclerosis protein 1 (TSC1) – TSC2 complex, when hypoxic condition is long-lasting (i.e., chronic hypoxia) and in conjunction with other stresses [65]. Overall, inhibition of mTOR results in changes in specific genes translation, contributing to a substantial difference in protein expression during hypoxia and influencing hypoxic-cell phenotype notably by altering metabolism, angiogenesis, autophagy and endoplasmic reticulum (ER) homeostasis [65]. Conversely, while mTOR is inhibited in hypoxic cells, in the context of cancer, hypoxic cells can re-establish the function of mTOR to control protein synthesis [65].

Among other stresses, hypoxia can cause accumulation of unfolded or misfolded proteins in the ER which activates the UPR [65], [85]. The latter is a signaling program meant to relieve ER stress by increasing the protein-folding capacity, enhancing the clearance of unfolded proteins or by inhibiting protein translation [65], [85]. This is achieved through regulation of transcription and translation of specific genes such as ER chaperones or components of the endoplasmic reticulum-associated protein degradation (ERAD) pathway [65], [85]. Although generally aiming to promote cell survival by reducing ER stress, UPR will however trigger cellular death by autophagy or apoptosis if this stress persists [85].

Three UPR signaling pathways have been uncovered, all initiated by chaperone proteins among which the glucose-regulated protein 78 (GRP78) also known as binding immunoglobin protein (BiP) [86], [87]. Buildup of unfolded proteins initiates BiP released from ER membrane, in turn inducing RNA-like endoplasmic reticulum kinase (PERK), inositol-requiring enzyme 1α (IRE1α), and activating transcription factor 6 (ATF6) [65], [86], [87].

First, PERK activation results in selective translation of proteins such as activating transcription factor 4 (ATF4), growth arrest and DNA damage inducible protein (GADD34), and CCAAT/enhancer binding homologous protein (CHOP) [86]. ATF4 restores ER homeostasis by modulating gene expression involved in amino acid biosynthesis, anti-oxidative responses, protein folding and in maintaining redox homeostasis [86], [88]. Of note, ATF4 can also induce cellular death via CHOP activation [86]. Meanwhile, GADD34 allows restoration of protein synthesis by mediating dephosphorylation of eukaryotic initiation factor 2 (eIF2), upon stress recovery [86], [89]. As already mentioned, CHOP activation stimulated by ATF4 will result in cell death [86].

Second, IRE1α degrades selected mRNA by regulated IRE1-dependent decay (RIDD) to reduce protein synthesis and decrease ER load. Additionally, IRE1α release transcriptionally active x-box binding protein 1 (XBP1) to restore ER homeostasis. IRE1α can also activate a proapoptotic signal by activation of c-Junk N-terminal kinase 1 (JNK1).

Third, similarly to PERK and IRE1α, ATF6 also promotes restoration of ER homeostasis, this time, by promoting protein chaperone and lipid synthesis, stimulating ER-degradation, and enhancing N-glycosylation [86]. Again, ATF6 can also contribute to cell death by inducing CHOP [86].

Furthermore, all hypoxia-response pathways are interconnected. Indeed, there is an interplay between HIF, mTOR and UPR. For example, UPR signaling promotes the response to hypoxia by phosphorylation and activation of HIF-1α and ATF4 and IRE1α cooperate with HIF-1α to activate downstream target genes. More broadly, this interplay is part of a generalized response to hypoxia, notably by interacting with HIF-1α thus enhancing HIF-1α target genes. mTOR can also promote HIF-1α stabilization and accumulation as a mean to start the transcription of necessary genes for cellular adaptation [65], [86], [90].

Overall, all these pathways result in cellular adaptation to hypoxia via complex metabolic and phenotypic changes involving a numerous set of genes. Alternatively, when hypoxic stress is prolonged and cells fail to adapt, cellular death is triggered.

2.1.1.4 Hypoxia-Response Pathways, Downstream Genes and Impact on Cancer

As previously discussed, multiple pathways trigger the cellular response to hypoxia with the aim of promoting transcription of a set of genes allowing the cell to adapt and survive under hypoxic conditions. Indeed, hypoxia-response pathways participate in multiple biological processes such as angiogenesis, cell metabolism, cell proliferation and differentiation, immune response, metastasis progression or cell death evasion, all of which promotes a more aggressive phenotype in the context of cancer.

More than 70 genes have already been identified to be putative HIF1A targets, an ever increasing number thanks to the democratization of transcriptomics [91], [92], [93], [94], [95]. Here, I describe a few examples of how these genes allow cancer cells to survive in hypoxic conditions and how hypoxia promotes a more aggressive phenotype.

As previously mentioned, hypoxic cells will promote angiogenesis to try to mitigate hypoxia by increasing blood flow. Known factors such as vascular endothelial growth factor A (VEGFA) promote angiogenesis by inducing proliferation and migration of vascular endothelial cells [96]. Upregulation of VEGFA in tumors leads to erratic neovascularization that fails to support adequate blood supply thus worsens local hypoxia [20]. Moreover, this neovascularization is leaky due to high permeability, facilitating tumor cell intra- and extravasation which increases the risk of metastasis.

The propensity of tumor cells to be highly proliferative translates into increased glucose uptake to maintain ATP production via glycolysis: the Warburg effect [20], [63], [97] (Figure 2-4). Activation of the Warburg effect relies on HIFs and MYC response to high proliferation rate and hypoxia, with HIF-1α being the main actor promoting this switch [63]. Indeed, HIF-1α promotes anaerobic metabolism shift by activating glycolysis regulators such as recombinant phosphoglycerate kinase 1 (PGK1) or pyruvate dehydrogenase kinase 1 (PDK1).

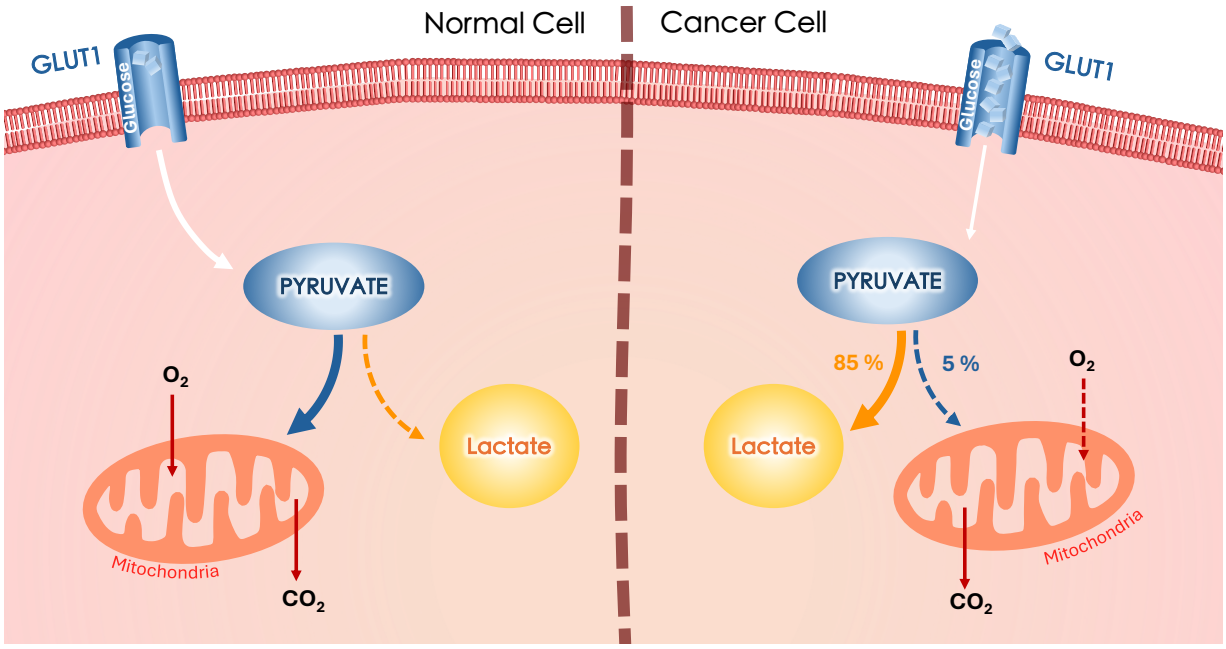

Figure 2-4 The increased glucose uptake to maintain ATP production via glycolysis : the Warburg effect. Adapted from Cramer et al. [1]

GLUT-1, encoded by solute carrier family 2 member 1 (SLC2A1), is a part of the GLUT family of membrane transporters proteins facilitating the translocation of glucose across cells [1]. GLUT-1 is widely represented across healthy tissue but is overexpressed in malignant cells to match their high glucose uptake. In short, glucose enters the cell via GLUT1 and is converted into pyruvate through glycolysis. Induction of PDK1 decreases mitochondrial utilization of the resulting pyruvate, therefore decreasing its transformation into acetyl-CoA to generate ATP [98], [99]. The rest of the pyruvate will be oxidized into lactate, the accumulation of which results in an increase of ATP and a reduction of ROS production [20], [63], [97]. This mechanism is one of the many by which hypoxic cells can evade apoptosis [63], [99].

Moreover, the accumulation of lactate and H^+ induces intracellular acidification [63], [100]. Therefore, hypoxic cells need to ensure pH homeostasis to survive [100]. In order to do so, carbonic anhydrase IX (CAIX) catalyzes the transformation of carbon dioxide (CO_2) in bicarbonate anion (HCO_3^-) and both CO_2 and lactic acid are buffered by HCO_3^-. As a result, CAIX contributes to the maintenance of a favorable pH promoting cell survival, but hydration of carbon dioxide also increases extracellular acidity by generating H^+.

The resulting acidic tumor microenvironment (TME) is a key feature of hypoxic tumors [100]. In turn, TME acidification promotes tumor growth and tumor cell invasion through breakdown of the extra cellular matrix (ECM), while reducing immune cell invasion [100], [101].

Hypoxic cells also have the ability to evade cell death partly due to their increased capacity of surviving with extensive DNA damages and by increasing anti-apoptotic proteins levels [62], [102]. For example, increased expression of BCL2 interacting protein 3 (BNIP3) and BCL2 interacting protein 3 like (BNIP3L) results in autophagy, a survival mechanism that promotes tumor progression [103]. While autophagy has been described as a type of cell death, autophagy plays a crucial role in the context of hypoxia and energy depletion by maintaining ATP production and other macromolecular synthesis, thus acting as a pro-survival pathway [103]. Furthermore, hypoxia also induces expression of drug resistance genes belonging to the ATP-binding cassette (ABC) transporter family. ABC proteins pump the drug out, in turn reducing intracellular drug concentration, thus limiting cellular death [63], [104]. For example, ABC Subfamily B Member 1 (ABCB1) (encoding for P-glycoprotein), ABC Subfamily C Member 1 (ABCC1) (encoding for multidrug resistance-associated protein 1, MDR1) and ABC subfamily G member 2 (encoding for ABCG2) are directly regulated by HIF-1α. In addition, promoters of ABCB1, ABCC1 and ABCG2 contain HREs sensitive to HIF-1α transcriptional regulation [104].

As previously stated, hypoxia also plays a role in metastasis progression by regulating cell and TME remodeling [105]. Cytoskeleton remodeling, as a part of epithelial-mesenchymal transition (EMT), is necessary for cancer cells to invade tissue and perform intra- and extravasation [106]. For example, vimentin (VIM), a known EMT marker, coordinates the dynamics of actin filaments and microtubules promoting cell motility [107]. Furthermore, Prolyl 4-Hydroxylase Subunit Alpha 1 (P4HA1), by hydroxylation and deposition of collagen in the ECM, generates a pro-invasive environment [105], [108].

Interestingly, hypoxia can also induce cell cycle arrest through multiple HIFs and UPR-regulated transcriptions factors [7], [109], [110]. HIF1 and UPR-dependent upregulation of CDK cyclin inhibitors p21 and p27, induce cell cycle arrest in G1 phase by counteracting cell proliferation, promoted by HIFs-dependent upregulation of Myc [7], [109], [110], [111]. This cycle arrest in G1 phase will play an important role in how hypoxic cells respond to chemotherapy, which will be discussed later.

However hypoxic cells can also evade cell cycle arrest depending on their expression of minichromosome maintenance complex (MCM) protein family, cell type-specific and cell cycle phase-specific HIF-1α and HIF-2α activity and effect on Myc, or even Myc itself [7], [110].

Overall, these 12 genes (VEGFA, PGK1, PDK1, GLUT1, CAIX, BNIP3, BNIP3L, ABCB1, ABCC1, ABCG2, VIM and P4HA1) confer an invasive, metabolically-enhanced, drug-resistant and apoptosis-evading phenotype to hypoxic cells. Despite these genes being but a fraction of the downstream targets of the hypoxia-response pathways, they already draw the portrait of the aggressive nature of hypoxic tumors. Even worse, hypoxia limits the efficacy of conventional cancer therapies, which I will describe in the following section.

2.2 Hypoxia and Cancer Treatment

Cancer treatment is supported by 4 pillars: surgery, radiotherapy, chemotherapy and targeted therapy (including immunotherapy). While surgery is also negatively impacted by hypoxia, it is evidently out of the scope of my Ph.D thesis [112]. As such, the following section will describe the mode of action of the other 3 modalities, and how hypoxia negatively impacts their efficacy.

2.2.1.1 Radiotherapy

Radiotherapy (RT) plays a major part in cancer management, as an estimated 50% of all patients will benefit from it at some point during their treatment [2], [113], [114], [115], [116], [117]. Regardless of the type of radiation, the damaging effects of ionizing radiation (IR) are caused by the ejection of electrons from molecules within the cell, i.e. their ionization [2]. While the radiation itself can "directly" induce damages by ionization, most molecular damages are "indirectly" dealt by the cascade of ejected electrons, in turn ionizing molecules along their track. As the speed of the electron decreases, collisions and subsequent ionization become more frequent, leading to the formation of clusters of ionizations.

Most of the deposited energy by IR is absorbed by water as it accounts for approximately 80% of the composition of the cell. Ionized water leads to a rapid production of reactive radical intermediates which interact with other molecules within the cell, such as DNA, causing the "indirect effect". As DNA is the largest molecule in the cell it makes for an "easy" target for IR. Furthermore, DNA exists in only 2 copies with a limited turnover and is vital for cellular functions, making it a perfect target in the context of cancer treatment. Thus, when clusters of ionizations are formed in DNA, breaking chemical bonds and disrupting its structure and function, they eventually lead to mitotic catastrophe and cell death as the cell simply cannot cope. The most damaging oxidizing agent is the hydroxyl radical (OH•) which chemically reacts with the DNA, producing a radical: DNA•. When in range, this radical can potentially lead to sustained DNA damages. However, when DNA• is produced, it enters a competition for reduction or oxidation. Reduction can restore the DNA to its original form through -SH containing compounds such as glutathione or cysteine. On the other hand, oxidation can fix or make damages permanent via the interaction between DNA• and O_2.

Thus, in hypoxia or in the presence of reducing species, DNA damages are not fixed, i.e., not permanent, and the DNA is ultimately restored. Therefore, hypoxia has a direct negative impact on the efficacy of RT. As such, enhancement of radiation damage by oxygen, or rather the degree of cell sensitization through oxygen can be characterized as the oxygen enhancement ratio (OER). OER is defined as the ratio of doses required to give the same level of biological effect (e.g. cell surviving fraction) in function of oxygen level, normoxia (or physoxia in patient) or hypoxia.

The OER can be as high as 2.5 to 3.3 for most mammalian cells *in vitro* and most tissues *in vivo* when treated with doses of x- or γ- radiation greater than 3 Gy [1], [2]. Although decrease of OER is observed at doses lower than 3 Gy, close to the clinical dose of 2 Gy used for fractionated treatment, Wouters and Brown demonstrated that cells at intermediate level of oxygenation can lead to significant radioresistance during fractionated RT [118].

Indeed, hypoxia-induced radioresistance begins to be observed *in vitro* at $pO_2 = 20$ mmHg, results in an OER of 2 at $pO_2 = 3$ mmHg and confers full resistance at $pO_2 < 0.2$ mmHg. Similar findings are observed clinically in many cancer types, where hypoxia content is an important predictor of poor response to radiotherapy and therefore of poor clinical outcome [119]. In addition, hypoxic cancer cells may have varying competence to undergo DNA-repair mechanisms, whether homologous recombination (HR), Non-homologous end joining (NHEJ) or nucleotide excision repair (NER) [1], [2]. As a matter of fact, HR deficiency has been shown to sensitize hypoxic cells to ionizing radiation, thereby reducing the OER [120].

Finally, cells are known to be more sensitive to RT in phases G2 and M and more resistant in phase G1 and S. As such, hypoxia-induced cell cycle arrest in G1 phase further reduces the efficacy of RT [2].

2.2.1.2 Chemotherapy and Hypoxia-Related Chemoresistance

Chemotherapy (CT) refers to the use of a toxic agent to treat cancer, and can be divided in 3 major categories: antimicrotubular agents (e.g., anthracyclines, taxanes), alkylating agents (e.g., cisplatin), and antimetabolite (e.g., 5-Fluorouracil) [121].

Antimicrotubular agents are divided in multiples categories, among which anthracyclines and taxanes. Doxorubicin is one of the most well-known CT and belongs to the anthracycline's family. Its main mechanism of action can be summarized as DNA intercalation, disruption of topoisomerase-mediated repairs and free radicals-mediated cellular damages [121], [122]. Paclitaxel, a taxane agent, works by disrupting polymerization and depolymerization equilibrium of microtubules, in turn causing abnormal cellular function leading to apoptosis. Specifically, paclitaxel is a M-phase-specific microtubule assembly inhibitor [121]. Further research indicated that paclitaxel can induce apoptosis by binding to B-cell leukemia 2 (Bcl-2) and thus interrupt its function [123].

Alkylating agents work by cross-linking their unstable alkyl group ($R\text{-}CH_2^+$) with the DNA bases, inflicting DNA-damages, making DNA strands unable to uncoil or separate hence stopping DNA replication and triggering cell death [121], [123].

Lastly, antimetabolite agents, for example 5-Fluorouracil (5-FU), interfere with DNA synthesis and repair by blocking incorporation of the thymidine nucleotide into the DNA strand during the S phase of the cell cycle [121], [124]. Importantly, various structural, physico-chemical and biological effects of cancer hypoxia foster chemoresistance and/or drastically limit CT efficacy. First, CT cannot properly be delivered to hypoxic niches as the erratic vasculature caused by hypoxia limits penetration of the chemotherapeutic compound. Second, as most CT agents are weak basis, low TME pH characteristic of hypoxia limits their efficacy. Indeed, the ion trapping model explains this phenomenon, as weakly basic compounds will concentrate in acidic regions instead of reaching their intracellular targets [11], [125], [126], [127]. Third, hypoxic cells further reduce CT efficacy by way of promoting the activity of drug efflux transporters (e.g. MDR1), thereby actively reducing intracellular drug concentration [128]. Then, as hypoxic cells are less proliferative, CT agents relying on DNA or RNA replication, and thus cell proliferation, are less cytotoxic. This has been widely documented across a large range of CT such as the ones already mentioned [11], [129], [130], [131], [132], [133].

2.2.1.3 Targeted Therapies

Compounds specifically tailored to target hypoxic cells have demonstrated their efficacy *in vitro* and *in vivo*, with a few under clinical investigation.

Hypoxia-activated prodrugs (HAPs) are a group of targeted therapies that are selectively activated under hypoxia, making them more cytotoxic to hypoxic cells [30]. Multiple HAPs have been developed since the 1980s, but all of them failed to be translated to the clinic despite their antineoplastic effect being proven preclinically [30]. Indeed, all clinical trials were unsuccessful due to either, poor efficacy, intense adverse effects, or a combination of both [30], [32].

The most common HAPs are tirapazamine (TPZ or SR-4233) and evofosfamide (TH-302). TPZ, one of the first compound to specifically target hypoxic cells, was discovered and developed by Brown and Lee in 1986. Activation of TPZ, enabled by local absence of O_2, results in production of free radical species and subsequent topoisomerase II-mediated induction of double-strand DNA breaks [9], [31], [32]. However, TPZ failed to translate into clinical studies due to non-negligeable adverse effects without higher local tumor control or better overall survival. Of note, this failure could be partially attributed to poor patient stratification for hypoxia [30], [134].

Evofosfamide has a similar mechanism of action as TPZ. Upon activation in hypoxic regions, evofosfamide is converted into its active form dibromo isophosphoramide mustard, a potent alkylator acting as a DNA cross-linking agent [30], [135]. Contrary to TPZ, evofosfamide has been tested in clinical trials since 2007, and still remains a drug of interest despite reported limited efficacy. Indeed, 2 new clinical trials starting in early 2025 are investigating efficacy of evofosfamide as a combination therapy. The first one will be a combination of evofosfamide with androgen receptor-signaling inhibitor therapy in castrate resistant prostate cancer (NCT06836726), while the second one is a combination with both zalifrelimab and balstilimab in advanced or metastatic castration-resistant prostate cancer, pancreatic cancer, and human papilloma virus (HPV)-negative squamous cell carcinoma of the head and neck (SCCHN) (NCT06782555).

Another approach consists of designing compounds selectively targeting hypoxia-specific genes and proteins. Evidently, inhibition of HIFs and mTOR has been investigated as part of this strategy.

HIF1 inhibitors, such a dichloroacetate (DCA) and digoxin, have demonstrated their efficacy in preclinical studies [67]. DCA decreases HIF1 transcription through inhibition of PDK and digoxin decreases HIF-1α through direct inhibition of HIF1 [136], [137]. Both of these drugs have reached clinical phase, phase I for DCA and phase II for digoxin [80]. However, no phase II clinical trials involving DCA has been reported, despite promising results in phase I [138]. On the other hand, digoxin phase II clinical trial failed to obtain results due to low patient enrollment (only 6) and insufficient amount of tissue samples to analyze [136], [139]. Lastly, EZN-2968, an antisense oligonucleotide inhibitor of HIF-1α was tested in 1 pilot study and 2 phase I clinicals trials. Again, no phase II study was launched despite promising results.

Meanwhile, mTOR inhibition strategy led to the development of everolimus [140]. While still being investigated in multiple clinical trials and being approved by the FDA in 2009, high toxicity and treatment-related mortality were reported and one important challenge is to properly identify biomarkers that predict response to everolimus (e.g., hypoxic biomarker) [141], [142].

On the other hand, the HIF-2α inhibitor belzutifan was approved by the FDA in December 2023 for patients with advanced renal cell carcinoma [143]. As of today, it is one of the only drugs that showed promising results in targeting hypoxia in renal cell carcinoma [29]. Other clinical studies are currently ongoing to test its efficacy in patients diagnosed with other cancer types (NCT02974738, NCT04976634). Importantly, 80% of clear renal cell carcinomas are known to present accumulation of HIF-2α, due to the loss of VHL gene and its protein pVHL [29], [144]. In this case, HIFs genes and pathways are constitutively activated and hijacked, thus promoting tumor growth and survival [145]. As such, belzutifan shuts down these pathways independently of hypoxia levels, leading to its demonstrable efficacy.

Like CT, the delivery of any targeted therapy is limited by the ability of compounds to diffuse inside the tumor and by some of the aforementioned resistance mechanisms. Overall, very few hypoxia-targeted therapies have successfully transferred from bench to patients, partly due to inadequacies between pre-clinical and clinical results.

Finally, regarding immunotherapy, hypoxic TME is highly immunosuppressive due to both its acidic pH and key signaling pathways [146]. For example, the hypoxia-mediated anaerobic glycolysis in tumor cells results in the excretion of adenosine, a potent suppressor of T-cells [147] Similarly, natural killer cells undergo profound metabolic reprogramming, changing both their function antitumor function and their phenotype. In addition, contrary to tumor cells, most immune cells cannot survive in the highly acidic hypoxic regions of the tumor [12], [36], [148].

All therapies described within the past sections, and virtually all non-surgical cancer therapies, are negatively impacted by tumor hypoxia. Whether physico-chemical or biological, the impact of hypoxia on cancer therapy efficacy must be adequately recapitulated at the fundamental and pre-clinical levels to improve the efficacy of cancer treatment modalities and the success rate of antitumor drugs.

2.3 Soft-tissue Sarcomas

Soft tissue sarcomas (STSs) account for 1% of all cancers in adults and 20 % of pediatric cancers [13], [15]. STSs are a rare type of cancer originating from mesenchymal cells, which is to say from any soft tissue : muscle, fat, blood vessels, nerves, tendons, linings of the joint etc. [13], [15]. While treatment protocol of STSs patients depends on tumor grade, most large high-grade STSs are treated with a combination of RT and limb-sparing surgical resection. RT is preferentially given before surgery (i.e. neoadjuvant RT) to limit long-term RT-related toxicities [16]. Adjuvant CT can be prescribed for patient with stage II diseases and above, although its efficacy is questionable as no significant differences in either relapse-free survival or overall survival are observed [149]. Despite achieving excellent local tumor control through neoadjuvant RT + surgery, metastases remain the main cause of death for around half patients diagnosed with ST, with their overall survival measured in mere months [150]. For metastatic patients, administration of anthracycline CT doxorubicin is considered standard of care, despite extremely poor ~20% response rates [17], [151].

As mentioned above, STSs is a highly metastatic cancer type, which is due in part to the hypoxic nature of STSs [150]. Indeed, STSs are characterized by a 45 % incidence of tumors harboring hypoxia, associated with worsened clinical outcome [152], [153], [154]. For example, a decrease in the 18 months disease-free survival from 70 % to 35 % is observed in soft tissue sarcomas (STSs) exhibiting hypoxia [20], [155].

Overall, STSs are a perfect example of the impact of hypoxia in cancer: hypoxia renders STSs resistant to both RT and CT, and increases aggressivity and metastatic potential. Although the focus of my thesis is on STSs, these findings can be generalized to other cancer types such as glioblastomas, head and neck carcinomas or breast and ovarian cancer, all of which are aggressive cancers with poor prognosis.

As such, studying hypoxia at the fundamental and translational level, would be of major interest for treatment development and could hopefully help improve patient survival, particularly in the context of STSs.

2.4 Preclinical Study of Hypoxia

2.4.1.1 Preclinical Models

Treatment discovery and development at the fundamental and preclinical levels rely on a variety of *in vitro*, *ex vivo* and *in vivo* tumor models, each corresponding to increasing level of complexity. The following sub-sections will describe the main approaches for these tumor models, along with their advantages and some of their limitations.

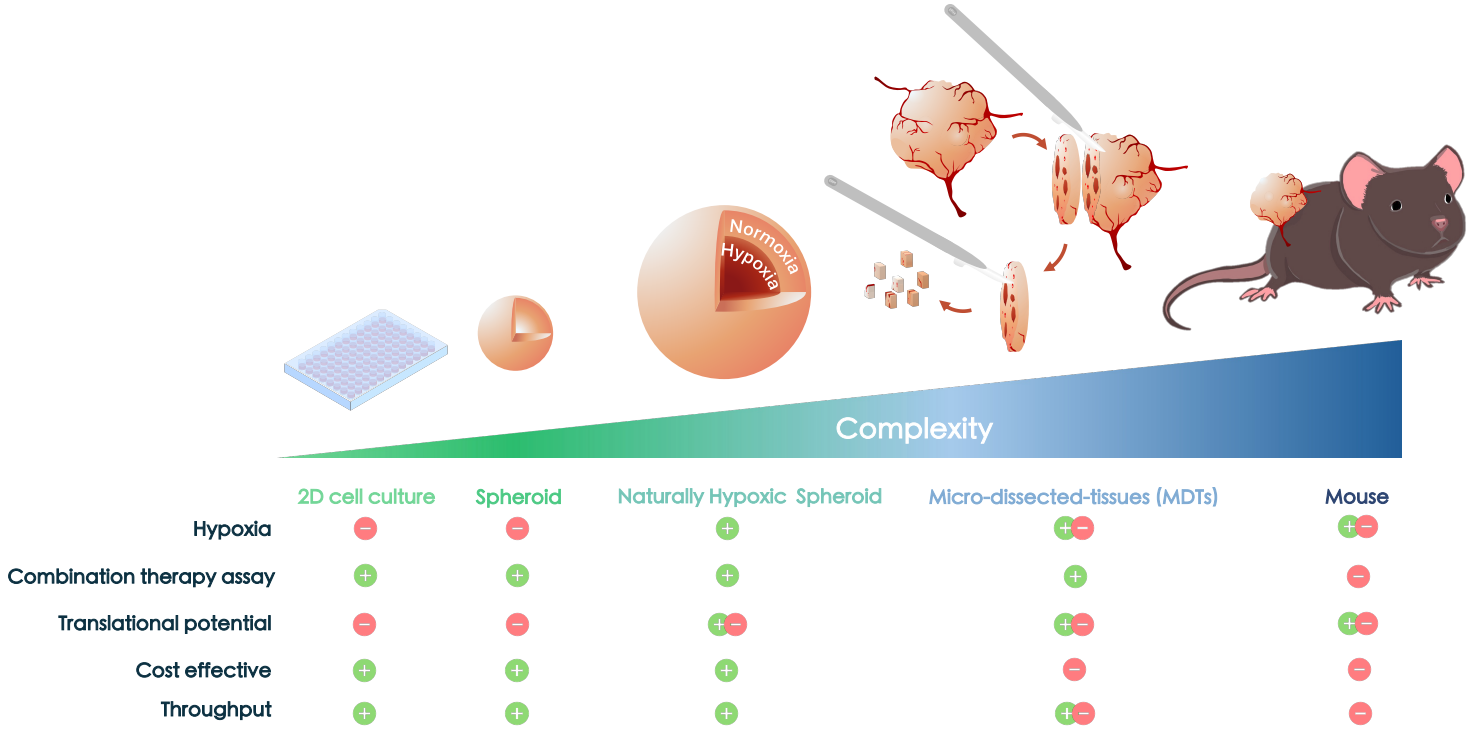

Figure 2-5 Preclinical Models, Advantages and Limitations

2.4.1.2 In vitro and Ex Vivo Models

Since the 1900s, 2D cell culture has been extensively used in cancer research thanks to its simplicity and high reproducibility, while being cheap and high-throughput [45], [156]. Despite being the most commonly used *in vitro* model for cancer treatment development, 2D cell culture is known for its limitations in representing tissue cells and recognized inability to mimic 3D cell organization and tumor kinetics [45], [156].

Indeed, the lack of tridimensionality of 2D cell culture cannot be eaisily reproduce either the diffusion-limited oxygen and nutrients gradients or the multi-layered structure of solid tumors, making them inadequate for the study of hypoxia and for treatment development [41], [45], [156]. Although 2D has certainly demonstrated its usefulness in elucidating the mechanisms of hypoxia at the molecular and cellular level, 3D incorporates structural and physical aspect of in vivo tumors especially relevant for tissue oxygenation. (Figure 2-5)

Therefore, overcoming 2D cell culture limitations by engineering more relevant tumor models for preclinical cancer research is necessary to improve treatment discovery and decrease failure rate *in vivo* [156]. As such, 3D tumor models have regained popularity for the past 15 years, despite being first introduced more than 50 years ago [41], [157]. 3D tumor models consist of either 3D cell culture (spheroids) or *ex vivo* culture of tissue explants. Advantages of these models is their ability to preserve the natural shape and spatial distribution of the cells, recapitulate oxygen and nutrient gradients as well as preserving cell-cell interactions [41], [156]. Thus, 3D tumor model can emulate hallmarks of cancer, among which the topic of interest of my thesis: hypoxia. With this, 3D *in vitro* and *ex vivo* models have been garnering interest in cancer research and treatment development [156]. (Figure 2-5)

Tumor spheroids, defined as compact cell aggregates, can be generated using various methods that are categorized in 2 groups: scaffold-free and scaffold-based. In scaffold-free culture, the 4 types of techniques of spheroids production can be summarized as agitation-based, hanging drop, liquid overlay and microfluidics [49], [156], [158]. Agitation-based techniques consist of continuously stirring adherent cells to prevent adhesion to the culture vessel, until they aggregate into a spheroid [48], [158], [159]. Hanging drop technique takes advantage of the surface tension of petri dish coverslips to generate multiple droplets of cell suspension. Thanks to gravity, cells will fall at the bottom of the drop and self-aggregate [160]. Liquid overlay technique relies on surface treatment of culture vessel that prevents cell attachment, such as ultra-low attachment (ULA) well plate. As adherent cells are used and as they cannot adhere to the bottom of the plate, they will adhere to one another and ultimately from a spheroid [41], [52], [159]. Microfluidics techniques work in a similar fashion to the other methods, albeit in a miniaturized setup, and will be discussed later. While agitation-base, hanging drop and liquid overlay are inexpensive methods to produce a large number of spheroids they require lots of reagent and do not necessary allow the generation of size-controlled spheroids [45], [161].

What's more, these techniques are not always compatible with other assays: it is not possible to efficiently image or retrieve spheroids inside a spinning flask or in a hanging drop, and any analyte secreted (e.g., lactate dehydrogenase or LDH, ATP, cell-free DNA) is extremely diluted, thus making the technique incompatible with liquid-based assays. In scaffold-based techniques, spheroids are grown and cultured in a natural (collagen, alginate, chitosan) or synthetic (polyethylene glycol, polylactic acid) gel-based matrix. Apart from issues regarding high batch-variability for scaffold materials, spheroids cannot easily be harvested for either bioanalysis or imaging. In addition, there is a growing concern regarding biocompatibility and toxicity of compounds used for polymerization of both synthetic and natural polymers [162].

Tumor spheroids are usually smaller than 450 µm of diameter. As the expression of hypoxia in solid tumors begins to appear 150 µm away from blood vessels due to diffusion limitations, a spheroid of ~ 450 µm would barely have hypoxia, if any at all. A few studies have generated spheroids larger than 500 µm, thus naturally harboring a hypoxic core [41], [158], [163] Still, these spheroids must be grown over more than 10 days to reach the desired size, albeit with high variability and with the caveat of relying on complex experimental setups (e.g., scaffolds, collagen matrix, etc). For example, Xavierselvan et al. had to grow their FaDu spheroids over 25 days in a ULA well-plate to reach a diameter of 650 µm [164]. Finally, although co-culture spheroid models have been described, most spheroids are made of only one tumor cell line and do not recapitulate the structural and biological effects of intratumoral stroma [41], [161], [165], [166].

To increase complexity, plate-based methods to culture *ex vivo* tumor explants have been reported [165], [167]. Broadly speaking, these methods consist of harvesting tumor samples from either patients or mouse models, preparing them in the form of slices or spheroid-like biopsies, and culturing them using plate-based methodologies [165], [168], [169]. Overall, these methods are tedious, experimentally-heavy and require access to *in vivo* tumor models, drastically limiting their throughput. Furthermore, mainly designed to preserve tumor heterogeneity and stromal content, these approaches often view hypoxia as an issue rather than a characteristic to actively try to emulate [165], [170].

As such, despite their 3D conformation, most spheroids and *ex vivo* tumor explants share with 2D the *de facto* absence of hypoxia. However, *in vivo* models could potentially alleviate those limitations.

2.4.1.3 *In vivo* Models

In vivo tumor models, usually mice, inherently recapitulate all major hallmarks found clinically in tumors.

In vivo tumor models usually result from the inoculation of human cancer cell suspension or grafting of fragments of patient-derived primary tumor. In this context, genetically-engineered immunodeficient mice are required to prevent tumor cells or graft rejection, therefore failing to emulate the immune component of tumor response. The development of humanized mice models partly addresses these issues by allowing grafting of both human cancer cells and human immune cells, but have limited ability to generate antigen specific antibody response [171]. Another model is the syngeneic mice model, where an immunocompetent mouse is subcutaneously or orthotopically injected with mouse tumor cell lines, this time preserving the immune component but being limited the low amount of available cell lines and their clinical relevance [50]. Moreover, genetically engineered mice models that spontaneously develop cancers, driven by altered expression of oncogenes of tumor suppressors, has been developed and applied to the study of tumorigenesis. As only few models are available, their use in anti-cancer treatment development is currently limited [50].

While mice models are wildly used in cancer research and are essential to capture the global response of tested treatment (e.g., abscopal effect, toxicity, etc.) before clinical trials, they are tedious to work with. First, *in vivo* models are expensive due to the number of animals needed to extract enough data, are time-consuming, can require high maintenance from the animal facility, and have a low to medium throughput. (Figure 2-5)

Second, *in vivo* tumor models do not provide complete control over how much tumor cells are under hypoxia, or if there is hypoxia at all. Indeed, *in vivo* tumors need to be large enough to increase the probability of harboring significant hypoxia, usually already close to the limit accepted by the regulatory bodies being 1.5 cm in all direction [43]. Therefore, studies investigating treatment efficacy over the course of weeks cannot be performed as the tumor quickly reaches maximum size in control groups.

Third, if one wants to assess hypoxia content in live animals before treatment administration, this must be performed with needle-type O_2 electrodes or complex imaging techniques (e.g., PET, fMRI) [172]. Those kinds of equipment are expensive, require qualified personnel, and are therefore not necessarily available in all research center and animal facilities. The alternative is postmortem assessment by immunofluorescence (IF) or immunohistochemistry (IHC) labelling of tissue section, a post-hoc destructive process.

For all these reasons, animal models are ill-adapted for the first step of preclinical studies, especially when taking hypoxia into account.

Importantly, the President of the United States of America signed in to law in 2022 the FDA Modernization Act 2.0. This bill allows and encourages the use of "cell-based assays, microphysiological systems, or bioprinted or computer models" as alternatives to animal models for purposes of drug and biological product development [173]. In January 2025, another proposal to mandate the FDA to update its regulation within 12 months regarding animal use in research has been introduced in the US Senate [174]. Similarly, the European Medicines Agency (EMA) has implemented new measures in 2021 to minimize animal testing during medicines development, by encouraging alternative approaches such as "tests based on human and animal cells, organoids, organ-on-chips and in silico modelling" [175].

Thus, developing simple preclinical tools to study hypoxia, its impact on cancer and on cancer treatment, while yielding high throughput results to identify prognostic biomarkers and druggable targets is extremely relevant and timely.

2.4.1.4 Hypoxia in Preclinical Models

Based on my previous statement regarding hypoxia in *in vivo* models, i.e. their complexity regarding the study of hypoxia and the necessity of using alternative models, going back to *in vitro* or *ex vivo* models is warranted. (Figure 2-5)

In vitro study of hypoxia involves complex experimental setups to control oxygen level, or the use of chemicals acting as oxygen scavengers or interacting with the hypoxia-response pathways. These methods are used to artificially induce hypoxia in both 2D and 3D *in vitro* and *ex vivo* models (e.g., spheroids, tumor explants). However, these approaches are not without issues: do not be too excited, we are not out of the water yet.

2.4.1.5 Chemical Induction of Hypoxia

Cobalt chloride ($CoCl_2$) is commonly used to induce hypoxia and is believed to work through inhibition of PHD, in turn blocking HIF-1α degradation and subsequently initiating the HIFs-dependent hypoxia-response pathway [176]. Yet, mechanisms of hypoxia-induction by $CoCl_2$ are not fully elucidated and give rise to upregulation of genes unrelated to hypoxia [42], [177], [178], [179]. Briefly, $CoCl_2$ diluted in sterile water is added to cell culture medium for at least 2 hours to induce stabilization of HIF-1α. However, cells have to be incubated in $CoCl_2$-supplemented culture medium for 24h to 72h to observe downstream effects of HIF-1α stabilization. Furthermore, amount of $CoCl_2$ required to induce hypoxia has been shown to vary between cell lines (100 µM – 300 µM), with $CoCl_2$ being cytotoxic at all such concentrations (IC_{50} = 30 – 125 µM). [177]

Other chemicals such as dimethyloxaloglycine (DMOG) and deferoxamine (DFO) also inhibit PHD activity, albeit by different mechanisms, again allowing HIF-1α stabilization [177]. While these chemicals are frequently used to induce hypoxia in *in vitro* setting, they only mimic parts of hypoxia [42], [179]. Indeed, they fail to impact other hypoxia-response pathways such as UPR or mTOR response, thus inadequately recapitulating the full breadth of the effects of hypoxia on tumor cells [42], [177].

Oxygen-scavenging compounds (e.g., sodium sulfite) directly limiting oxygen concentration have also been reported [180], [181]. However, their use is most prevalent in the field of microfluidics, which will be the topic of one of the following sections.

Overall, chemically-induced hypoxia fails to recapitulate the complex multi-layered structure of varying oxygenation status and cell phenotypes (e.g. proliferating cells, senescent cells, necrotic cells etc.) found *in vivo* in solid tumors, making them ill-suited for translational research.

2.4.1.6 Non-chemical Induction of Hypoxia

The most prevalent methods to artificially induce hypoxia are hypoxic chambers (airtight plastic container), oxygen-controlled incubators or hypoxic glove-box, all operating in a similar fashion (Figure 2-6). They consist of injecting nitrogen into a confined environment to flush the oxygen out, creating an oxygen-controlled culture environment at a desired oxygen concentration.

However, maintaining a controlled level of oxygen during the course of experiment can be challenging. For example, this equipment constantly consumes large quantities of nitrogen gas to maintain the target oxygen concentration, and the lower said target the faster the nitrogen is consumed. On a side note, this approach also makes researchers extremely dependent on the supply chain to perform basic experiments, the limits of which became apparent during the COVID-19 pandemic.

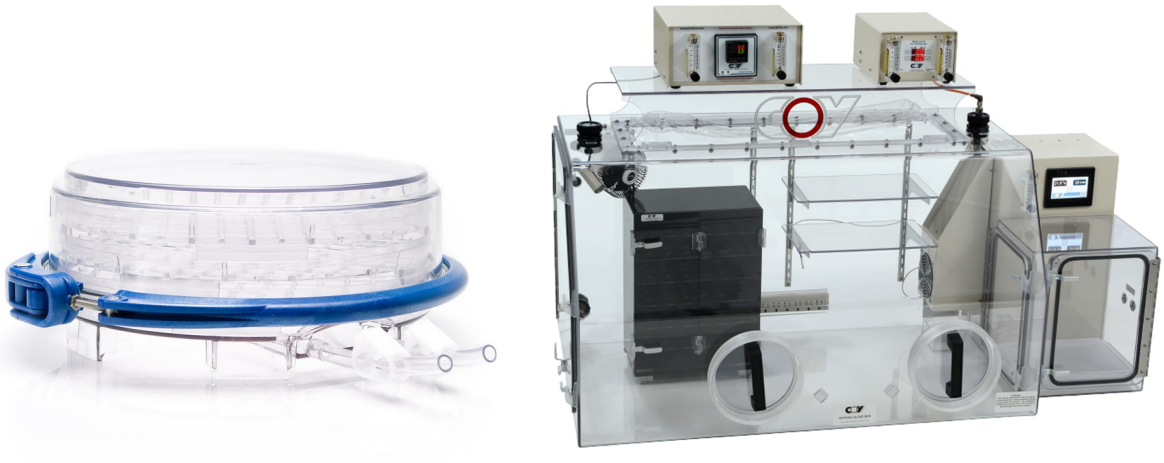

Figure 2-6 Examples of hypoxic chamber (STEMCELL Technologies, left) and hypoxic glove-box (Coy Laboratories, right) systems.

Regarding hypoxic chambers and oxygen-controlled incubators, one issue is that once biological samples must remain inside or else they would automatically reoxygenate. For example, in the case of oxygen-controlled incubators an action as simple as opening the door could potentially jeopardize the whole experiment. Similarly, any experiment requiring media change, drug testing or irradiation would involve taking the samples out of the setup, thereby re-exposing it to ambient air. Overall, these methods drastically limit the bioassays that can be performed or impose a major burden on researchers to mitigate their issues.

By contrast, most of these issues are avoided when using hypoxic glove-boxes. They consist of a glove-box workstation composed of an incubator and a bench with controlled oxygen

concentration, allowing maintenance of hypoxic conditions during cell culture. Nonetheless, all reagents for cell culture, treatment or live-bioassays also need to be maintained under low oxygen level to avoid reoxygenation through the dissolved oxygen they contain. Additionally, leaving cell culture media or other reagents in low oxygen environment will affect their pH, increasing their acidity as carbon dioxide can be dissolved at a higher concentration, possibly leading to uncontrolled adverse effect. Moreover, treatment with RT is still realistically impossible to perform within this setup, *de facto* incompatible with external beam irradiators. Therefore, the same issue as for hypoxic chambers and oxygen-controlled incubators would arise: reoxygenation of the biological samples when performing basic experiments (e.g., RT, live imaging).

Finally, as for chemical induction of hypoxia, non-chemical induction cannot produce gradients of hypoxia found *in vivo*, a level of complexity necessary for translational research. Overall, none of those methods allow the study of the interaction between hypoxic and normoxic cells as all of the cells would be subjected to the same oxygen level or lack thereof.

So, we are back to square one: generating hypoxic tumor models is a tedious and imprecise process, often incompatible with treatment evaluation and translational cancer research.

2.5 Microfluidics in Cancer Research

Microfluidics is the field of miniaturized design allowing the manipulation of microliters of fluids. Following the same idea as electronic miniaturization, microfluidics enables the miniaturization of research laboratories in multiple fields and is also colloquially referred to as “lab on a chip”. For the past decades, microfluidic technologies have been used and developed for biological applications as they uniquely combine high design versatility, cost-effectiveness, user-friendliness, and multiplexing capability with the capacity to develop increasingly complex biological models and bioassays directly on-chip. Thanks to the advent and democratization of microfabrication techniques, such as 3D-printers and computer numerical control (CNC) milling machines, design and fabrication of customized microfluidic devices for specific applications are now easily feasible. For all these reasons, microfluidics has proven to be a great tool in cancer research. [35], [41], [51], [182], [183], [184].

As previously stated, despite 3D *in vitro* tumor models being more relevant than 2D cell culture, their plate-based culture presents a variety of challenges to researchers. Indeed, spheroids generation methods are not user friendly, often time-consuming, require lots of reagent and do not necessary allow the generation of size-controlled spheroids. Similarly, *ex vivo* tissue samples are difficult to maintain for multiple days without inducing a significant decrease in viability. Fortunately, the boom of microfluidics for biological applications in the last decades cemented microfluidic devices as a tool of choice for the culture of 3D tumor models. As these 3D tumor models are especially relevant regarding drug uptake dynamics and intratumoral drug distribution and as on-chip treatment can be easily performed, drug screening became one main avenue for the development of robust on-chip 3D-tumor models [185], [186], [187], [188]. As such, the use of on-chip 3D tumor models for treatment screening application has increased in microfluidic literature over the last 10 years [185], [189], [190], [191].

2.5.1.1 Microfluidic Chip Materials for 3D Tumor Model Culture

Microfluidic devices or chips are commonly made of rigid polymer, inorganic materials, PDMS or even paper, all of which having pros and cons [192]. Glass, thermoplastics and PDMS still remain the most widely used materials thanks to their durability, versatility, biocompatibility and inexpensiveness [192], [193]. Glass and thermoplastic-based microfluidic devices can easily be mass-produced with high reproducibility and high resolution. Additionally, techniques such as hot embossing, laser engraving or micro-milling are used to manufacture intricate designs [192], [193]. Furthermore, the transparency and rigidity of both glass and thermoplastics such as polymethyl methacrylate (PMMA) make them compatible with microscopy techniques and equipment [192], [193].

Meanwhile, PDMS can be a bit more challenging. PDMS chips must be handmade through a method called soft-lithography [194], [195]. Soft lithography consists of the assembly of two (or more) parts made in soft polymer materials, here PDMS. First, negative molds of the device made of ultraviolet (UV) resin, thermoplastic or PMMA are either 3D-printed, embossed or micromachined [192]. Second, unpolymerized PDMS – usually a mix of 10 parts elastomer to 1 part encapsulating agent for biological purpose – is poured into the molds and polymerized using heat. Once polymerized, the parts of the device are manually sealed together after a short exposure to atmospheric plasma [192], [194], [195].

Briefly, exposing surfaces to atmospheric plasma activates the inert polymer surface by forming highly reactive species, in the case of PDMS reactive hydroxyl group, (-OH) are formed [196]. Once both surfaces are activated and assembled, covalent bonds between both surfaces are created, leading to a long-term sealing of the device [196]. However, resolution and intricacy of the design are limited by both the mold and soft lithography itself, as the manufacturer must be able to unmold the PDMS. Additionally, despite being transparent, PDMS chips can be ill-adapted for microscopy analysis as PDMS is a soft material: chips can bend on top of the objective thus affecting the focus and the quality of the resulting images.

Despite these aforementioned limitations, PDMS remains the polymer of choice for biology applications thanks to its biocompatibility, its transparency to both light and oxygen, and its radiocompatibility [54], [197], [198]. In addition, the flexibility of PDMS is a major advantage when one wants to retrieve the biological samples as the chip can easily be peeled or cut with any sharp object. Furthermore, chips made with PDMS through soft-lithography are affordable (0.20 CAD$/g, 1 device ~ 20-50 g) and do not require complex and expensive machinery to produce them: just a 3D printer, an oven and a plasma generator.

2.5.1.2 Microfluidic Chip-Based Methods for 3D Tumor Model Culture

As previously stated, the vast majority of non-commercial microfluidic chips are made of PDMS, a transparent, oxygen-permeable, water-equivalent (a critical property for RT) and biocompatible silicon material. Its physico-chemical properties make ideal for cancer research, as tumor models can be cultured, treated, imaged and analyzed on-chip [54], [55].

In addition, microfluidic chips can alleviate many problems found in existing *in vitro* tools for cancer research, such as facilitating formation of size-controlled spheroids in a high throughput fashion while being faster and less expensive than other spheroid cell culture methods [41]. Similarly, on-chip culture of *ex vivo* tumor samples like micro-dissected tissues (MDTs) and tissue slices has been demonstrated to alleviate the issues of poor tissue viability found in plate-based methods [165].

Indeed, multiple strategies have been developed to form and culture spheroids on microfluidic chips such as emulsion techniques, hanging droplets, microtraps, or microwells which allows the devices to be tailored to match experimental requirements [199]. The selection of the spheroid generation technique depends on the design of the chip itself, and vice versa. As such, microfluidic chips can be either perfused or non-perfused depending on experimental purposes and requirements, although perfused systems can be cumbersome.

The emulsion technique relies on a flow-focusing droplet generator and generally consists of a 3-inlets chip: one for the cell suspension and two for the non-miscible with water liquid (e.g., oil) [199], [200]. Briefly, by adjusting the inflows depending on the liquids' viscosity and target droplet size, droplets of cell suspensions will be captured within the oil. An alternative is to use cell-dispensed hydrogel in lieu of cell suspension, with the general methodology being identical [199]. This method enables rapid and high-throughput production of spheroids, although their size is drastically limited by the maximum size of a droplet [199]. For example, Panuška et al. reported in 2024 a system to generate 800 µm droplets, resulting in only ~ 200 µm large spheroids [200]. Moreover, emulsion technique requires pressure-pumps, making it cumbersome to use in a standard biohood. In addition, spheroids are encapsulated in either oil or hydrogel which could alter further experimentation, e.g., chemo- or radiotherapy testing, or biological processing.

The on-chip hanging drop technique works in a similar fashion to its petri dish version. Briefly, chips generally consist of one channel with a rigid material (glass, PMMA, etc.) at the bottom and a holed PDMS slab as the roof. Then, a cell suspension is pipetted into the channel and the chip is flipped upside-down for droplet formation. Thanks to gravity, cells sediment at the bottom of the droplet and ultimately aggregate into a spheroid. However, this method shares the same limitations as the petri dish method: not user-friendly, no easy retrieval of the spheroids, only for small spheroids. Indeed, the maximum size of a spheroid is drastically limited by the maximum size of the droplet. The latter is in turn limited by its maximum weight, above which gravity prevails over surface tension, making the droplet fall.

The microtraps techniques consist of multiple U-shaped microstructures laterally placed inside of a channel, trapping cell upon cell suspension injection. However, this method requires a constant flow to keep the cells tightly packed inside the trap ensuring spheroid formation and once formed, to keep the spheroid in place. As such, this method requires using syringe pumps, thereby making it not user friendly and cumbersome to use in standard biohoods and incubators.

Lastly, the microwell technique is the most straight forward method for spheroid generation. Chip design generally consists of a one channel PDMS chip with microwells at the bottom, with many shapes and sizes of wells having been reported in the literature. Briefly, the inside of the chip is first treated with a surfactant (e.g. Pluronic®, a poly(ethylene glycol)-block-poly(propylene glycol)-block-poly(ethylene glycol)) to prevent cell adhesion. As the cell suspension is pipetted directly inside the channel, cells sediment inside each well thanks to gravity and ultimately aggregate into a spheroid. Mainly, this technique allows user-friendly and high-throughput generation of uniformly-sized spheroids. Moreover, the size of the spheroid is directly a function of the size and shape of the well and of the concentration of the cell suspension, making this method easily tunable to reach any desired spheroid size. Additionally, tumor cell size and cell line-specific ability to tightly aggregate could also influence spheroid dimensions and sphericity. As such, previous work from our lab demonstrated applications of the microwells technique for spheroid generation in PDMS microfluidic chips [14], [33], [53], [55]. Rousset et al. (2017) cemented the principle and design rules of microfluidic device for 3D tumor model culture using the microwell technique. Following his work, Patra et al. (2019) engineered a microfluidic device for the culture of 120 sarcoma spheroids while only using less than 200 µL of reagents, compatible with on-chip CT (doxorubicin) and RT treatment.

Principles for on-chip methods of *ex vivo* culture of tumor models are analogous to plate-based methods: retrieving and processing tumor tissue into smaller fragments or slices. Similarly to *in vitro* on-chip methods, some of the issues found in plate-based *ex vivo* culture can be alleviated by on-chip culture of tissue slices or MDTs. Indeed, Astolfi et al. (2016), Simeone et al. (2019) and Dorrigiv et al. (2021, 2023) demonstrated ability to trap large numbers of on-chip MDT explants, in a comparatively easier fashion than standard *ex vivo* methods, and showcased applications in translational cancer research [46], [165], [201], [202]. Similarly, Carr et al, Cheah et al. and Kennedy et al. (U. Hull, UK) have designed microfluidic casings for user-friendly culture and irradiation of *ex vivo* tumor slices [203], [204], [205].

Overall, microfluidics and its many advantages can be of great use in improving the current landscape of *in vitro* and *ex vivo* tumor models and treatment evaluation, but what about hypoxia?

2.5.1.3 Current Landscape of Hypoxia on-Chip in Cancer Research.

Although 3D tumor culture has benefitted greatly from the development and adoption of microfluidic chips, this has not fully translated to the field of hypoxia research. Indeed, numerous groups using microfluidics to study hypoxia do not take advantage of using 3D culture, using 2D cell culture instead, and the few that are still rely on either chemical or non-chemical artificial induction [181], [206], [207], [208], [209], [210], [211], [212], [213], [214], [215], [216], [217], [218], [219], [220].

For example, Barmaki et al. (2020) used the oxygen scavenger sodium sulfite in culture medium to generate hypoxia in 2D cell culture, while the whole setup is being perfused [181]. Similarly, Takahashi et al. (2023) uses a complex circulating mix of humidified nitrogen, O_2 and CO_2 gas perfusing 2D cell culture on-chip (Figure 2-7) [221]. Furthermore, both these examples and multiple other similar studies are only generating hypoxia at one specific O_2 concentration, without generating gradients [181], [206], [214], [221], [222].

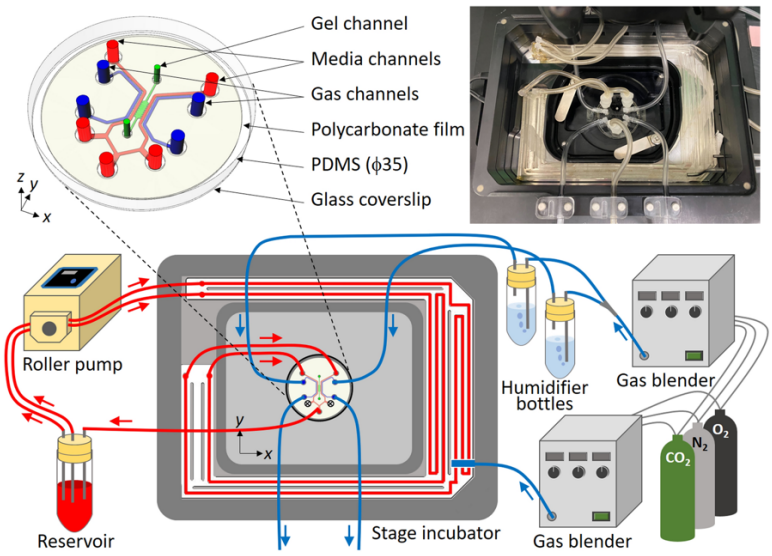

Figure 2-7 Microfluidic setup for hypoxia generation on 2D cell culture

Takahashi et al. chip. The microfluidic device is placed in a stage incubator to maintain temperature. The chip is perfused with humidified gas mixture of nitrogen, O_2 and CO_2 and with culture medium. Red and blue arrows indicate flow direction of the culture medium and gas mixture, respectively. A photograph of the chip and the flow channel placed in the stage incubator [221].

Alternatively, multiple groups did generate hypoxia gradients on chip, albeit in 2D or 3D-like models. Oh et al. (2022) engineered a device and generate a gradient of O_2 by integrating a polycarbonate film into their device, acting as an oxygen barrier, and seeded either a cell suspension (2D model) or a cell suspension-scaffold gel mix (3D-like model) (Figure 2-8, A). I qualified the cell suspension-scaffold gel mix as a 3D-like model as there is no cell-cell junction in 3D or dense aggregation, but rather of a 3 cells thick slab [217]. Similarly, others have engineered chips to generate gradients of hypoxia but again in 2D cell culture, all of them using artificial methods of induction (Figure 2-8, B) [214], [215], [216], [223], [224], [225].

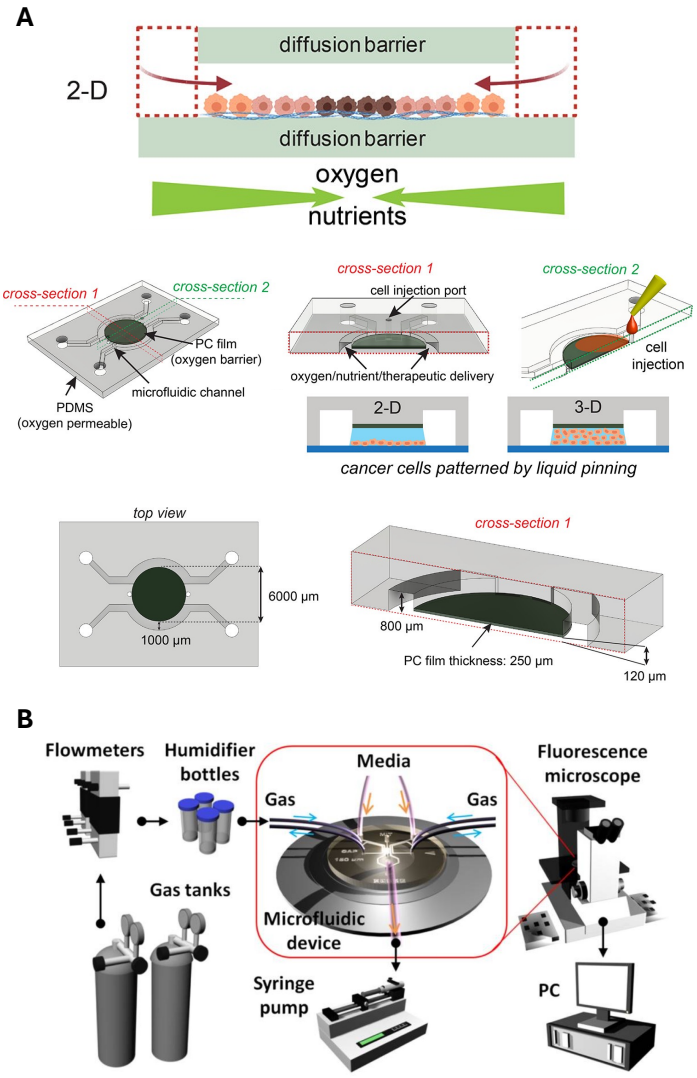

Figure 2-8 Microfluidic setups for hypoxia gradient generation on 2D cell culture.

(A) Oh et al. chip. [217] (B) Funamoto et al. chip. This perfused chip can generate both uniform and gradient hypoxia by injecting nitrogen. Their objective is to follow 3D movements of cancer cell embedded in a matrix, in normoxic versus hypoxic conditions. [215]

Only a few teams have combined both 3D models and hypoxia, again using small 3D models (diameter < 500 µm) and artificially inducing hypoxia. Barisam et al. (2022) designed a perfused chip on which they can culture 16 “spheroids” (or rather loose cell aggregates according to their images) of ~ 500 µm and incubated their chip in an oxygen-controlled incubator (Figure 2-9, A)[206]. However, they are not able to retrieve their spheroids from the device, instead resorting to systematically dissociating them using trypsin before bioanalysis.

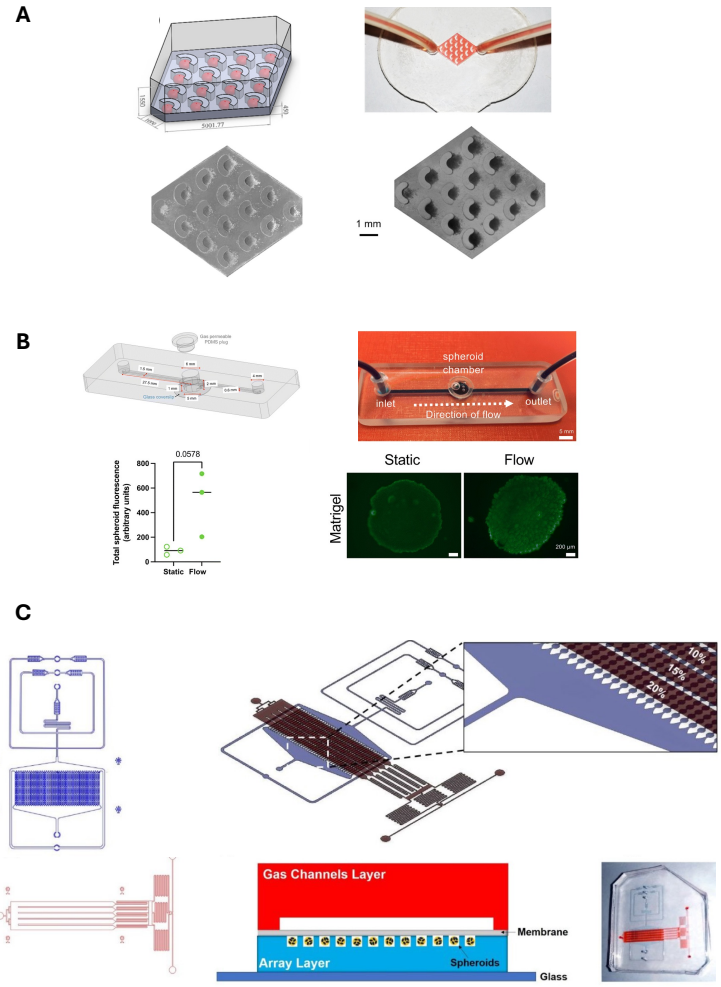

Figure 2-9 Microfluidic setup for spheroid culture with artificial induction of hypoxia

(A) Barisam et al. chip (B) Pyne et al. chip (C) Fridman et al. chip. They generate on-chip spheroids and artificially induce hypoxia by injecting nitrogen inside a gas channel in the device. They can generate multiple oxygen concentrations on the same chip thanks to the design. They generate a gradient across their chip rather than inside the same spheroid.

Similarly, Pyne et al. (2024) engineered another perfused chip in which they can culture one spheroid (Figure 2-9, B) [207]. However, despite their spheroid being larger than 1 mm of diameter, technically far exceeding the threshold for diffusion-driven hypoxia, they still use a hypoxic glove-box at 1 % of O_2 for their study. In addition, rather than on-chip generation, they form their spheroid using a ULA 96 well-plate (outside of the chip), transfer it onto their device and add Matrigel (scaffold material). Of note, given the concentration of Matrigel they used (50 %), and based on my own experiments, the total absence of spheroid invasion into Matrigel is curious.

To add to the mystery, their staining of live cells indicates that only the outer rim of the spheroid is alive for their "static" (no-flow) condition, and no other staining was conducted. Overall, given the only image presented in the article, it is difficult to gauge if their spheroid is a tightly packed sphere or a loose aggregate of cells, is hypoxic or not, or is even alive at all. [207] As a final example, Geyer et al. (2023) used a commercial device from MIMETAS to generate extremely small patient derived spheroids (that they define as organoids) of less than 150 µm of diameter. As the other groups, they then placed the device in a controlled-oxygen incubator, at 1 % of O_2. [208]

Notably, none of those group studied the impact of oxygen gradient in spheroids, missing one of the important characteristics of tumor hypoxia: the interplay between hypoxic and normoxic cells (Figure 2-9, C).

Finally, besides not generating large spheroids, artificially inducing hypoxia or only working with 2D models, all of these devices have in common their complexity to use and to potentially transfer to other research groups.

This is also true when looking at groups using 3D *ex vivo* models on-chip who, despite investigating treatment response, either never studied the presence or the impact of hypoxia in these models [46], [201], [202], [203], [204], [205], [226], [227], [228], [229], [230], [231]. As previously mentioned, hypoxia is often defined as a limitation in tumor explants rather than a characteristic of interest.

2.5.1.4 Tools for Improved Hypoxia on-Chip.

Fortunately, the fields of microfluidics, 3D biology, physics, biochemistry and engineering already possess all the necessary tools to address this issue. The following section will describe how elements from each of these fields can be harnessed to purposefully design a device for the culture of naturally hypoxic tumor spheroids.

2.5.1.5 Theoretical Basis for Oxygen and Glucose Consumption

As previously mentioned, hypoxia and lack of nutrients is most often thought of as a limitation in the field of on-chip tumor models rather than a relevant characteristic to be actively pursued.

The target size of on-chip spheroids, and therefore that of the microwell, is therefore generally limited by the need for these spheroids to not lack either glucose or oxygen. To ensure so, researchers can easily model oxygen and glucose consumption of their on-chip tumor models using Michaelis-Menten kinetics, the parameters of which are either tabulated or can be derived experimentally.

This equation describes the diffusive process where a species being consumed is written as:

$$\frac{\partial C}{\partial t} = D\nabla^2 C - \frac{qC}{C + K_M} \tag{2.1}$$

With C the concentration of the species, D its diffusion coefficient, q its consumption rate and Km the Michaelis-Menten constant.

Thankfully, this complex equation can be greatly simplified in the case of O_2 given the characteristics of PDMS chips and a few relevant assumptions.

First, as PDMS is extremely oxygen permeable, the volume of culture medium outside of the spheroid can be considered infinite and fully saturated in oxygen at all times. Steady-state!

$$\frac{\partial C}{\partial t} = 0 \tag{2.2}$$

Then, as spheroids can be reasonably approximated to perfect spheres, the 3D equations can be reduced to a 1D problem (Figure 2-10).

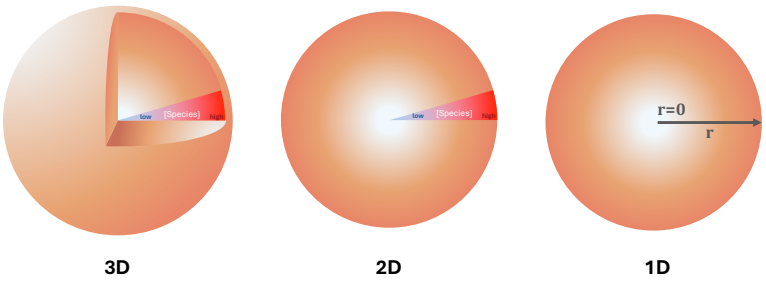

Figure 2-10 From a 3D to a simple 1D problem.

Still, 2D is often preferred for data visualization, drawing a visual parallel with IF staining of spheroids.

With only the radial component remaining, equation (2.1) then becomes:

$$0 = D\frac{1}{r^2}\frac{\partial}{\partial r}\left(r^2\frac{\partial C}{\partial r}\right) - \frac{qC}{C + K_M} \tag{2.3}$$

To further simplify this equation, the consumption of the species can be considered occurring at the constant rate q. Furthermore, the use of the microwell method is especially useful. Given that a high number of cells are seeded at the same time, the cell aggregate/spheroid bypasses the initial growth phase, and its size reaches a plateau within a few days. Indeed, spheroids generated on chip get denser rather than larger over the course of the first few days. As such, variation of spheroid diameter does not need to be considered within the model [232]. However, it could be argued that this densification changes the value of q, and the model should as such be considered valid only when the maximum density is reached.

Therefore, by integrating twice, equation (2.3) becomes:

$$r^2\frac{\partial C}{\partial r} = \frac{qr^3}{3D} + A \tag{2.4}$$

$$C(r) = \frac{qr^2}{6D} + \frac{A}{r} + B \tag{2.5}$$

A and B are integration constants, and their expressions can be found by setting the boundary conditions of the problem. First, assuming finite concentration at the center of the spheroid leads to $A = 0$ based on equation 2.4. The second boundary serves to link both domains (spheroid and culture medium) by defining $C(r = r_{tot}) = C_0$, leading to $B = C_0 - \frac{qr_{tot}^2}{6D}$. The value for C_0 is generally the oxygen saturation of water (159 mmHg) but can be refined to the exact value of oxygen saturation in culture medium in a 37°C 5% CO_2 incubator (141 mmHg) [233]. Obviously, in the case of a low-O_2 incubator, C_0 would change accordingly.

$$C(r) = C_0 + \frac{q}{6D}(r^2 - r_{tot}^2) \tag{2.6}$$

The radius at which the spheroid would start containing hypoxia can be calculated by solving for $r = r_H$ so that the concentration is equal to the threshold for hypoxia $C(r) = C_H$, defined as total absence of oxygen, the Michaelis-Menten constant itself or the 10 mmHg (1.3% pO_2) threshold for CAIX expression.

This approach was used by Astolfi et al. and Rousset et al. to define limits for on-chip MDT and spheroid size, with the calculation being easily solved by hand. This limit is generally around 210 µm of radius, and can vary slightly depending on the cell type [46], [227].

In 1955, a similar approach was taken by Thomlinson and Gray in their seminal paper on modelling of tumor cells oxygen consumption based on histological data [4]. Their histological criterion was necrosis instead of hypoxia staining, assuming total absence of oxygen instead of a defined concentration, and the pattern of necrosis within their tumor samples led them to use cylindrical coordinate system instead of spherical coordinates. Still, the symmetry of the problem leads to a 1D/steady-state simplification of the governing equation, leading to a critical radius of 145 µm.

More recently, Grimes et al. calculated a theoretical hypoxic radius using the previously described approximations, and compared it to EF5-stained slices of tumor spheroids of varying sizes [47]. EF5 binding occurs at 10 mmHg, giving them spatial information on hypoxia content and a reference point for future oxygen concentration modeling. Although their purpose was to use this approach to estimate oxygen consumption rate of an individual cell, their framework experimentally validated the formula for hypoxic content of a tumor spheroid as a function of its size.

Finally, similarly to O_2, glucose consumption can be modeled using the equation 2.1. However, contrary to O_2, glucose is not replenished, and we cannot use the steady state approximation. Therefore, the concentration of such nutrients must be computed with a Multiphysics simulation software such as COMSOL Multiphysics®. Still, Rousset et al. demonstrated that based on the volumes of various microfluidic channels and the number of cells within the devices, medium should be changed every 24h to ensure that glucose levels remain above threshold without perifusion. Similarly, Dorrigiv et al. showcased the glucose uptake of MDTs and tissue slices over the course of 24 h, again confirming the need for daily media change.

2.5.1.6 General Framework for Hypoxic Spheroid Generation

Going back to equation 2.6 and to Grimes et al.'s observations: if one wanted to purposefully generate a hypoxic spheroid, its size should simply be increased to above the theoretical hypoxia radius threshold, $r_{critic} = 210$ for Astolfi et al. or, $211\ \mu m < r_{critic} < 255\ \mu m$ for Grimes et al. Therefore, a spheroid should theoretically be of ~ 450 µm of diameter to observe few cells under hypoxia. As shown by Grimes et al., this criterion can be used to derive a theoretical formula to select the target size of a spheroid to yield a given hypoxic content.

From equation 2.6 we can get the formula for the radial depth as a function of local oxygen concentration:

$$r = \sqrt{r_{tot}^2 + \frac{6D(C(r) - C_0)}{q}} \tag{2.7}$$

If we set C(r) = C_H = 10 mmHg, we can calculate:

$$r_H = \sqrt{r_{tot}^2 + \frac{6D(C_H - C_0)}{q}} \tag{2.8}$$

With r_{tot} the total radius of the spheroid and r_H the radius of the hypoxic region.

If we then set an arbitrary criterion of α so that $\alpha = \frac{r_H}{r_{tot}}$, we get:

$$r_{tot} = \sqrt{\frac{6D(C_0 - C_H)}{q(1 - \alpha^2)}} \tag{2.9}$$

For visualization and for experimental purposes, the α criterion can be very simply adapted to the second dimension, i.e. a slice of spheroid, or the third, i.e. the volume of the spheroid:

$$\beta = \frac{A_H}{A_{tot}} = \alpha^2 \tag{2.10}$$

$$\gamma = \frac{V_H}{V_{tot}} = \alpha^3 \tag{2.11}$$

For example, if β = 0.5, α = 0.70, we get r_{tot} = 700 μm if we use critical radius data (~ 210 μm) from Astolfi et al. and Grimes et al. However, if we use the histological data for normoxic radius (~ 150 μm) from Thomlinson and Gray and Grimes et al., we get r_{tot} = 450 μm.

This difference of radius demonstrates the limits of theoretical approximations and the usefulness of more complex finite-element modeling of oxygen consumption, notably by taking the Michaelis-Menten kinetics into account. Still, these calculations provide guidance for experimental purposes and microfluidic chip design. Once again, the microwell method comes to our aid: experimentally adjusting spheroid size simply requires adjusting cell seeding concentration and well dimensions. The generation of incrementally larger spheroids based on theoretical calculations should predictably yield spheroids of gradually higher hypoxic content, CQFD.

2.6 Literature Review: Take Home Message

Throughout this review, I described how hypoxia is a complex biological phenomenon that greatly impacts cancer patients by negatively impact their prognosis, notably by reducing the efficacy of all anti-cancer treatments. STS is a perfect case study for tumor hypoxia and its impact, with no current treatment targeting or counteracting hypoxia being clinically-available. Therefore, it is of the utmost importance to study hypoxia and its impact on cancer and anti-cancer treatment at the fundamental and preclinical levels, to develop efficient treatment strategies that take hypoxia into account.

As I have shown, there is an apparent lack of user-friendly preclinical tools to study hypoxia and its impact on anti-cancer treatments in a clinically-relevant fashion. The current landscape of preclinical tools to study hypoxia are either animal models, highly variable and low throughput, or *in vitro*/*ex vivo* models for which hypoxia must be artificially induced. Despite the many advantages of microfluidics for cancer research, researchers must still resort to artificial induction of hypoxia, which does not recapitulate its clinical hallmarks. In addition, most experimental setups are cumbersome, complex, hard to use and prone to uncontrolled biases. This explains, in part, why none of these methods are broadly adopted by the translational cancer research community, slowing down important research to improve cancer patient outcomes.

By harnessing elements from microfluidics, 3D biology, physics, biochemistry and engineering, one can derive general principles for user-friendly on-chip generation and culture of tumor spheroids of predictable size and hypoxic content.

CHAPTER 3 Research Rationale, Main Goal and Objectives

Based on the observation that microfluidics has major advantages for 3D culture that were not properly exploited for the study of hypoxia, my Ph.D project focused on bridging the gap between clinically-relevant hypoxia research and user-friendliness. Providing researchers with a versatile tool to integrate hypoxia to any and all fundamental and preclinical cancer research avenues would address the current unmet need in the field in a timely fashion given the recent FDA Modernization Act 2.0 and the new implemented measures by the EMA.

Therefore, my overarching goal is to provide a user-friendly and robust tool to study hypoxia at the fundamental and preclinical level for translational cancer research. Based on the literature review I defined a set of specifications that my design would need to meet.

Project name

Hypoxic-Core Spheroid on a Chip

Overview

The main goal of this project is to provide a user-friendly and robust tool to easily integrate hypoxia to preclinical cancer research pipelines.

Objectives

1. Engineer a compact, user-friendly and efficient microfluidic device for the culture of large tumor spheroids.
2. Demonstrate that large tumor spheroids on chip are naturally hypoxic, and respond to oxygen-dependent treatment accordingly.
3. Demonstrate that hypoxic-core spheroids recapitulate key hallmarks of clinical hypoxia on-chip

3.1 Hypoxic-Core Spheroid on-Chip: Proof of Concept

Objective 1: Engineer a compact, user-friendly and efficient microfluidic device for the culture of large tumor spheroids.

Specifications Sheet of Objective 1

Requirements	♦ The chip must have a straightforward user-friendly design ♦ The chip must have a straightforward manufacturing ♦ The chip must be compatible with a multichannel pipette ♦ The chip must be Autoclavable, biocompatible ♦ The chip must generate spheroids larger than 450 µm of diameter ♦ Larger spheroids naturally express hypoxia
Technical Specifications	♦ Chip must be made of PDMS to ensure constant supply of oxygen ♦ Chip must be made through soft lithography ♦ Mold must either be 3D-printed with Asiga MAX X27 or micromachined from a PMMA slab with Modela MDX-40A 3D Milling Machine ♦ Microfluidic chip must not be perfused or perifused ♦ Chip must contain multiple spheroids (at least 5) to ensure biological reproducibility ♦ Spheroids must be dense ♦ Spheroid diameter must be larger than 450 µm ♦ Spheroids must be generated in less than a week to be competitive to plate-based method ♦ Chip channel must contain enough culture media to ensure sufficient nutrients and metabolites to sustain multiple spheroids over 24 h ♦ Spheroid must be positive for hypoxia-related gold standard proteins (e.g., CAIX, HIF-1α) or known hypoxia marker (e.g., pimonidazole, EF-5: a nitroimidazole derivative)
Issues and Concerns	♦ Some cell lines might not form spheroids ♦ Spheroid might not be larger than 450 µm using the microwell technique ♦ There might not be enough nutrients and metabolites in the culture media to sustain culture of multiple spheroids larger than 450 µm over 24 h

	♦ Spheroids larger than 450 µm might still be negative for hypoxia-related gold standard proteins known hypoxia marker ♦ Positive controls of hypoxia might inaccurately represent controls for hypoxia
Assumptions	♦ Microwell technique allows generation of size-controlled spheroids ♦ Spheroid size is a function of well dimensions and cell seeding concentration ♦ Spheroids with a diameter < 450 µm do not exhibit hypoxia ♦ Spheroids with a diameter > 450 µm should exhibit hypoxia ♦ Spheroids with a diameter > 900 µm should exhibit ~50 % of hypoxia on the central slice ♦ Glucose concentration in culture medium is sufficient to sustain ~900 µm spheroids over 24 h
Out of Scope	♦ Investigation of treatment response

3.2 Hypoxic-Core Spheroid on-Chip: Validation of Hypoxia

Objective 2: Demonstrate that large tumor spheroids on chip are naturally hypoxic, and respond to oxygen-dependent treatment accordingly.

Specifications Sheet of Objective 2

Requirements	♦ The chip must generate naturally hypoxic spheroids from multiple cell lines ♦ Establish a finite-element model of oxygen concentration within the naturally hypoxic spheroids to corroborate experimental data and previously-published models ♦ The chip must be radiocompatible ♦ The chip must be compatible with research center cabinet irradiator (GammaCell irradiator) ♦ Convince biologists that spheroids can naturally exhibit hypoxia without the use of artificial methods of induction
Technical Specifications	♦ Chip must be made of PDMS to ensure constant supply of oxygen ♦ Chip must be made through soft lithography ♦ Mold must either be micromachined from a PMMA slab with Modela MDX-40A 3D Milling Machine to ensure absence of chip defects ♦ Microfluidic chip must not be perfused or perifused ♦ Chip must contain multiple spheroids (at least 15) to ensure biological reproducibility and sufficient biological material ♦ At least 2 cell lines must be used to generated naturally hypoxic spheroids ♦ Spheroids must be dense ♦ Spheroid diameter must theoretically be larger than 900 µm to ensure that ~ 50 % of the cross-section area is hypoxic ♦ Spheroid must be positive for 2 hypoxia-related gold standard proteins: CAIX and HIF-1α ♦ Spheroid must be radioresistant ♦ Spheroid must be sensitive to known HAPs (e.g, TPZ, evofosfamide)
Issues and Concerns	♦ Theoretical criterion for 900 µm spheroids might experimentally yield more or less than ~50 % of their cross-section area

	♦ 50 % of the cross-section area only represent ~30 % of spheroid volume and might not be enough to observe relevant biological effects ♦ Spheroids might not express both CAIX and HIF-1α ♦ Spheroids might not be radioresistant ♦ Spheroids might not respond to HAPs as expected ♦ Positive controls of hypoxia might inaccurately represent controls for hypoxia ♦ Positive controls cannot be properly treated with RT or HAPs due to reoxygenation, therefore generating unwanted biases
Assumptions	♦ Microwell technique allows generation of size-controlled spheroids ♦ Spheroid size is a function of well dimensions and cell seeding concentration ♦ Spheroids with a diameter < 450 µm do not exhibit hypoxia ♦ Spheroids with a diameter > 450 µm should exhibit hypoxia ♦ Spheroids with a diameter > 900 µm should exhibit ~50 % of hypoxia on the central slice ♦ Glucose concentration in culture medium is sufficient to sustain ~900 µm spheroids over 24 h
Out of Scope	♦ Investigation of other hypoxia-related genes ♦ Investigation of chemoresistance ♦ Investigation of aggressivity ♦ Investigation of immunoresistance

3.3 Hypoxic-Core Spheroid on-Chip: Characterization of Hallmarks of Hypoxia

Objective 3: Demonstrate that hypoxic-core spheroids recapitulate key hallmarks of clinical hypoxia on-chip.

Specifications Sheet of Objective 3

Requirements	♦ The chip must follow identical requirements to objectives 1 and 2 ♦ Larger HyCo spheroids must exhibit hallmarks of clinical hypoxia ♦ Convince biologists that spheroids can naturally exhibit hypoxia (without the use of artificial methods of induction) using standard and robust bioassays
Technical Specifications	♦ Chip must be made of PDMS to ensure constant supply of oxygen ♦ Chip must be made through soft lithography ♦ Microfluidic chip must not be perfused or perifused ♦ Chip must contain multiple spheroids (at least 15) to ensure biological reproducibility and sufficient biological material ♦ At least 2 cell lines must be used to generated naturally hypoxic spheroids ♦ Spheroids must be dense ♦ Spheroids diameter must theoretically be larger than 900 µm to ensure that ~ 50 % of the cross-section area is hypoxic ♦ Spheroids must be positive for 2 hypoxia-related gold standard proteins: CAIX and HIF-1α ♦ Spheroids must express known downstream target genes of hypoxia ♦ Spheroids must be radioresistant ♦ Spheroids must be chemoresistant ♦ Spheroids must exhibit a more aggressive phenotype ♦ Spheroids must have a different phenotype to that of smaller normoxic spheroids ♦ Must use standard and robust bioassays (PCR, RNAseq, clonogenic assay, etc.)
Issues and Concerns	♦ 900 µm spheroids might not exhibit hypoxia in ~50 % of their cross-section area ♦ 50 % of the cross-section area only represent ~30 % of spheroid volume and might not be enough to observe biological effects

	♦ Spheroids might not be radioresistant ♦ Spheroids might not chemoresistant ♦ Spheroids might not express both CAIX and HIF-1α ♦ Spheroids might not express known downstream target genes of hypoxia ♦ Naturally hypoxic spheroids might not have a significantly different phenotype to that of smaller normoxic one ♦ Assays performed might still be insufficient to convince potential users of the robustness of naturally hypoxic spheroid on chip ♦ Use of microfluidics might be a barrier to the adoption of the device as microfluidics has yet to be standardized
Assumptions	♦ Microwell technique allows generation of size-controlled spheroids ♦ Spheroid size is a function of well dimensions and cell seeding concentration ♦ Spheroids with a diameter < 450 µm do not exhibit hypoxia ♦ Spheroids with a diameter > 450 µm should exhibit hypoxia ♦ Spheroids with a diameter > 900 µm should exhibit ~50 % of hypoxia on the central slice ♦ Glucose concentration in culture medium is sufficient to sustain ~900 µm spheroids over 24 h
Out of Scope	♦ Investigation of immunoresistance

3.4 SWOT Analysis

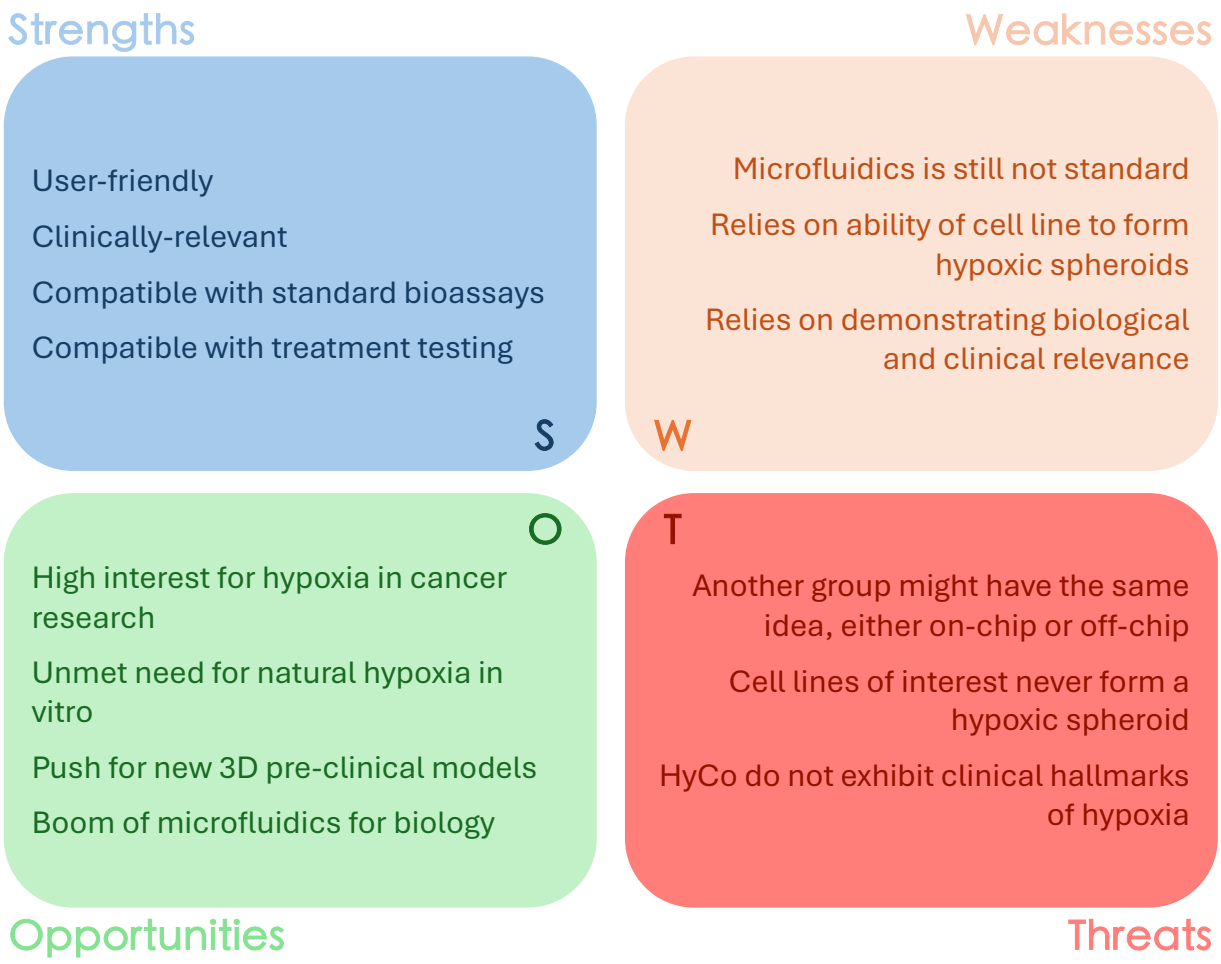

Figure 3-1 SWOT Analysis of Hypoxic-Core Spheroids on a Chip

CHAPTER 4 ARTICLE 1: HYPOXIC JUMBO SPHEROIDS ON-A-CHIP (HONACHIP): INSIGHTS INTO TREATMENT EFFICACY

4.1 Background Information and author contributions

This chapter presents my 1st published article, which showcases the microfluidic chip, the generation of large "jumbo" spheroid naturally exhibiting a hypoxic core, and their use to investigate treatment synergies. This paper establishes the basis of my work: the design of the chip, the method for the generation of large spheroids and how to apply this method to test different treatment combinations. As STSs is a case study of hypoxia, I used 2 STSs cell lines: one commercial and one patient-derived. In this publication, I demonstrate how "jumbo" spheroids express significantly more hypoxia-related gold standard protein compared to smaller normoxic ones. Based on these results we designed a finite element model of oxygen consumption as a function of spheroid size. Then, as a proof of application of the microfluidic chip, spheroids were exposed to both TPZ, a hypoxia prodrug, and RT. Finally, we discussed the limitations and the work that still has to be done to prove that "jumbo" spheroids are indeed expressing clinical hallmarks of hypoxia.

As a first author, I contributed to about 90 % of this article. I designed and manufactured the microfluidic chips. Although Ouafa Najyb, Audrey Glory and Julie Lafontaine trained me to do all bioassays, I did all the experiments myself once trained. Rodin Chermat helped me with the design of the *in silico* model and with data analysis. I did all the statistical analysis, wrote the paper and designed the figures. Audrey Glory, Ouafa Najyb, Rodin Chermat and Julie Lafontaine guided me in the design of the study and the revision of the manuscript. Thomas Gervais and Philip Wong provided support and supervised the research. All authors have reviewed the article and agree with these contributions.

The article was submitted on July 8th, 2021, and accepted on August 6th, 2021 in Cancers, volume 13, issue 16 [Special Issue Modeling Cancer in Microfluidic Chips)], article number 4046. The article is reproduced from [33] under an open access Creative Common CC BY license (CC BY 4.0).

4.2 Authors and Affiliations

Elena Refet-Mollof [1,2], Ouafa Najyb [2], Rodin Chermat [1,2], Audrey Glory [2], Julie Lafontaine [2], Philip Wong [2,3,4,5,*], and Thomas Gervais [1,2,6,*]

[1], Insitute of Biomedical Engineering, Polytechnique Montréal, 2500 Chemin de Polytechnique, Montréal, QC H3T 1J4, Canada

[2], Institut du Cancer de Montréal, (ICM), Centre de Recherche du Centre Hospitalier de l'Université de Montréal (CRCHUM), 900 St. Denis Street, Montréal, QC H2X 0A9, Canada

[3], Department of Radiation Oncology, Centre Hospitalier de l'Université de Montréal (CHUM), 1051 Sanguinet Street, Montréal, QC H2X 3E4, Canada

[4], Department of Radiation Oncology, Princess Margaret Cancer Centre, 610 University Avenue, Toronto, ON M5G 2M9, Canada

[5], Department of Radiation Oncology, University of Toronto, 149 College Street, Suite 504, Toronto, ON M5T 1P5, Canada

[6], Department of Engineering Physics, Polytechnique Montréal, 2500 Chemin de Polytechnique, Montréal, QC H3T 1J4, Canada

***** Correspondence: philip.wong@rmp.uhn.ca (P.W.); thomas.gervais@polymtl.ca (T.G.)

4.3 Simple Summary

Hypoxia is found in half of the solid cancers and is a major contributor to treatment resistance and promotion of metastasis, leading to shortened patient survival. No user-friendly in vitro preclinical tool exists to study natural chronic hypoxia. The aim of this study was to design a microfluidic device allowing easy culture, maintenance, treatment, and analysis of naturally hypoxic sarcoma spheroids. We confirmed that our jumbo spheroids (>750 μm) contained hypoxic cores, as they expressed the hypoxic marker protein Carbonic Anhydrase IX (CAIX). Quantification of DNA strand breaks from radiotherapy and a hypoxia pro-drug demonstrated hypoxia-dependent treatment responses. Our novel microfluidic device is versatile and convenient for both fundamental and preclinical research, to better understand and treat hypoxic tumors.

4.4 Abstract

Hypoxia is a key characteristic of the tumor microenvironment, too rarely considered during drug development due to the lack of a user-friendly method to culture naturally hypoxic 3D tumor models. In this study, we used soft lithography to engineer a microfluidic platform allowing the culture of up to 240 naturally hypoxic tumor spheroids within an 80 mm by 82.5 mm chip. These jumbo spheroids on a chip are the largest to date (>750 μm), and express gold-standard hypoxic protein CAIX at their core only, a feature absent from smaller spheroids of the same cell lines. Using histopathology, we investigated response to combined radiotherapy (RT) and hypoxic prodrug Tirapazamine (TPZ) on our jumbo spheroids produced using two sarcoma cell lines (STS117 and SK-LMS-1). Our results demonstrate that TPZ preferentially targets the hypoxic core (STS117: $p = 0.0009$; SK-LMS-1: $p = 0.0038$), but the spheroids' hypoxic core harbored as much DNA damages 24 h after irradiation as normoxic spheroid cells. These results validate our microfluidic device and jumbo spheroids as potent fundamental and pre-clinical tools for the study of hypoxia and its effects on treatment response.

4.5 Introduction

Hypoxia is found in 50% to 60% of solid cancers and accounts for 19% to 70% of tumor volume [9], [152]. Since the 1950s, hypoxia has been identified as a major contributor to treatment resistance, associated with poor prognosis, metastasis progression and tumor aggressiveness [4], [234], [235]. For example, soft tissue sarcomas (STSs) are prone to forming large and highly hypoxic tumors, leading to increased risk of metastasis [15], [236]. Therefore, investigating combination therapies to target multiple molecular pathways involved in metastasis, such as hypoxia, could potentially improve patient prognosis [237]. The study of hypoxia and its implications on radioresistance have been a topic of interest in fundamental, pre-clinical and clinical research, culminating in 2019 with the Nobel Prize in Physiology or Medicine [64].

In solid tumors, hypoxia is characterized by a lower oxygen concentration than physoxia and appears around 100 µm to 200 µm away from a blood vessel, due to poor and abnormal vasculature [35], [238] (Figure 1). Hypoxia is also characterized by the expression of specific genes and proteins belonging to the Hypoxia Responsive Element (HRE) pathway [1], [5], [91] such as Hypoxia Inducible Factor 1 alpha (HIF1-α) protein and one of its downstream targets, Carbonic Anhydrase IX (CAIX), [1], [9], [130]. Multiple studies demonstrated a correlation between the expression of hypoxia markers such as CAIX and poor prognosis in soft-tissue sarcomas [19], [239], [240], [241].

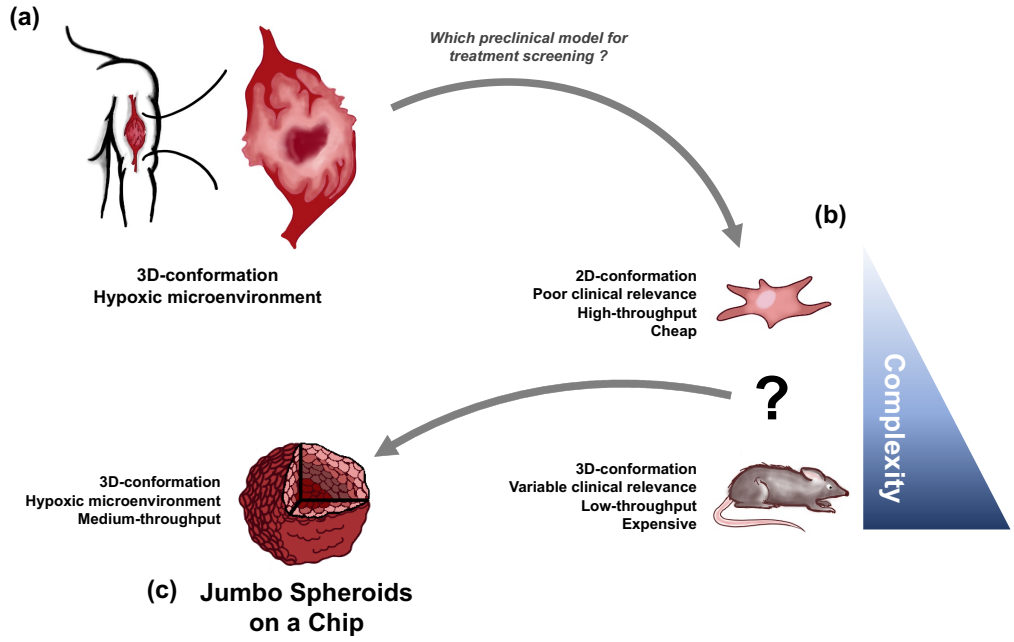

Figure 4-1 Paradigm for HOnAChip

(a) Solid tumors are complex naturally hypoxic 3D-structures. **(b)** Preclinical models of solid tumors fail to easily mimic clinically-relevant characteristics of solid tumors. **(c)** HOnAChip jumbo spheroids are easily-produced naturally hypoxic tumor spheroids, in a microfluidic device compatible with drug testing, radiotherapy and bioanalysis.

The efficacy of radiotherapy (RT) is directly linked to hypoxia as oxygen is required to permanently fix DNA damages caused by RT-induced radical species [9], [242]. This leads to an oxygen enhancement ratio (OER) of 2–3:1, meaning that there are 2 to 3 times less radiobiological effects in hypoxic cells than in normoxic ones [62]. Moreover, chemoresistance arises from the inability of the abnormal vasculature to properly deliver therapeutic agents to the hypoxic core [1], [9]. Finally, hypoxia fosters immunoresistance as immune cells cannot survive in the highly acidic hypoxic microenvironment [12], [243], [244], [245].

Tirapazamine (TPZ, SR-4233), a non-toxic prodrug, was discovered and developed by Brown and Lee in 1986 as an alternative chemotherapy and is one of the first compounds to specifically target hypoxic cells [31]. Activation of TPZ, enabled by local absence of oxygen, results in the production of free radical species and subsequent topoisomerase II-mediated induction of double-strand DNA breaks [31], [246]. By acting as a complementary cytotoxin and selectively killing hypoxic cells, the most radioresistant cells in tumors, TPZ enhances the antitumor effects of radiation [9]. Nevertheless, TPZ, as with other hypoxic prodrugs or HIF-targeting agents, failed to translate to clinical improvement [32]. Few drugs in development take hypoxia into account, in part due to the lack of solid user-friendly translational models on which one can study hypoxia and its effects on drugs and RT [8], [9], [247]. Therefore, there is an unmet need to study the biology of hypoxia at a fundamental and translational level in order to develop better treatment modalities [41].

As of today, no preclinical *in vitro* tool exists to study hypoxia without artificially inducing it, either with a hypoxic chamber, low O_2 incubator, chemical such as cobalt chloride ($CoCl_2$) or other HIF-1 alpha inhibitors [35], [39], [41], [233]. Artificially inducing hypoxia can present many challenges regarding cell culture and maintaining hypoxia, mainly during treatment or bioanalysis [35], [39], [41]. Furthermore, artificially hypoxic small spheroids do not recapitulate the oxygen gradients found in normal tumors [41].

Microfluidic technologies have enabled the formation of size-controlled 3D cell cultures with medium to high throughput while being less expensive, more reliable, user-friendly, and faster than other 3D cell culture methods or *in vivo* techniques [53], [227], [248], [249]. Indeed, animal models are expensive and time-consuming, making them impractical (and ethically questionable) for the first steps of fundamental knowledge finding and pre-clinical studies (Figure 1). Microfluidic 3D tumor models, also called tumor spheroids, can be treated with RT, chemotherapy or drug combinations directly on a chip while being more relevant than 2D cell culture [41], [53], [227], [248], [250], [251].

It has been reported that spheroids must theoretically have a radius of at least 100 µm to 200 µm, depending on the cell type, to be able to naturally produce gradients of oxygen concentration [35]. However, spheroids must exceed this theoretical threshold to recreate clinically relevant aspects of tumor biology, mainly the coexistence of hypoxic and normoxic cells population in the same structure [41], [163]. Few microfluidic devices allow the culture of spheroids large enough (>500 µm of diameter) to adequately mimic tumor geometry, naturally express hypoxia and be useful for bioanalytical and pharmaceutical purposes [41], [163]. Indeed, spheroid size and density, growth conditions and analytical endpoints have to be taken into careful consideration during the design of a microfluidic chip [41], [163], [252].

In this study we introduce a simple microfluidic tool capable of reliably producing up to 240 tumor spheroids of >750 µm diameter, the largest spheroids produced on chip so far. We demonstrated how naturally hypoxic spheroids can be used to assess the response to oxygen-dependent treatments TPZ and RT. Results are supported by *in silico* modeling of oxygen transport and consumption, spatial distribution of gold-standard hypoxic protein, and treatment response measured by immunostaining down to the core of the spheroids.

4.6 Materials and Methods

4.6.1 Microfluidic Chip

4.6.1.1 Microfluidic Device Fabrication

The top and bottom layers of the chip were cast in polymethyl siloxane (PDMS) Dow SYLGARD 184 Silicone Elastomer Clear (Ellsworth Adhesive, Stoney Creek, ON, Canada) with a 1:10 ratio of Dow SYLGARD 184 curing agent (Dow Corning, Midland, MI, USA). The PDMS-filled molds were placed in a desiccator for 20 min to remove unwanted air bubbles, and then cured at 80 °C for 45 min in a Precision Compact oven (Thermo Fisher Scientific, Saint-Laurent, QC, Canada). Top and bottom layers were unmolded and assembled manually after a 30 s exposure to atmospheric plasma using Enercon plasma gun (Enercon Industries Corporation, Menomonee Falls, WI, USA). Molds fabrication is presented in Appendix A1.

4.6.1.2 Microfluidic Device Preparation for Cell Culture

Once the chips were assembled, they were individually put inside an autoclavable box before being autoclaved. Afterwards, chip channels were successively washed once with isopropanol to remove air bubbles, three times with sterilized deionized water and three times with PEG-PPG-PEG, Pluronic® F-108 (Sigma-Aldrich Canada Co, Oakville, ON, Canada) to prevent attachment of biological material. Prepared devices were incubated for 24 h at 37 °C in 5% CO_2 incubator. Then, chip channels were washed three times with sterilized deionized water and three times with appropriate supplemented culture media before seeding.

4.6.1.3 Cell Culture

4.6.1.3.1 Cell Culture

SK-LMS-1 Human leiomyosarcoma cell line was procured from ATCC (HTB-88, ATCC, Manassas, VA, USA). STS117 Human soft-tissue-sarcoma (STS) primary cell line harboring a loss of function mutation TP53 was derived from patients' primary extremity STS diagnosed as an undifferentiated pleomorphic sarcoma. STS117 cell line was kindly provided by Dr. R. Gladdy (Mount Sinai Hospital, Toronto, ON, Canada) [240]. SK-LMS-1 was cultured in EMEM (Wisent Inc., St-Bruno, QC, Canada), STS117 was cultured in DMEM F12 (Wisent Inc.), both supplemented with 10% Fetal Bovine Serum (FBS) (Gibco, Thermo Fisher Scientific, Saint-Laurent, QC, Canada) and 1% Penicillin–Streptomycin solution (Wisent Inc.).

SK-LMS-1 and STS117 cells were maintained by subculturing at 80% confluency. Briefly, the medium was aspirated, cells were washed with Phosphate Buffer Saline (PBS) (Wisent Inc.) and were trypsinized with 0.025% trypsin EDTA (Wisent Inc.) for 2–3 min at 37 °C. Once cells are detached, supplemented medium was added to stop the enzymatic reaction, and the cell suspension was centrifuged for 5 min at 1500 rpm. The cell pellets were resuspended in the appropriate volume to perform seeding in the microfluidic devices.

4.6.1.3.2 Spheroid Formation

Upon preparation of the microfluidic device, suspended cells were seeded at a concentration of 3 × 10^6 cells/mL. An amount of 200 µL of cell suspension was pipetted in the device thrice in the inlet and thrice in the outlet for homogenization. The medium was then changed every 24 h until spheroid were formed 2 days after seeding. Control spheroids formation and hypoxia induction for control spheroids methods are presented in Appendix A2.

4.6.2 Hypoxic Protein Analysis

4.6.2.1 Western Blot

The top layer of the device was peeled off manually to allow spheroids retrieval. Fifteen spheroids were pipetted into Eppendorf tubes, washed twice with PBS and centrifugated at 2 min^{-1}.g for 2 min. PBS was then removed, and samples were put on ice. Spheroids were then homogenized 3 times 3 s using a sonicator (XL-2000, Misonix, Cole-Parmer Canada Company, Montréal, QC, Canada) in RIPA lysis buffer (Sigma-Aldrich, Louis, MO,USA) supplemented with Phosphatase Inhibitor PhosSTOP (1:1000) (Roche, Sigma-Aldrich) and cOmplete™ Protease Inhibitor Cocktail (1:10,000) (Roche, Sigma-Aldrich) to prevent denaturation. Then samples were centrifugated for 15 min at 13,000 rpm at 4 °C (Biofuge pico, Heraeus, Kendro Laboratory Products, Asheville, NC, USA). Protein concentration was determined by BCA Protein Assay (Bio-Rad Laboratories Ltd, Saint-Laurent, QC, Canada and lysates concentrations were standardized to 1 µg/µL by diluting in 4X Laemmli buffer (Bio-Rad, Hercules, CA, USA) and 100 mM DTT. Before blotting, samples were heated at 100 °C for 7 min. Then, 30 g of cell lysates were loaded in precast gels 4–15% Mini-PROTEAN® TGX™ (Bio-Rad) and transferred onto PVDF membrane (Immobilon-P, Merck Millipore, Sigma-Aldrich). PBST (PBS 1X, 0.1% Tween-20) and 5% skim milk solution was used for blocking.

Membranes were then incubated, at 4 °C overnight, with primary antibody diluted in blocking buffer; 1:750 rabbit anti-HIF1-α (ab179483, Abcam, Waltham, MA, USA), 1:2000 rabbit anti-CAIX (ab15086, Abcam, USA) and 1:20,000 mouse anti β-actin (A-5441, Sigma-Aldrich). After washing with PBST buffer, membranes were incubated 1 h at room temperature in HRP (CellSignaling, Withby, ON, Canada) diluted in blocking buffer. Then, membranes were rinsed, incubated for 1 min with SuperSignal™ West Pico PLUS Chemiluminescent Substrate (ThermoFisher Scientific, Waltham, MA, USA) and imaged on Bio-Rad ChemiDoc MP Imaging system (Bio-Rad). Chemiluminescent intensities were measured and HIF1-α and CAIX levels were normalized by β-actin levels to eliminate influence of loading differences. The ratios were then normalized to the positive control.

4.6.3 Immunofluorescence

Two days after seeding or 24 h after treatment, spheroids were washed 3 times with PBS directly in the device and fixed with Formalin 10% (Fisher Scientific Company, Toronto, ON, Canada) for 45 min. Then, spheroids were washed 5 times with PBS, the top layer of the chip was peeled off to proceed to inclusion of 5 spheroids in optical cutting compound OCT (Leica, Buffalo Grove, IL, USA). Included samples were left overnight to sediment, thereby insuring homogeneous z-levels across samples. Afterwards, included samples are frozen on dry ice and stored at −80 °C. Frozen samples were sectioned using Leica Cryostat (Leica, Buffalo Grove, IL, USA) with a 5 µm thickness at −20 °C. Sections were incubated for 1 h at room temperature with blocking buffer (PBS 1X, 3% IgG-free, Protease-free BSA, 0.5% Triton 100 10X). Sections were then incubated in blocking buffer with rabbit anti-CAIX (1:1000) (PA1-16592, ThermoFisher Scientific, Waltham, MA, USA) and mouse anti-γH2AX (1:250) (05-636, EMP Millipore) overnight at 4 °C. After washing 3 times with PBS, sections were incubated in secondary antibody buffer (PBS 1X, 3% BSA) with AlexaFluor-647 antibody (1:750) (A31573, Invitrogen, USA) and AlexaFluor-488 antibody (1:750) (A31571, Invitrogen, ThermoFisher Scientific, Waltham, MA, USA) for 1 h at room temperature. Afterwards, sections were stained with DAPI (1:5000 from 5 mg/mL stock solution) (D3571, Invitrogen, USA) to stain nuclei. Then, sections were mounted with ProLong™ Gold Antifade Mountant (P36934, Invitrogen, ThermoFisher Scientific, Waltham, MA, USA). Images were obtained on a Zeiss fluorescence microscope with Axio-Vision 4.0 software (Carl Zeiss AG, Jena, Germany). Images were analyzed using ImageJ (ImageJ, Fiji General Public License). Image analysis is described in Appendix A3.

4.6.4 In silico Modeling of Oxygen Consumption

A finite element method with the commercial COMSOL Multiphysics® software was used to model the oxygen consumption in our jumbo and small spheroids. A 2D-symmetry approximation was used to draw the spheroids as perfect circles, with a previously estimated mean diameter. Oxygen consumption was defined by a reaction equation with Michaelis–Menten kinetics, using a method derived from Grimes et al. [47]. Briefly, Michaelis–Menten parameters were set for our jumbo spheroids so that CAIX expression threshold of 10 mmHg (0.0126 mM) was crossed at the estimated mean depth of hypoxic region. After adjusting the oxygen consumption rates for size, the model was then applied to small spheroids. Michaelis–Menten constant was set at 4.63×10^{-3} mol/m^3 [227]. Oxygen consumption rates applied to the models can be found in Table 1.

Table 4-1 Parameters used in the oxygen consumption in silico model

Spheroids	Oxygen Consumption Rate [mol/.s]
SKLMS1 jumbo	3.65×10^{-2}
STS117 jumbo	4.07×10^{-2}
SKLMS1 small	2.61×10^{-2}
STS117 small	2.33×10^{-2}

4.6.5 Treatment Modalities

4.6.5.1 Tirapazamine (TPZ)

Serial dilution of Tirapazamine (SML0552, Sigma; dissolved in DMSO at 50 mM) in proper culture media was performed to reach desired concentration of 10 µM and 35 µM (a dose within the range used in human trial [32]) (control: culture media, 1:1500 DMSO). Treatment with TPZ was performed 2 days after seeding by pipetting 5 × 200 µL in each channel to ensure homogeneity. Then, devices were incubated for 24 h at 37 °C in 5% CO_2 incubator.

4.6.5.2 Conventional Radiotherapy

Two days after seeding, fresh media were added to each channel before irradiation of spheroids directly on chip using the Gammacell 3000 irradiator (Best Theratronics, Ottawa, ON, Canada) at defined doses (0, 2, 4 and 8 Gy).

4.6.5.3 Combination Therapy

Combination of TPZ and radiation therapy was performed directly on a chip. Spheroids were irradiated 2 days after seeding at 0, 2, 4 or 8 Gy, then treated with either 0, 10 or 35 µM of TPZ and incubated for 24 h at 37 °C in 5% CO_2 incubator. Then, spheroids were retrieved 24 h after treatment and analyzed by IF assay as previously described.

4.6.6 Statistical Analysis

Statistical analysis was conducted using GraphPad Prism (Version 9.0.1, GraphPad, San Diego, CA, USA). Gaussian distribution of SK-LMS-1 and STS117 jumbo spheroids diameter were assessed by performing a Shapiro-Wilk lognormality and normality test. Distribution of samples passed the normality test if $p > 0.05$. For Western blot analysis mean fold changes in proteins in negative control (small-normoxic), positive control (small-hypoxic) and jumbo spheroids were analyzed for significance using an ordinary one-way ANOVA with Tukey's multiple comparisons test. For IF analysis, comparison of γH2AX foci per nuclei area between normoxic and hypoxic region of jumbo spheroids cross-section, when treated with either TPZ or RT alone, were analyzed for significance using an ordinary one-way ANOVA with Šídák's multiple comparisons test. Comparison of γH2AX foci per nuclei area in normoxic and hypoxic region of jumbo spheroids cross-section, when treated with a combination of TPZ and RT, were analyzed for significance using an ordinary one-way ANOVA with Tukey's multiple comparisons test.

4.7 Results

4.7.1 The Microfluidic Chip Allows Formation of Size-Controlled Jumbo Spheroids

The microfluidic chip consists of 16 independent channels, each containing 15 wells allowing formation of one jumbo spheroid each (Figure 2a). Hexagonal-shape wells were chosen to optimize the number and volume of wells per channel (Figure 2a). Final dimensions for the wells are 1.6 mm for the inscribed diameter and a depth of 1.2 mm. The chip was optimized to be the same dimension as a 96-well plate, as well as being compatible with an 8-channels multipipette and for each channel to fit in a histology cassette. In comparison with a 96-well plate, this microfluidic chip allows the formation of 240 jumbo spheroids, i.e., 3 times more spheroids per mm2, while using 2 times less reagent than in standard protocols [253]. In addition, this chip is optically translucent, allowing imaging of spheroids with brightfield microscopy, and can be cut with a scalpel or a razor blade for experimental purposes (Figure 2b). Sterilization of the chip can be performed using a standard autoclave and the chips can be kept for at least one year after fabrication without alteration of their physicochemical properties.

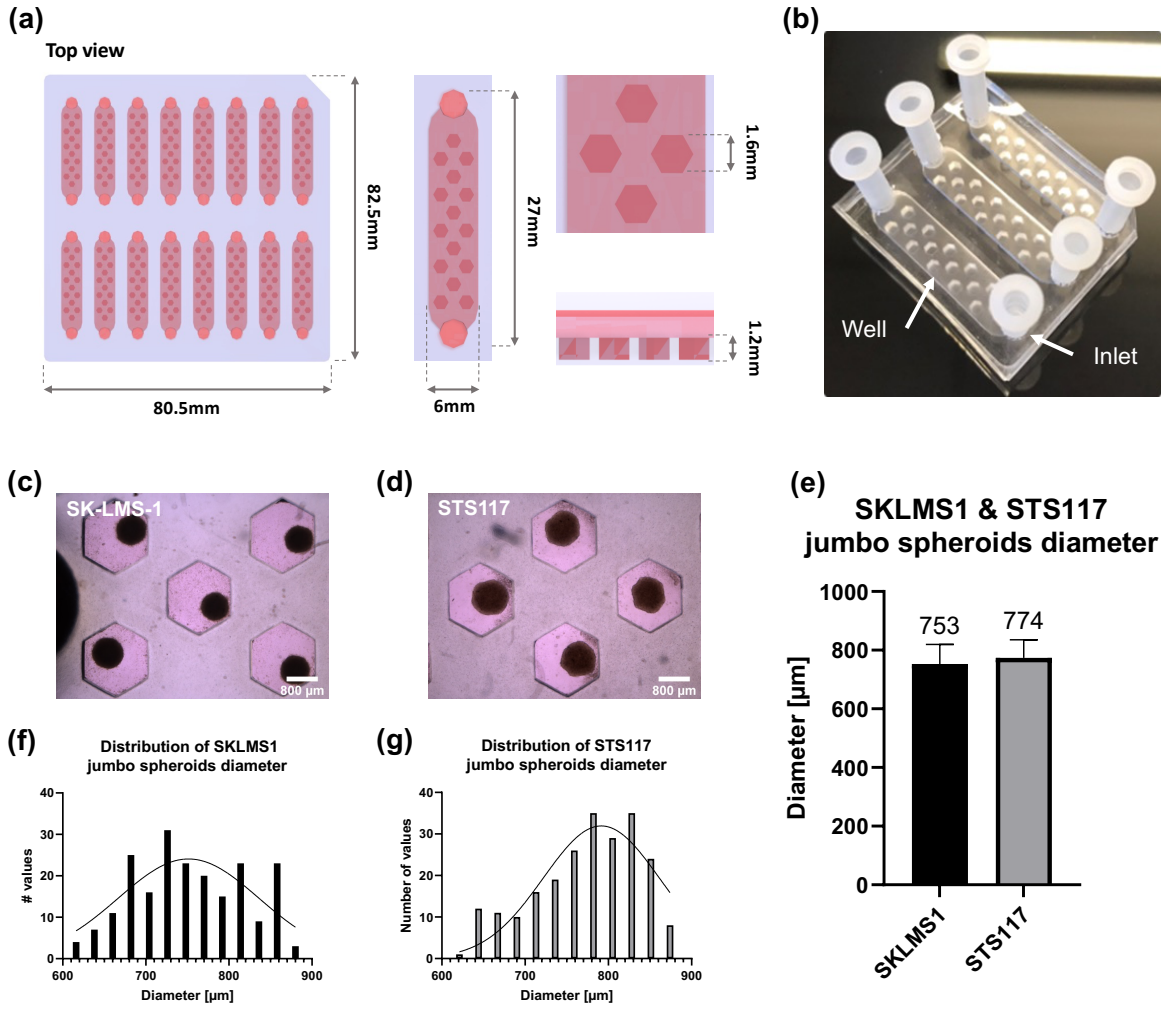

Figure 4-2 Spheroids of 2 sarcoma cell lines are successfully formed 2 days after seeding and present a controlled diameter

(a) 3D-render of assembled chip. (**b)** Image of assembled chip. Plastic inlets are separate from the chip and added for experimental purposes. **(c) (d)** Brightfield image of SK-LMS-1 (c) and STS117 (d) jumbo spheroids 2 days after seeding. (**e).** Mean diameter of SK-LMS-1 and STS117 jumbo spheroids 2 days after seeding. Diameter of SK-LMS-1 spheroids is 753 ± 67 µm, n=210. Diameter of STS117 spheroids is 774 ± 62 µm, n=227. Values are presented as mean ± SD. Results were obtained across more than 3 repetitions. (**f) (g)** Distribution of SK-LMS-1 (f) & STS117 (g) jumbo spheroids diameter. In both cell lines, spheroids diameters follow a Gaussian distribution (SK-LMS-1 : p=0.53, STS117 : p=0.69).

In both cell lines, spheroids are successfully formed 2 days after seeding and present a homogeneous diameter following a gaussian distribution (Figure 2c,d,f,g). SK-LMS-1 jumbo spheroids have a diameter of 753 ± 67 μm and STS117 jumbo spheroids have a diameter of 774 ± 62 μm (Figure 2e).

4.7.2 Presence of Hypoxia in Small vs. Jumbo Spheroids

A high expression of HIF1-α was observed in Western blots of SK-LMS-1 spheroids, regardless of their size (Figures 3a,b and S1). Although there is a high expression of HIF1-α protein in SK-LMS-1 jumbo spheroids, no statistical difference between small-normoxic spheroids (negative control, < 450 μm), small-hypoxic spheroids incubated for 24 h in 2% O2 incubator (positive control, method in Appendix A2) and jumbo spheroids was observed (Figure 3b). In contrast, Western blot analysis for STS117 showed the expected variation in protein levels (Figures 3d,e and S1). STS117 small-hypoxic and jumbo spheroids expressed 2.7 times and 2.3 times more HIF-α, respectively, than small-normoxic ones (Figure 3e). No statistical difference was observed between STS117 jumbo spheroids and small-hypoxic ones.

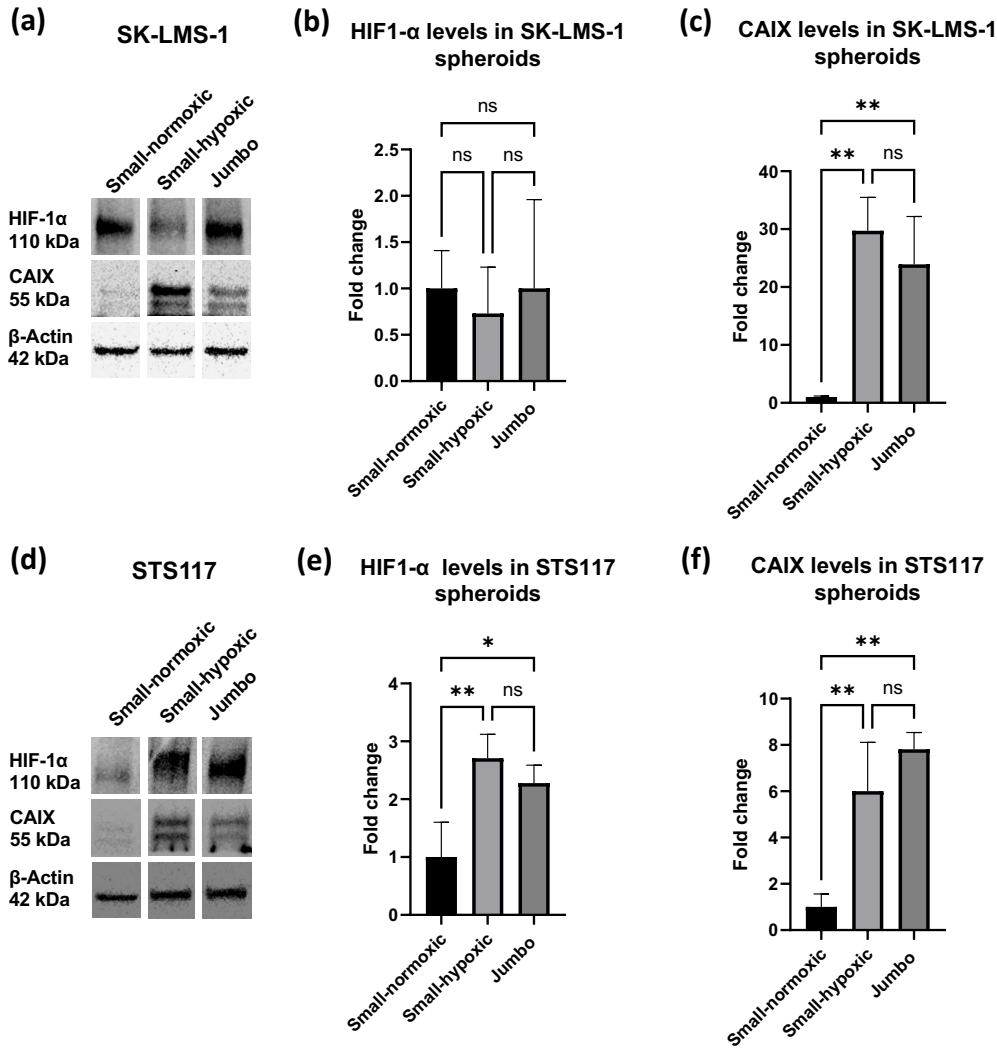

Figure 4-3 In both cell lines, CAIX expression increases significantly in jumbo spheroids, consistent with presence of hypoxia.

(a) (d) CAIX and HIF-1α expression in SK-LMS-1 (a) and STS117 (d) small-normoxic (diameter < 450 μm), small-hypoxic and jumbo (diameter > 750 μm) spheroids. **(b) (e)** Fold change of HIF1-α protein in SK-LMS-1 (b) and STS117 (e) small-normoxic, small-hypoxic and jumbo spheroids (STS117: small-normoxic vs small-hypoxic: p=0.0089; small-normoxic vs jumbo : p=0.0320). **(c) (f)** Fold change of CAIX protein in SK-LMS-1 (c) and STS117 (f) small-normoxic, small-hypoxic and jumbo spheroids (SK-LMS-1: small-normoxic vs small-hypoxic: p=0.0022; small-normoxic vs jumbo : p=0.0069), (STS117: small-normoxic vs small-hypoxic : p=0.0087; small-normoxic vs jumbo : p=0.0018). Values are presented as mean ± SD (standard deviation), N=3 with more than 15 spheroids per repetition, * $p<0.05$, ** $p<0.005$.

CAIX expression levels were consistent with our expectations in both cell-lines, namely a low expression of CAIX in small-normoxic spheroids and a high expression of CAIX in small-hypoxic and jumbo spheroids (Figure 3a–c,f). Indeed, SK-LMS-1 small-hypoxic and jumbo spheroids expressed 30 times and 24 times more CAIX, respectively, than small-normoxic spheroids (Figure 3c). No statistical difference was observed between SK-LMS-1 jumbo spheroids and positive control. Similarly, in STS117, small-hypoxic and jumbo spheroids expressed 6 times and 7.8 times more CAIX, respectively, than small-normoxic spheroids (Figure 3f).

An immunofluorescence assay (IF) was performed to localize the expression of CAIX in small-normoxic, small-hypoxic, and jumbo spheroids cross-section. As expected, in both SK-LMS-1 and STS117, CAIX is localized in the core of the jumbo spheroids (Figure 4a,b). Respectively, 45% of SK-LMS-1 jumbo spheroids cross-section area and 49% of STS117 jumbo spheroids cross section area are CAIX-positive (Figure 4c).

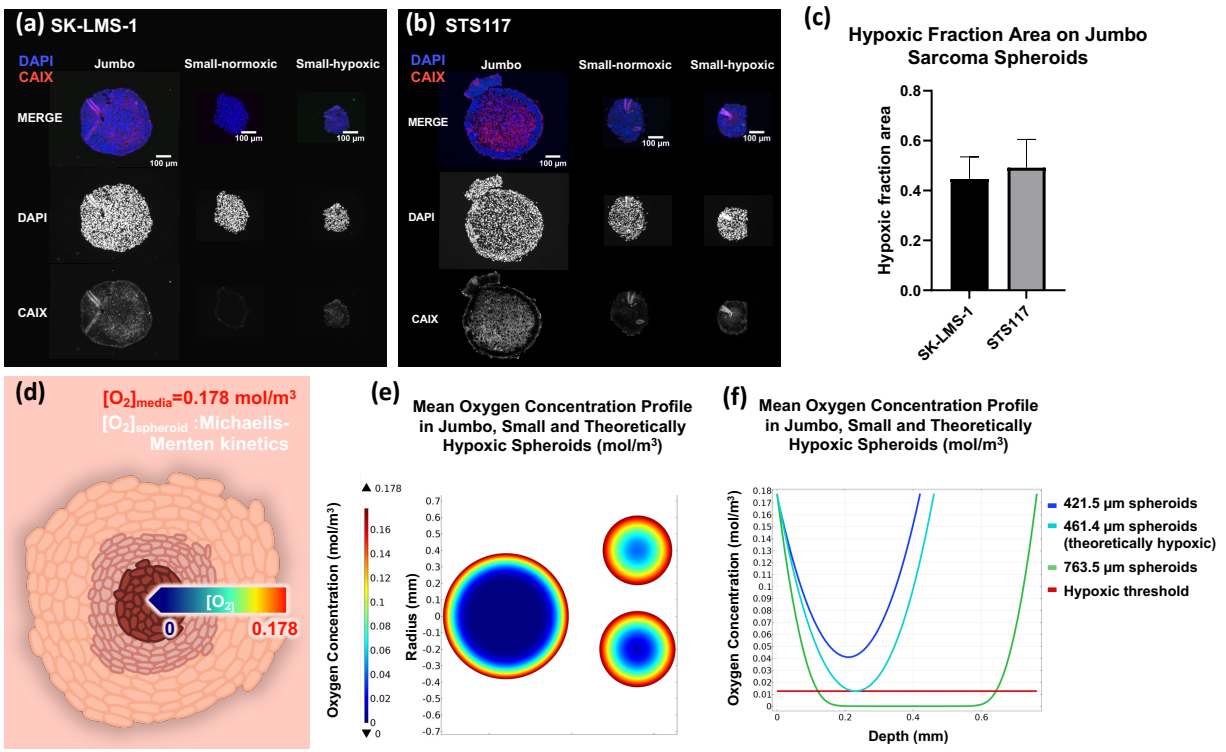

Figure 4-4 Hypoxia is localized in the core of jumbo spheroids at expected depths.

(a) (b) CAIX (red) staining in SK-LMS-1 (a) and STS117 (b) small (normoxic and hypoxic controls) and jumbo spheroids using anti-CAIX antibody. N=3 with more than 3 spheroids per repetition. Scale bar = 100µm. **(c)** Hypoxic fraction area on jumbo sarcoma spheroids. 45 % ± 8.9 % of SK-LMS-1 and 49 % ± 11.4 % of STS117 cross section area express CAIX and is defined as hypoxic area. Resulted are presented as mean ± SD. N=3. **(d)** Schematic of oxygen consumption modelling in jumbo spheroids. Michaelis-Menten parameters for oxygen consumption are derived from CAIX staining. (**e)** Mean oxygen concentration profile in jumbo and small spheroids cross-section. **(f)** Graph of mean oxygen concentration in small, jumbo and theoretically hypoxic spheroids cross-section.

For both cell lines, small-normoxic spheroids expressed significantly less CAIX signal than small-hypoxic ones (Figure A1) CAIX was expressed all over the section of small-hypoxic spheroids, as expected for hypoxia-induced spheroids (Figure 4a,b).

Using the IF results, we calculated the mean depth of hypoxic regions in our jumbo spheroids as:

$$d_h = r \times \left(1 - \sqrt{\frac{A_h}{A}}\right)$$

With the mean hypoxic depth, r the mean total radius, and the hypoxic fraction area in our jumbo spheroids with A_h the CAIX-positive area and A the total area of the spheroid (based on the CAIX expression in the IF). This gave us an estimated hypoxic depth of 120 µm in jumbo spheroids. Given these values, we built a numerical model of oxygen consumption in both our jumbo and small spheroids to understand why small spheroids (<450 µm) did not express CAIX (Figure 4d). As shown in Figure 4e,f, in a model specifically built so that CAIX-expression threshold is crossed at the previously calculated depth, the same threshold is never crossed in smaller spheroids. Using our model, we estimated that STSs spheroids should theoretically be at least 461.4 µm wide for the first cell to cross the hypoxic threshold, confirming the necessity of spheroids larger than 750 µm to have a meaningful number of hypoxic cells.

4.7.3 Evaluation of Treatment Response in Jumbo Spheroids

SK-LMS-1 and STS117 spheroids were treated with RT (0, 2, 4, 8 Gy) and TPZ (0, 10, 35 µM; a dose within the range used in human trial [32]), both of which inflict DNA damages as their main mode of action [1]. As previously stated, TPZ preferentially causes single- and double-DNA strand breaks in hypoxic cells [254]. Therefore, cytotoxicity of TPZ in both SK-LMS-1 and STS117 jumbo spheroids was assessed by quantifying double strand DNA breaks using γH2AX marker by IF. First, we compared the number of γH2AX foci per nuclei area in the CAIX-positive region (hypoxic region) versus CAIX-negative region (normoxic region) of the jumbo spheroids cross-section, in both cell lines, when treated with either TPZ or RT only.

Both SK-LMS-1 and STS117 hypoxic regions show a dose–response relationship to TPZ (Figure 5a,d). Indeed, there is a dose-dependent response in hypoxic regions only, with significant differences between 0 µM and 10 µM for SK-LMS-1, between 10 µM and 35 µM for STS117, and 0 µM and 35 µM for both cell lines (Figure 5b,e). Moreover, at 35 µM there is a significant difference between the hypoxic regions and the normoxic regions, confirming that TPZ induces DNA damages preferentially to hypoxic regions as previously demonstrated in the literature (Figure 5b,e).

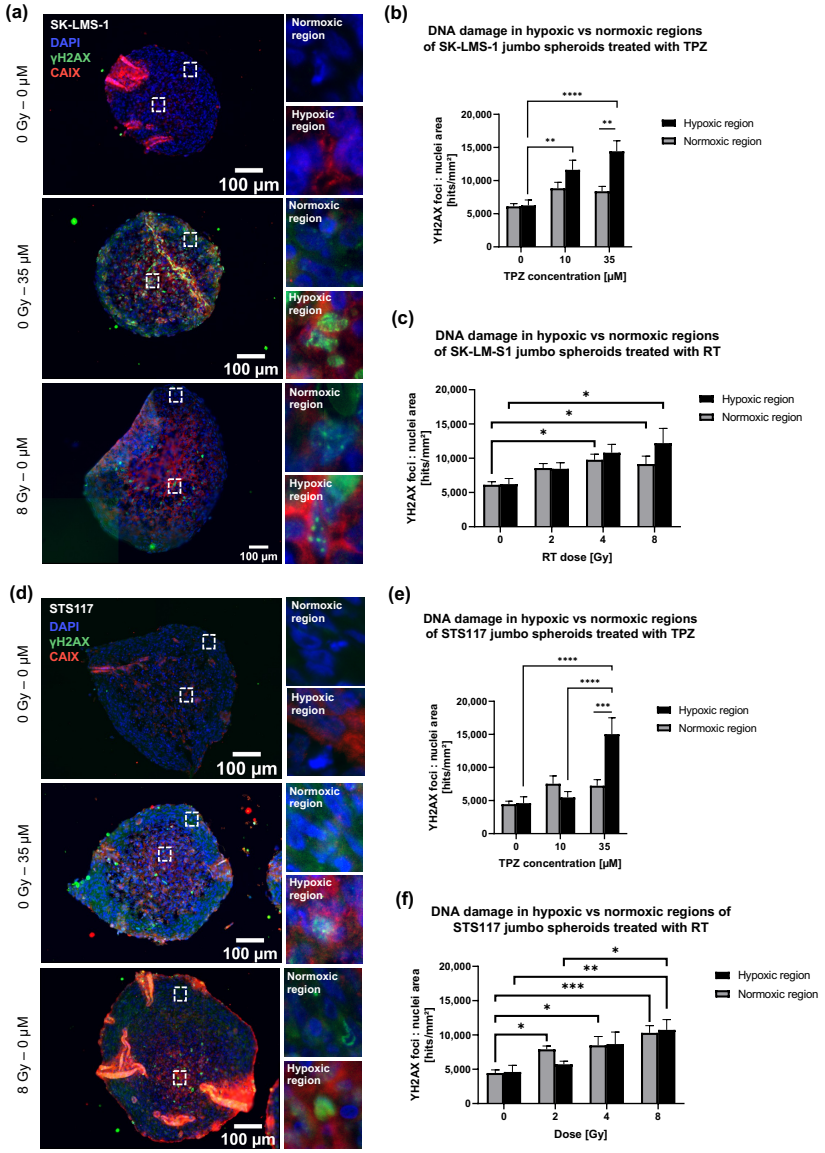

Figure 4-5 Contrary to RT alone treatment with TPZ alone resulted in oxygen-dependent responses.

(a) (d) DNA damages (γH2AX, green), hypoxia (CAIX, red) and nuclei (DAPI, blue) staining in SK-LMS-1 (a) and STS117 (d) jumbo spheroids treated with either 35 UM of TPZ or 8 Gy of RT**. (b) (c) (e) (f)** DNA damages in hypoxic (H) versus normoxic (N) regions of SK-LMS-1 and STS117 jumbo spheroids treated with either TPZ alone (b) (e) or with RT alone (c) (f) (**SK-LMS-1: H:** 0 – 10 µM: p=0.0038, 0 – 35 µM: p<0.0001; **35 µM:** H vs N: p=0.0096), (**STS117: H**: 0 – 35 µM: p<0.0001, 10 – 35 µM: p<0.0001; **35 µM:** H vs N: p=0.0009), (**SK-LMS-1: H:** 0 – 8 Gy: p=0.0157; **N:** 0 – 4 Gy: p=0.0111, 0 – 8 Gy: p=0.043), (**STS117: H**: 0 – 8 Gy: p=0.0076, 2 – 8 Gy: p=0.0429; **N:** 0 – 2 Gy p=0.0387, 0 – 4 Gy: p=0.0125, 0 – 8 Gy: p=0.0002). From γH2AX IF staining foci were counted and normalized per nuclei area. Values are presented as mean ± standard error of the mean (SEM), N=3-4, 2-4 spheroids per repetition, * p<0.05, ** p<0.005, *** p<0.0005, **** p<0.0001.

However, no statistical differences were observed between normoxic and hypoxic regions of STS117 and SK-LMS-1 jumbo spheroids when treated with RT only (Figure 5c,f). The increase in γH2AX foci per nuclei area is dose-dependent in both cell lines regardless of the region. In the absence of TPZ, significant differences are observed in hypoxic regions between 0 Gy and 8 Gy for both cell lines, and 2 Gy and 8 Gy for STS117 (Figure 5c,f). These differences are already observed between 0 Gy and 4 Gy, and 0 Gy and 8 Gy in SK-LMS-1 normoxic regions, and between 0 Gy and 2 Gy, 0 Gy and 4 Gy and, 0 Gy and 8 Gy in STS117 normoxic regions (Figure 5c,f). Despite no significant differences between regions for a given radiation dose, these results could indicate that a higher radiation dose is required to yield significant DNA damages in hypoxic regions than in normoxic regions.

Then, we investigated the combined effects of TPZ and RT and compared the DNA damages in each region separately. For SK-LMS-1, at 10 μM of TPZ, significant differences are observed between 0 Gy and 8 Gy, 2 Gy and 8 Gy, and 4 Gy and 8 Gy in both hypoxic and normoxic regions (Figure 6a,b). For STS117, at 10 μM of TPZ, significant differences are observed only between 0 Gy and 8 Gy in both hypoxic and normoxic regions (Figure 6c,d).

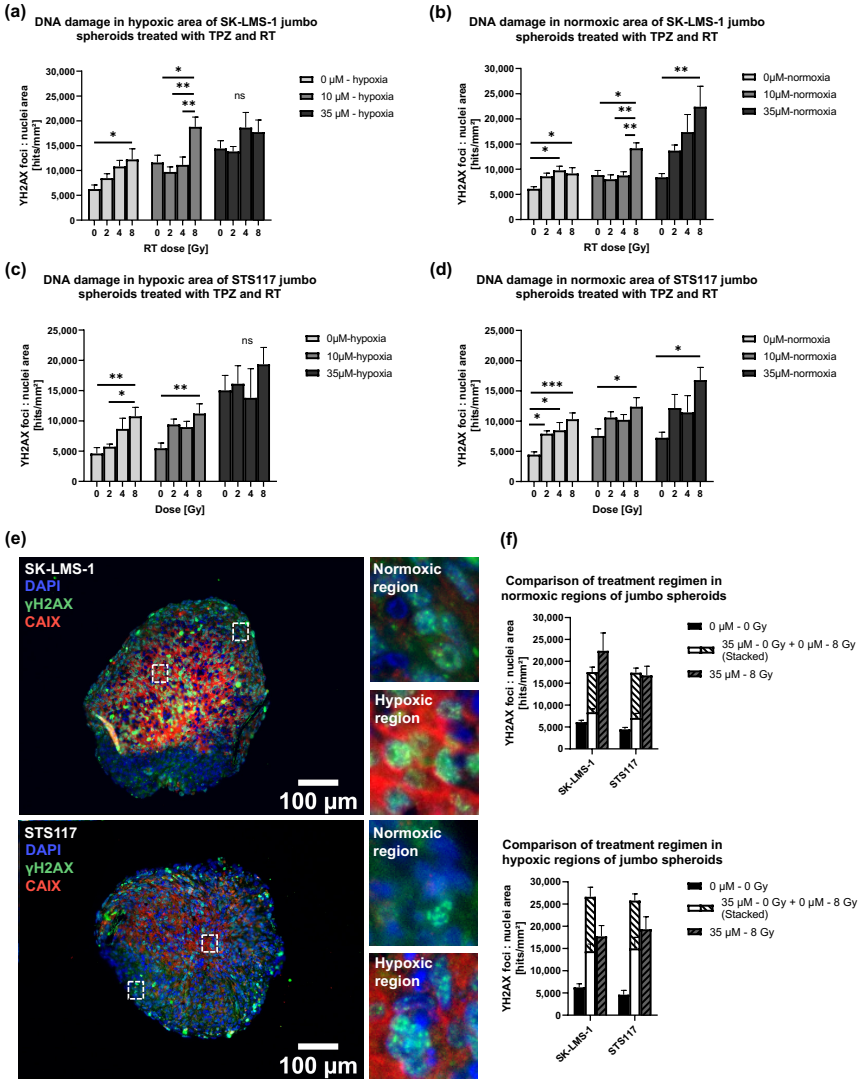

Figure 4-6 Combination of RT and TPZ resulted in oxygen-dependent responses.

(a) (b) (c) (d) DNA damages in hypoxic area (a), (c) and normoxic area (b), (d) of SK-LMS-1 and STS117 jumbo spheroids treated with TPZ and RT, (**SK-LMS-1: H: 10 µM:** 0 – 8 Gy: p=0.018, 2 – 8 Gy: p=0.0023, 4 – 8 Gy: p=0.0076; **N: 10 µM:** 0 – 8 Gy: p=0.0015, 2 – 8Gy: p=0.0003, 4 – 8 Gy: p=0.0008; **N: 35 µM:** 0 – 8 Gy: p=0.0077), (**STS117: H**: **10 µM:** 0 – 8 Gy: p=0.0072; **N: 10 µM:** 0 – 8 Gy: p=0.0294; **N: 35 µM:** 0 – 8 Gy: p=0.0126)**. (e)** DNA damages (γH2AX, green), hypoxia (CAIX, red) and nuclei (DAPI, blue) staining in SK-LMS-1 and STS117 jumbo spheroids treated with 35 µM of TPZ and 8 Gy of RT. **(f)** Comparison of treatment regimen in normoxic of hypoxic regions of jumbo spheroids. From γH2AX IF staining foci were counted and normalized per nuclei area. Values are presented as mean ± standard error of the mean (SEM), N=3-4, 2-4 spheroids per repetition, * $p<0.05$, ** $p<0.005$, *** $p<0.0005$.

In the normoxic regions of both cell lines, at 35 μM of TPZ, RT retains its observed dose-dependent DNA damage increase (Figure 6b,d). Furthermore, for SK-LMS-1 and STS117, combination therapy of 35 μM and 8 Gy appears to yield similar damages than the sum of each condition alone (Figure 6e,f). In the hypoxic regions of both cell lines, there are no significant differences between each RT dose (either 0 Gy, 2 Gy, 4 Gy and 8 Gy) when jumbo spheroids are treated with 35 μM of TPZ (Figure 6a,c). Although the difference is not significant, combination therapy of 35 μM and 8 Gy appears to yield fewer damages than the sum of each condition alone (Figure 6e,f). These results could indicate additive effects of the combination therapy under normoxia, in SK-LMS-1 and STS117, respectively.

4.8 Discussion

Our microfluidic chip allows the formation of up to 240 size-controlled jumbo hypoxic spheroids in 48 h with minimal and user-friendly operation, on which rapid evaluation of treatment combination can be performed. Natural expression of hypoxia in our spheroids alleviates the challenges presented by artificial induction. Indeed, to artificially maintain culture media and cells under low pO_2, nitrogen needs to be injected in the chamber [35], [39]. This leads to a progressive acidification of the culture media, which has been shown to alter drug conformation and possibly inactivate them [1], [40]. Furthermore, studying RT on hypoxic cell cultures would either require for the whole chamber to fit in the irradiator or for the hypoxic environment to be interrupted for the duration of the treatment. Finally, artificial induction of hypoxia does not allow both normoxic and hypoxic regions within the same sample, thus making it less consistent with real tumor microenvironment. Furthermore, compared to hanging drops or spinner flask methods, our chip enables a precise control of spheroid size while being more ergonomic. Control of spheroids size is achieved by the optimization of cell density that needs to be seeded and by the size of the wells [250]. Compared to a 96-well plate, the increased number of samples per condition reduces the amount of reagent required and the experimental variability. Our device allows easy drug delivery, retrieval of samples for standard histopathology or bioanalysis and is fully compatible with RT.

Protein quantitation demonstrated higher levels of gold-standard hypoxic protein CAIX in our jumbo spheroids, illustrating the presence of chronic natural hypoxia without resorting to hypoxic chamber or chemicals. Quantitation of other gold-standard hypoxic protein HIF1-α yielded mixed results depending on the cell line, varying as expected between samples in STS117 but not in SK-LMS-1. As HIF1-α levels are known to vary between cell lines, our failure to correlate HIF1-α expression and hypoxia in SK-LMS-1 could be attributed to previously observed abnormal HIF1-α basal levels [255], [256]. Indeed, SK-LMS-1 exhibits an altered MYC pathway (amplification of *MYCBPAP* and deletion of *MLX* and *MXI1*) which has been shown to drive HIF1-α stabilization under normoxia [62], [257], [258], [259]. As 3D-conformation has been shown to influence gene expression and regulation in tumor cells, investigating *MYC*, *HIF1A*, *VHL* and *PHD* gene expression and relevant miRNAs levels could provide insights into the significance of HIF1-α levels in SK-LMS-1 jumbo spheroids [260]. SK-LMS1 may not be the best sarcoma model, but served to exemplify a model in which a disconnect between HIF1-α and CAIX occurs in the 3D model, which had been observed *in vivo* [261].

Overall, our results in jumbo spheroids indicate that CAIX is a more reliable marker of hypoxia across cell lines, as previously observed clinically [20], [262], [263], [264].

Histopathology analysis showed that CAIX-expressing cells were localized at the center of our jumbo spheroids, at depths similar to those found in the literature, strengthening our claim of natural expression of hypoxia [5]. CAIX/HIF1-α co-staining would have provided meaningful information on protein localization in our jumbo spheroids, especially for SK-LMS-1 as they expressed high level of HIF1-α even in normoxia, but proved extremely arduous and not cost-effective mainly due to the high HIF1-α antibody concentration required for IF [265]. Indeed, studies have highlighted how hazardous IF staining of HIF1-α is, often preferring CAIX or pimonidazole [237], [266], [267], [268]. The CAIX signal displayed at the rim of our jumbo spheroids is attributed, as other staining artifacts, to local folding of sample, and could be reduced by using positively charged glass slides.

Using an in silico model of oxygen consumption derived from IF results of jumbo spheroids, we were able to show that for STS cell lines, observed expression of hypoxia in jumbo spheroids implied an absence of hypoxia in smaller spheroids. This observation highlights how the link between spheroid cellular density and spheroid volume drives the oxygen consumption, hence the expression of hypoxia [99], [269]. Indeed, extremely high cellular density has been shown to upregulate HIF1-α even in 2D cell culture [99]. As the size of jumbo spheroids makes them too small to use microneedle probes, the standard method for pO2 measurements, our model is still limited by the assumption that CAIX begins to be expressed at 10 mmHg [47], [59], [266], [270], [271], [272].

We used our microfluidic device to test combined treatment of jumbo spheroids with conventional RT and widely used hypoxia pro-drug TPZ [32], [273], [274], [275]. As expected, TPZ was preferentially cytotoxic to CAIX-expressing cells in a dose-dependent manner, thereby cementing our spheroids as a naturally hypoxic 3D tumor model [246]. Surprisingly, both hypoxic and normoxic regions of our jumbo spheroids displayed a dose-response effect to RT, contradicting with expected hypoxia-associated radioresistance. A possible explanation could be that, although our spheroids are hypoxic enough to express CAIX, oxygen levels are still high enough to prevent radioresistance.

Indeed, an OER of 2 has been documented to appear below 3 mmHg, which according to our in silico model would only represent a fraction of our hypoxic core (Figure A2) [58]. Therefore, increasing the size of our jumbo spheroids might increase this fraction enough to observe radioresistance. Another explanation could be that 24 h after treatment, the oxygen-dependent DNA-repair in normoxic regions and the accumulation of DNA-damages in hypoxic regions are important enough to cancel out differences between these two regions [62], [276]. We chose to look at γH2AX staining 24 h after treatment, based on the study of Olive et al. [277], which aids in prediction of tumor response to treatment and gives us a better indication on treatment efficacy. As hypoxic cells are known to have impaired DNA-repair and a tendency to accumulate DNA damages, while DNA of normoxic cells can repair themselves more efficiently, investigating γH2AX foci 30 min after irradiation could reveal a potential hidden radioresistance in our jumbo spheroids [276], [277], [278].

Combination of RT and TPZ resulted in oxygen-dependent responses. Under hypoxia, RT loses its dose-response effect when combined with 35 µM of TPZ (a dose within the range used in human trial [32]) but not with 10 µM, suggesting that high concentration of TPZ masks additional effects of RT. However, under normoxia, 35 µM of TPZ increased efficiency of 8 Gy of RT additively for STS117 and SK-LMS-1, as previously observed in preclinical studies [279], [280].

At the clinical level, additional benefits of TPZ combined with RT and other chemotherapeutic agents such as cisplatin and carboplatin have not been demonstrated which could be explained by poor patient-stratification for hypoxia in most of these studies [134], [280]. Our results suggest that repurposing TPZ in combination with RT alone could yield meaningful results in soft tissue sarcoma treatment.

Finally, characterization of jumbo spheroids multilayered structure (presence of senescent, quiescent cell and/or necrotic cells) and expression of Hypoxia Responsive Element genes would provide meaningful information on our hypoxic tumor model, and how it can be used for the study of hypoxia.

4.9 Conclusions

To date, our spheroids are the largest (> 750 μm) on a chip and display a hypoxic core expressing gold-standard hypoxia-associated protein CAIX at the expected depth. Remarkably, this feature is absent in smaller spheroids of the same cell line, as shown both experimentally and in silico. The microfluidic format used is simple, reliable, and fully compatible with RT. As a proof of concept, jumbo spheroids were treated with TPZ hypoxic prodrug and RT, the efficacies of which are oxygen-dependent thus linked to hypoxia. In both the SK-LMS-1 and STS117 cell line, treatment with TPZ led to dose-dependent response in their hypoxic core only. Conversely, both hypoxic and normoxic regions of jumbo spheroids displayed a dose-response effect to RT, showing no evidence of radioresistance in the hypoxic core. Interestingly, the combination of both TPZ and RT resulted in an oxygen-dependent response. Overall, addition of 8 Gy of RT to 35 μM of TPZ yielded maximum DNA damages to both normoxic and hypoxic region, in an additive manner.

Finally, using our microfluidic device and our jumbo hypoxic spheroids to explore the biology of hypoxia and its implication on treatment resistance on a variety of cancer types would provide a useful preclinical tool for drug screening and treatment combinations.

CHAPTER 5 ARTICLE 2: HYPOXIC-CORE (HYCO) SPHEROIDS RECAPITULATE HALLMARKS OF CLINICAL HYPOXIA: A SIMPLE CHIP-BASED METHOD FOR TRANSLATIONAL ONCOLOGY

5.1 Background Information and author contribution

This chapter presents my 2nd soon to be submitted article, which showcases follow-up works of my 1st publication. This paper establishes the heart of my work. It delved deeper in the characterization of the "jumbo", now renamed hypoxic-core (HyCo) spheroids. The goal of this article is to demonstrate how this new *in vitro* model could enable preclinical researchers to easily incorporate hypoxia in their research hypothesis. The same chip design was used to generate HyCo spheroids from the same STSs cell lines as in the 1st publication. It then provides a thorough phenotypical characterization of HyCo spheroids and guidance towards how potential user could use the HyCo spheroids for drug screening or biomarker identification.

Again, as a first author, I contributed to about 90 % of this article. I designed and manufactured the microfluidic chips. As before, Julie Lafontaine trained me to do RTqPCR and I did all the experiments myself once trained, with the exception of clonogenic assays that were done by Rodin Chermat. I did all the statistical analysis, wrote the paper and designed the figures. Rodin Chermat and Julie Lafontaine guided me in the design of the study and the revision of the manuscript. Thomas Gervais and Philip Wong provided support and supervised the research. All authors have reviewed the article and agree with these contributions.

The article was submitted on April 3rd, and published on April 9th, 2025, in BioRxiv and will soon be submitted to Science Advances.

5.2 Authors and Affiliations

Elena Refet-Mollof [1,2,3], Rodin Chermat [1,2,3], Julie Lafontaine [2,3], David (Run Zhou) Ye[4], Thomas Gervais [1,2,3,5], Philip Wong [2,3,6]

[1], Biomedical Engineering Institute, Polytechnique Montréal, Montréal, Québec, Canada.

[2], Montréal Cancer Institute, Montréal, Québec, Canada.

[3], Research Center of the University Hospital of the University of Montréal, Montréal, Québec, Canada.

[4], Department of Ophthalmology, Mayo Clinic, Rochester, Minnesota, USA.

[5], Engineering Physics, Polytechnique Montréal, Montréal, Québec, Canada.

[6], Department of Radio-oncology, Princess Margaret Cancer Centre, UHN, University of Toronto, Toronto, Ontario, Canada

5.3 Abstract

Hypoxia influences the biology and response of cancers. No user-friendly device allows the study of hypoxia on highly-controlled clinically-relevant tumor models. Here, we describe how hypoxic-core (HyCo) spheroids generated using our unique non-perfused microfluidic device recapitulate key clinical hallmarks of hypoxia in vitro. Our PDMS-made system can generate up to 240 spheroids naturally exhibiting a diffusion-driven hypoxic core in only 4 days, here from two sarcoma cell lines. Compared to smaller normoxic spheroids from the same cell lines, known hypoxia-related genes are upregulated in HyCo spheroids. In addition, HyCo spheroids display hallmark hypoxia-induced resistance to radiotherapy and chemotherapy, along with increased invasiveness. Finally, to demonstrate applications of our HyCo spheroids and on-chip framework in drug development, we used our HyCo-derived gene expression dataset to select a drug candidate (diethyl-pythiDC) and confirmed its effect on spheroid invasiveness. Our results suggest that HyCo spheroids can be efficiently used as translational tools to integrate hypoxia in cancer research, without complex workflows or setups.

5.4 Teaser

On-chip spheroids with a natural hypoxic-core emulate clinical cancer hypoxia hallmarks essential for novel therapy development.

5.5 Introduction

Tumor hypoxia refers to intratumoral oxygenation lower than physiological levels and is known to directly increase tumor aggressivity, treatment resistance, metastasis progression and shorten cancer patient survival [4], [5], [281]. Cellular response to hypoxia involves activation of the hypoxia response pathway, a cascade of physiological and biological changes allowing hypoxic cells to survive in extreme conditions of low oxygen, low pH, and low concentration of nutrients [282], [283], [284]. These changes include increased glycolysis, angiogenesis, pH regulation, and endothelial to mesenchymal transition [284]. Moreover, the hypoxic microenvironment promotes tumor progression and metastasis by exacerbating cell motility and propensity to invade local tissue (i.e., the first step of the metastatic cascade) through both autocrine and paracrine mechanisms [6], [285], [286]. These mechanisms include secretion of growth factors and modulation of the expression of cell-cell or cell-extracellular matrix adhesion molecules [287]. In addition, hypoxia fosters pro-migratory and invasive phenotypes as well as regulating cell intravasation and extravasation, further contributing to metastasis progression [286], [287]. These combined effects will establish a vicious circle, as the increased tumor volume will result in greater depletion of oxygen and nutrients, further driving the aggressive phenotype [287].

Notably, hypoxia also contributes to anti-cancer treatment resistance [9], [62], [287], [288]. For example, radiotherapy (RT) efficacy is based on the generation of free radicals within the cell, among which the hydroxyl radical OH•, in turn producing radicals on the DNA (DNA•) [1]. As the fixation of these radicals into permanent DNA damage is an oxidative process, hypoxia directly results in decreased RT efficacy [1], [4], [289]. In addition, hypoxic cancer cells have acquired the ability to survive both RT-induced DNA damages and their extensive baseline genomic instability resulting from high cellular stress and impaired capacity for DNA-repair, further limiting the impact of RT [62]. Similarly, chemotherapies (CT) that target DNA are less efficient in hypoxic conditions [62], [276], [287], [290]. Furthermore, hypoxia increases the expression of a panel of genes involved in CT drug efflux (ATP-binding cassette family, e.g., ABCB1, ABCC1) thereby reducing intracellular drug concentration [291], [292].

Finally, similar observations can be made regarding immunotherapy, with hypoxia driving an immunosuppressive phenotype [36]. Mainly, immune cells cannot easily penetrate hypoxic regions, and the few cells that manage to do so are inactivated due to the acidity of the tumor microenvironment [36], [244].

Soft-tissue sarcoma (STS) is a rare groups of cancers in adults (less than 1%) but accounts for 20 % of pediatric solid malignant cancer [13], [15]. Originating from any soft tissues (e.g., muscle, fat, blood vessels, nerves, tendons, linings of the joints), about 45% of STSs harbor hypoxia, which is associated with worsened clinical outcome [152], [153], [154]. RT and limb-sparing surgical resection are the standard of care for most large high-grade STS, with RT being preferentially given before surgery (i.e. neoadjuvant RT) to limit long-term RT-related toxicities [16]. The value of adjuvant CT is questionable, with no significant differences observed in either relapse-free survival or overall survival (OS) [149]. Despite achieving excellent local tumor control through neoadjuvant RT + surgery, around half of patients subsequently develop metastases and their OS is often measured in months [150]. For metastatic patients, anthracycline CT is considered standard of care although response rates are extremely poor (e.g., ~20% for doxorubicin), and is sometimes combined with the alkylating agent ifosfamide [17], [151], [293]. Cisplatin, another widely-used alkylating agent, has shown poor efficacy in metastatic STSs. However multiple clinical trials using cisplatin in combination with other drugs are still ongoing (NCT06684327, NCT05057130, NCT04605770) [17]. As previously stated, the hypoxic nature of STSs likely renders them resistant to CT and radiotherapy, more aggressive and more metastatic, explaining poor patient survival rates [155], [294], [295]. As such, the validation of alternative treatment strategies taking hypoxia into account is required to reduce metastasis occurrence in STSs patients and increase disease-free survival.

However, there is an apparent lack of user-friendly devices allowing the study of tumor hypoxia in a controlled manner [35], [41], [233], [296]. Indeed, in vitro study of hypoxia often involves complex experimental setups to control the oxygen level either physically (e.g., hypoxia chambers) or chemically (e.g., cobalt chloride) [35], [39]. Generally speaking, physical methods do not allow long-term manipulation and RT/drug treatment of samples without removing the samples from the setup, thereby re-oxygenating them.

Additionally, oxygen level in such setups is controlled by injecting nitrogen, the resulting media acidification having been shown to induce uncontrolled biases in biology experiments [1], [40], [233]. Similarly, chemical induction can interact with other metabolic pathways than response to hypoxia and eventually affect treatment response evaluation [42]. Furthermore, none of these methods are able to capture the whole picture of clinical hypoxia, among which the complex interplay between hypoxic and normoxic cells within the same sample [35], [297]. Finally, discrepancies between in vitro methods of hypoxia induction limits the establishment of clinically-translatable signatures [37]. If in vivo tumor models can naturally exhibit hypoxia, duration of experiments is drastically limited by the need for these tumors to already be extremely large to be sufficiently hypoxic, close to the limit accepted by most ethics committees. Moreover, in vivo quantification of hypoxia is either a post-mortem process or requires complex imaging techniques and equipment [298]. As such, despite higher biological relevance, animal models are ill-suited for the study of hypoxia in early preclinical studies.

Microfluidics have eased cancer translational research and drug development for the past 20 years, enabling the culture and treatment of increasingly complex 3D tumor models in compact user-friendly systems [41], [54]. As the recently signed FDA Modernization Act 2.0, and the proposed FDA Modernization Act 3.0, allow and encourage “cell-based assays, microphysiological systems, or bioprinted or computer models” as alternatives to animal testing for purposes of drug and biological product development, the validation of microfluidic tools is both warranted and timely [173], [174]. In 2021, we reported a user-friendly non-perfused microfluidic chip on which users can culture up to 240 spheroids that naturally harbor both a normoxic shell and a hypoxic core [33]. In this study we delved deeper into the characterization and demonstration of translational applications of our in vitro models: the Hypoxic-Core (HyCo) spheroids. We show that our spheroid model displays key hallmarks of *in vivo* hypoxic STSs, including hypoxia-specific gene expression, treatment resistance and increased invasiveness. Then, we showcase how our on-chip model and methodology can be applied to data-driven treatment testing. Overall, we show that our on-chip tumor model provide cancer researchers with a simple yet clinically-relevant and powerful tool to study hypoxia and its impact on cancer treatment, as well as identifying potential prognostic biomarkers or druggable targets.

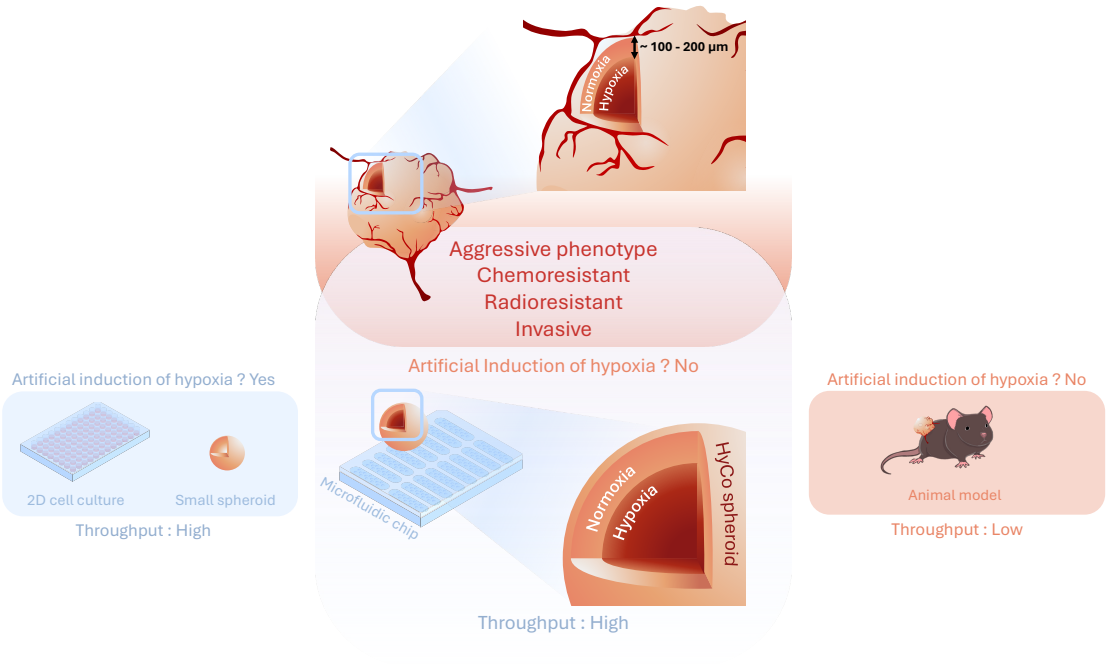

Figure 5-1 Paradigm for on-chip HyCo spheroids.

Soft-tissue sarcomas are hypoxic solid tumors, which contributes to their agressive phenotype, chemoresistance, radioresistance and increased invasiveness. On one hand, in vitro models are high-throughput but require artificial induction. On the other, animal models are naturally hypoxic but are low-throughput and cumbersome. In this study, we showcase how our chip-based high-throughput method generates naturally-hypoxic HyCo spheroids which recapitulate clinical hallmarks of tumor hypoxia, making them adapted for early preclinical studies

5.6 Results

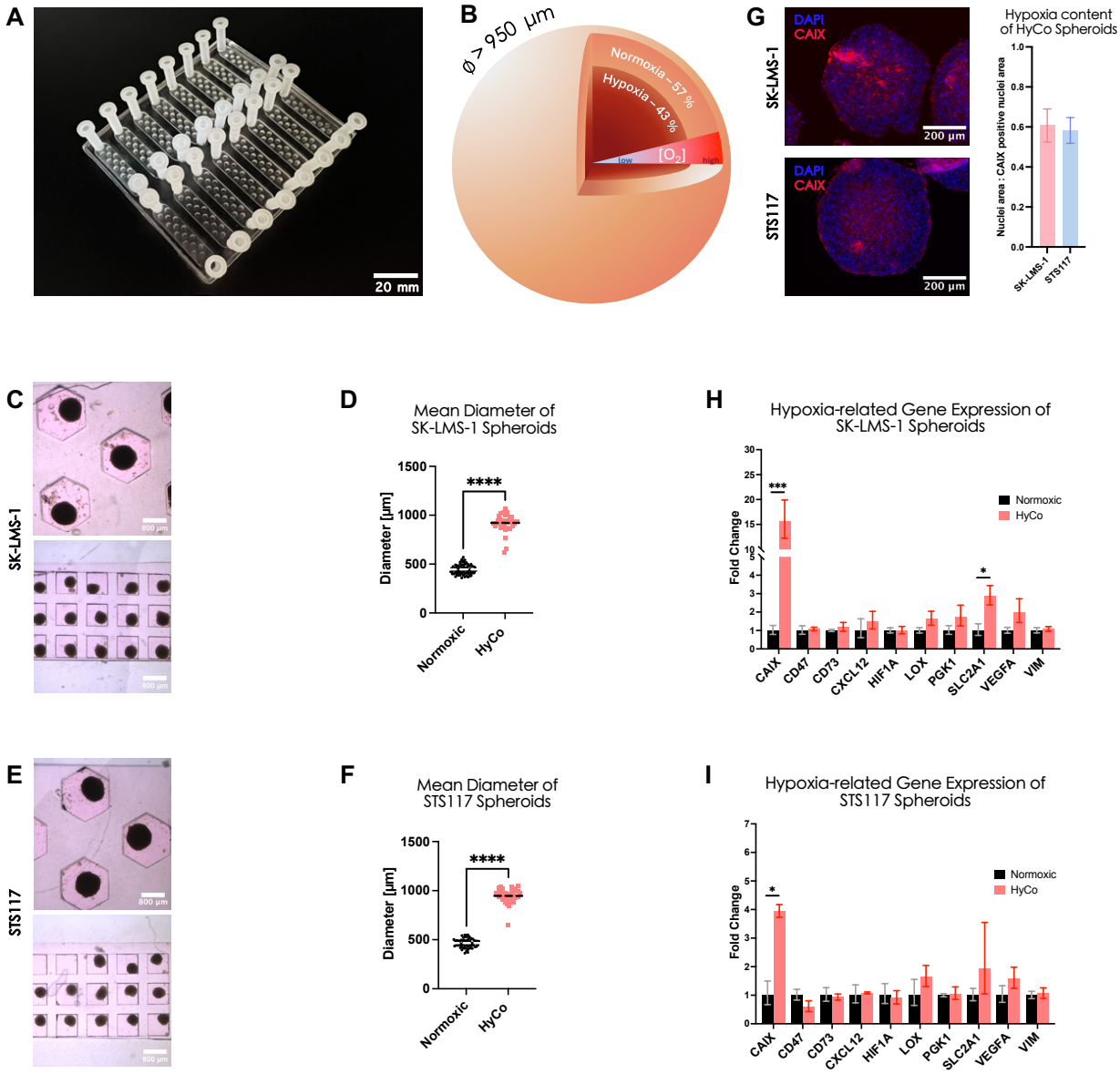

Figure 5-2 HyCo spheroids have an increased expression of hypoxia-related genes, for both SK-LMS-1 and STS117.

(A) Photograph of microfluidic chip for HyCo spheroid generation, culture and treatment. (B) 3D Schematic of HyCo spheroid with sectional view representing the 70:30 normoxic to hypoxic cells volumetric ratio. (C), (E) Brightfield images of SK-LMS-1 and STS117 HyCo and normoxic spheroids. (D), (F) Mean diameter of SK-LMS-1 and STS117 HyCo and normoxic spheroids (**** : p-value < 0.00001, N = 3 independent experiments, total of n= 33 to 79 spheroids, unpaired t-test). (G) Immunofluorescence images of SK-LMS-1 and STS117 HyCo spheroids stained for nuclei (DAPI, in blue) and hypoxia (CAIX, in red), along with quantification of CAIX-positive nuclei area ratio. (H), (I) RTqPCR of hypoxia-related genes expression (CAIX, CD47, CD73, CXCL12, GAPDH, HIF1A, LOX, PDK1, SCL2A1 VEGFA, VIM) in SK-LMS-1 and STS117 HyCo vs normoxic spheroid (mean ± SEM, N = 3 to 4 independent experiments).

5.6.1 HyCo spheroids generated on-chip overexpress key known hypoxia-related genes

Our microfluidic chips (Fig. 2A) are transparent, oxygen-permeable, radio-compatible, and allow formation of HyCo spheroids within 2 to 3 days for both SK-LMS-1 and STS117 cell lines. We selected 950 µm as the target diameter of HyCo spheroids based on our in-house in silico model of oxygen consumption [33]. At this size, approximately 43% of the spheroid volume or cellular content would theoretically grow under the 10 mmHg pO_2 threshold for CAIX-expression, ergo in hypoxia (Fig. 2B, Fig. S1). For SK-LMS-1, HyCo and normoxic spheroids harbor a mean diameter of 921 ± 90 µm and 446 ± 49 µm, respectively (Fig. 2C, D). For STS117 HyCo and normoxic spheroids harbor a mean diameter of 946 ± 75 µm and 465 ± 43 µm, respectively (Fig. 2E, F). It is worth noting that very few HyCo spheroids (3 SK-LMS-1 and 1 STS117, across 38 and 33 spheroids over 3 experiments) are much smaller than average and overlap with normoxic spheroid size distribution. In such cases, "small" HyCo spheroids were excluded from further experiment to prevent confounding effects. As such, as shown in Fig. 2G, our on-chip HyCo spheroids consistently exhibit a CAIX-expressing hypoxic core that occupies approximately 60 % of their cross-section. By extrapolating to the third dimension (Fig. 2B), our results indicate that approximately 45% of the total amount of cells in a HyCo spheroid are hypoxic, consistent with our in silico modeling (Fig. S1).

To probe whether ~ 45 % of hypoxic spheroid content was sufficient to induce observable downstream molecular responses, we performed a RTqPCR on a panel of 10 genes known to be upregulated under hypoxic conditions: CAIX, CD47, CD73, CXCL12, HIF1A, LOX, PGK1, SLC2A1, VEGFA and VIM. In both cell lines, most genes of the selected hypoxia-related panel are upregulated (fold-change > 1) except for CD47 in STS117 (Fig. 2H, I). For SK-LMS-1, CAIX (p-value = 0.02), CXCL12 (p-value = 0.21), LOX (p-value = 0.11), PGK1 (p-value = 0.23), SCL2A1 (p-value = 0.03) and VEGFA (p-value = 0.13) have a fold-change above 2 in HyCo spheroids. For STS117, CAIX (p-value = 0.04), LOX (p-value = 0.15), SCL2A1 (p-value = 0.31) and VEGFA (p-value = 0.19) have a fold-change above 2 in HyCo spheroids. Of note, HIF1A gene is not significantly upregulated, with a fold-change of only 1.35 ± 0.62 for SK-LMS-1 and 1.07 ± 0.22 for STS117.

Absence of HIF1A upregulation despite evidence of downstream effects of HIF1α stabilization has been previously reported for multiple cancers, and is observed here for our two sarcoma cell lines [299]. Overall, HyCo spheroids had increased expression of an array of known hypoxia-related genes in comparison to smaller normoxic spheroids, for both cell lines.

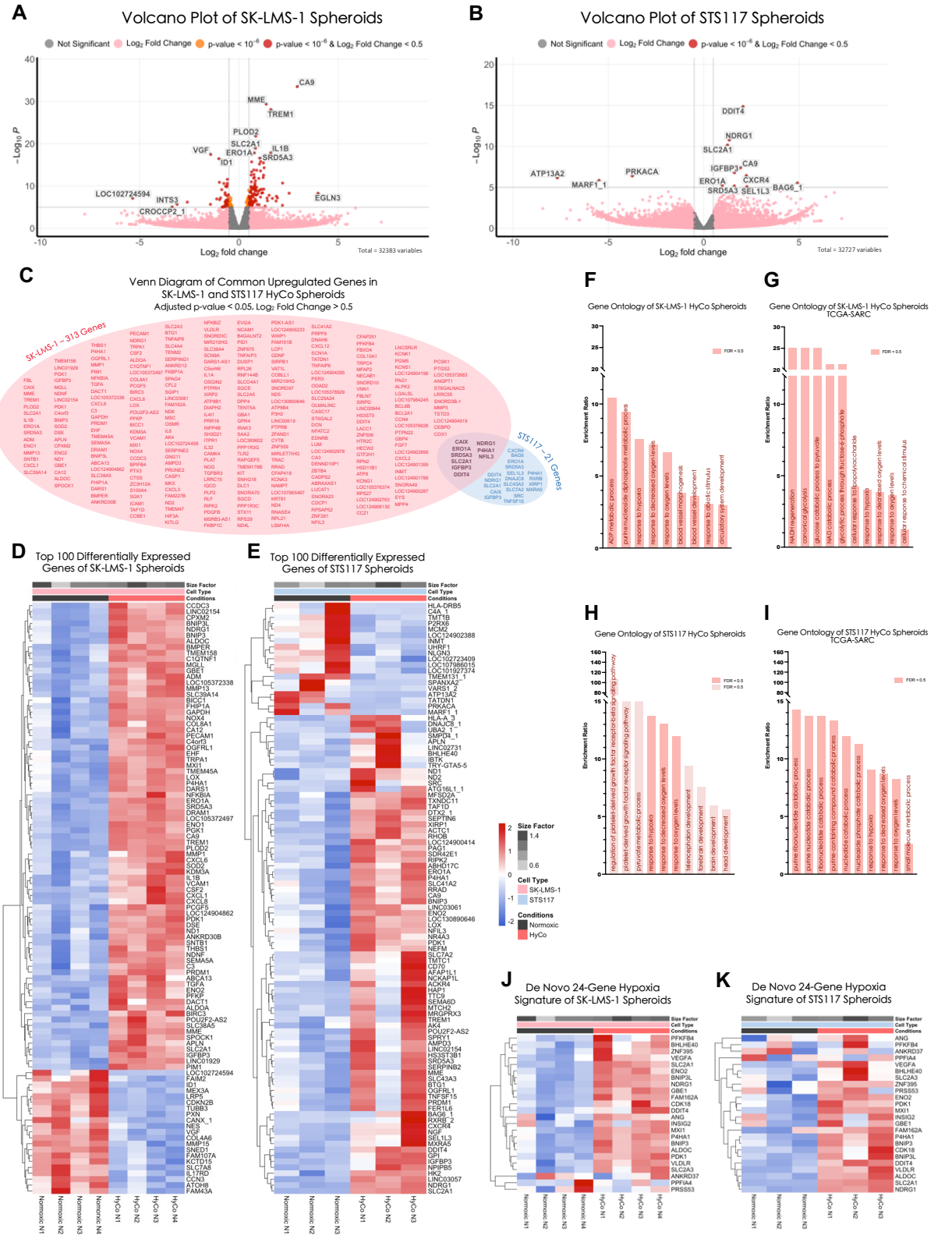

Figure 5-3 HyCo spheroids hypoxia-related genes signature correlates with STSs clinical data, for both SK-LMS-1 and STS117.

(A), (B) Volcano Plot of SK-LMS-1 and STS117 HyCo spheroids compared to normoxic spheroids. (C) Venn diagram of common upregulated genes in both SK-LMS-1 and STS117 HyCo spheroids (adjusted p-value < 0.05, Log_2 Fold Change > 0.5). (D), (E) Heatmap of top 100 differentially expressed genes of SK-LMS-1 and STS117 HyCo and normoxic spheroids. (F), (G) Gene ontology pathway enrichment ratio of SK-LMS-1 HyCo spheroids with whole human genome for reference and with TCGA-SARC for reference. (H), (I) Gene ontology pathway enrichment ratio of STS117 HyCo spheroids with whole human genome for reference and with TCGA-SARC for reference. For gene ontology analysis, False Discovery Rate (FDR) correction is applied using Benjamini-Hochberg (BH) method. (J), (K) Heatmap of de novo 24-gene hypoxia signature of SK-LMS-1 and STS117 HyCo and normoxic spheroids. All Heatmaps are clustered by Complete linkage with Euclidean distance and gene expression data are scaled by row (Z-score transformation) before clustering. All data comes from N = 3 to 4 independent experiments.

5.6.2 HyCo spheroids gene expression matches known soft-tissue sarcoma hypoxia signature

Following our RTqPCR, we profiled the bulk transcriptomes of HyCo and normoxic spheroids for SK-LMS-1 and STS117 (Fig. 3). As shown in the first Volcano plot (Fig. 3A), 112 genes are significantly upregulated (log_2 fold change > 0.5, p-value < 10e-6), and 43 genes are significantly downregulated (log_2 fold change < -0.5, p-value < 10e-6) for SK-LMS-1 HyCo spheroids. As shown in Fig. 3B., only 10 genes are significantly upregulated (log_2 fold change > 0.5, p-value < 10e-6), and 3 genes significantly downregulated (log_2 fold change < -0.5, p-value < 10e-6) for STS117 HyCo spheroids. Combined analysis of SK-LMS-1 and STS117 data identified shared upregulated genes for future experimental purposes (Fig. S2). For each cell line, we then ranked upregulated genes (log_2 fold change > 0.5) by their adjusted p-values. As shown in Fig. 3C, out of the 313 and 21 genes that were significanlty upregulated (adjusted p-value < 0.05) in SK-LMS-1 and STS117 respectively, there were 9 genes upregulated in both cell lines: CAIX, ERO1A, SRD5A3, SLC2A1, IGFBP3, DDIT4, NDRG1, P4HA1 and NFIL3.

To visualize gene expression across our samples, we generated heatmaps using the expression levels of the top 100 differentially expressed genes, for SK-LMS-1 and STS117 respectively (Fig. 3D, E). For SK-LMS-1, Unsupervised clustering of the spheroids based on the top 100 differentially expressed genes showed a clear divide between normoxic and HyCo spheroids in both cell lines, with 21 genes downregulated and 79 upregulated in the latter. Similarly, for STS117, 19 genes are downregulated and 81 are upregulated in HyCo spheroids. Based on whole human genome database (RampDB Genomics), gene ontology (GO) terms enriched in both SK-LMS-1 and STS117 HyCo spheroids include pathways in *response to hypoxia*, *response to oxygen level* and *response to decrease oxygen levels*. (Fig. 3F, H). Other GO terms enriched in SK-LMS-1 are related to metabolism switch and vasculogenesis, of which the relationship with hypoxia has been well-documented [35], [286]. For other pathways enriched in STS117 however, FDR are consistently above significance threshold and pathways such as *brain development* and *forebrain development* are, at first glance, unrelated to STSs response to hypoxia. Although the biological relevance of this finding cannot be entirely ruled out, considering the genome as a whole could lead to probability-based biases and misinterpretation of enriched pathways. Therefore, we performed gene ontology analysis using the human sarcoma-specific database (TCGA-SARC) as a reference to help us interpret our findings in the context of sarcomas. Based on TCGA-SARC database, GO terms enriched in HyCo spheroids of both cell lines now only include pathways linked to low oxygen levels and metabolic adaptation to hypoxia, in accordance with literature (Fig. 3G, I) [19].

Finally, we applied the *de novo* 24-gene hypoxia signature from Yang et al. to our data, with expression levels for SK-LMS-1 and STS117 spheroids illustrated in Fig. 3J and 3K [19]. Out of the 24 genes, 15 and 18 are upregulated ($\log_2$ fold change > 0.5) within HyCo spheroids for SK-LMS-1 and STS117 respectively (Fig. 3J, K). This showcases that HyCo spheroids gene signature matches that of Yang et al., which was selected based on its specificity to hypoxic STSs and its correlation with shorter pastient distant metastasis-free survival [19]. Overall, these results confirm the hypoxic nature of our HyCo spheroid model and its biological relevance in preclinical research.

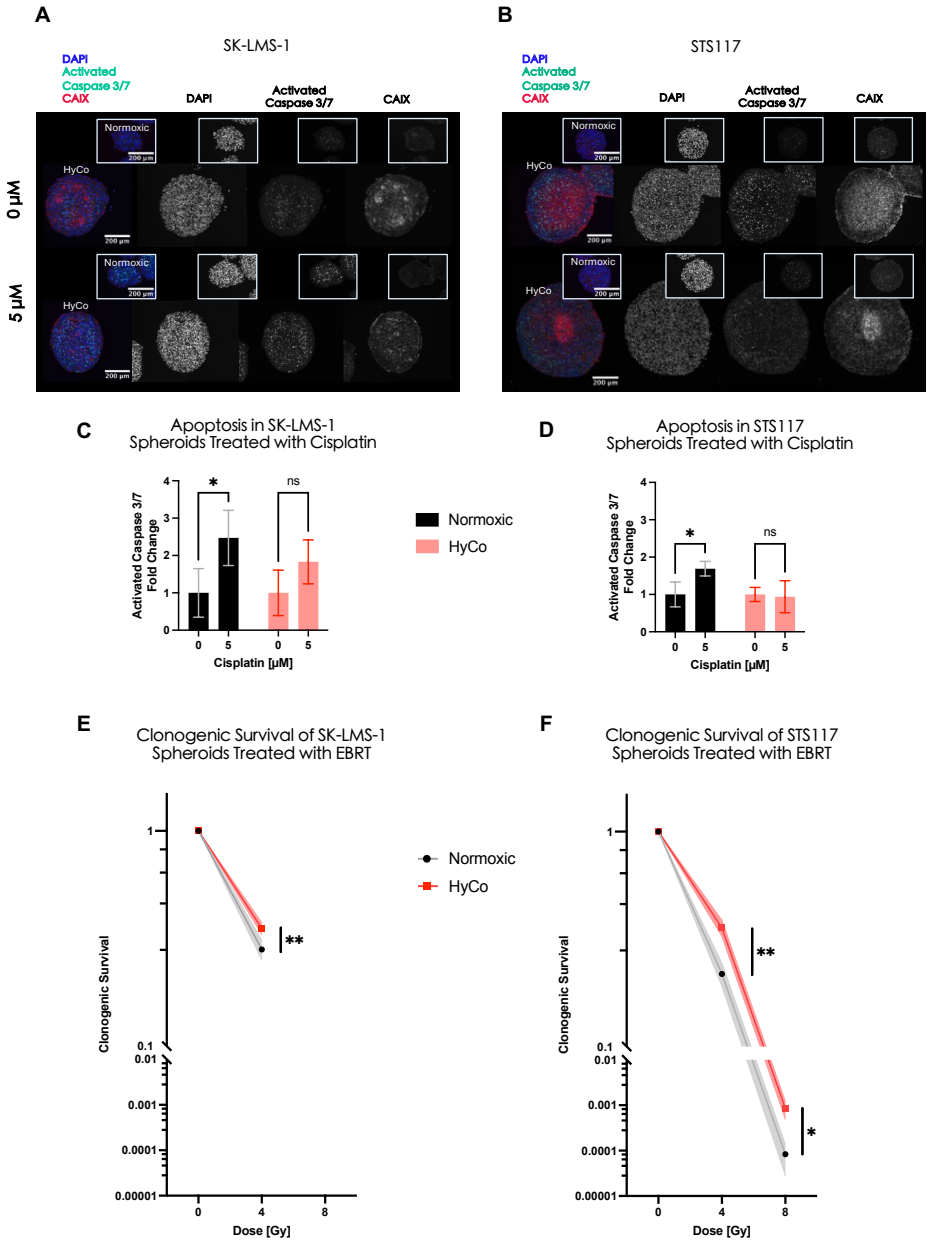

Figure 5-4 HyCo spheroids are resistant to both chemotherapy and radiotherapy compared to normoxic spheroids.

(A), (B) Immunofluorescence images of SK-LMS-1 and STS117 HyCo and normoxic spheroids after overnight exposure to 5µM of cisplatin, stained for nuclei (DAPI in blue), apoptosis (CellEvent ready probe 3/7 in green) and hypoxia (CAIX in red). (C), (D) Quantification of apoptosis signal (activated caspase 3/7) after overnight exposure to 5µM of cisplatin in SK-LMS-1 and STS117 HyCo and normoxic spheroids. Data are presented as mean ± SD, (*) : adjusted p-value < 0.05, N=3,4 independent experiments, n = 2 to 8 spheroids per repetitions, 2way ANOVA, Šidák's multiple comparisons test . (E), (F) Clonogenic survival curves of SK-LMS-1 and STS117 HyCo and normoxic spheroids after on-chip external beam radiotherapy treatment. Data are presented as mean ± SD, (*): adjusted p-value < 0.05, (**): adjusted p-value < 0.01, N=3 independent experiments, multiple unpaired t-test using Holm-Šidák method.

5.6.3 HyCo spheroids recapitulate clinically-observed hypoxia-induced treatment resistance

To further confirm the hallmark phenotypical behavior and more precisely the resistance to both chemo- and radiotherapy of our HyCo spheroids, we treated them with 5 µM of cisplatin or with 4 and 8 Gy external beam radiotherapy (EBRT). Cisplatin, a known alkylating chemotherapeutic agent, induces DNA-damages ultimately leading to apoptosis. Therefore, we evaluated cytotoxicity by quantifying accumulation of caspase 3 and 7 activation over 16 h. We selected cisplatin specifically for its poor response rate in STSs (10 %) and the well-established links between hypoxia and cisplatin resistance [17], [290]. Although EBRT also inflicts DNA-damages, we evaluated treatment efficacy by quantifying clonogenic survival to capture the long-term consequences of ionizing radiation on tumor cells.

For both cell lines, cisplatin-treated and non-treated HyCo spheroids display similar level of activated caspase 3 and 7, meaning there is no significant effect of cisplatin (Fig. 4A – D). By contrast, normoxic spheroids have 2.47 ± 0.74 times higher activated caspase 3 and 7 than HyCo (adjusted p-value < 0.05) for SK-LMS-1 (Fig. 4C), and 1.69 ± 0.20 (adjusted p-value < 0.05) for STS117 (Fig. 4D), showcasing that normoxic spheroids are more sensitive to cisplatin than HyCo spheroids of the same cell line. In addition, when separating the response to cisplatin between normoxic and hypoxic regions of HyCo spheroids, we observed that both regions exhibited lower activated caspase 3 and 7 than corresponding regions in normoxic spheroids (Fig. S1). Although not significant, this finding points towards paracrine signaling of cisplatin resistance from the hypoxic to the normoxic regions of HyCo spheroids.

Similarly, the clonogenic assay confirms the resistant behavior of HyCo spheroids for both cell lines after treatment with EBRT. SK-LMS-1 HyCo spheroids exhibit 1.26 ± 0.07 times more colonies than normoxic spheroids after exposure to 4Gy of EBRT (adjusted p-value < 0.01) (Fig. 4E). However, we observed no colonies when treated with 8 Gy of EBRT (Fig. 4E). STS117 HyCo spheroids exhibit 1.64 ± 0.07 times more colonies than normoxic spheroids after exposure to 4 Gy (adjusted p-value < 0.01) and 13.67 ± 8.04 times more colonies than normoxic spheroids after exposure to 8 Gy (adjusted p-value < 0.05) (Fig. 4F). From this data, STS117 cells appear more radioresistant than SK-LMS-1, as they are still able to form colonies after 8 Gy of EBRT even under normoxic conditions.

At 4 Gy however, normoxic STS117 spheroids are more sensitive than normoxic SK-LMS-1, while HyCo STS117 and HyCo SK-LMS-1 exhibit similar clonogenic survival. As such, hypoxia-induced radioresistance also appears more prominent for the STS117 cell line at 4 Gy. More broadly, the clonogenic assay indicates a dose response of HyCo and normoxic spheroids to EBRT regardless of cell line.

Overall, for both cell lines, HyCo spheroids are resistant to CT (cisplatin) and EBRT, therefore exhibiting an overall more resistant phenotype compared to their smaller normoxic counterpart.

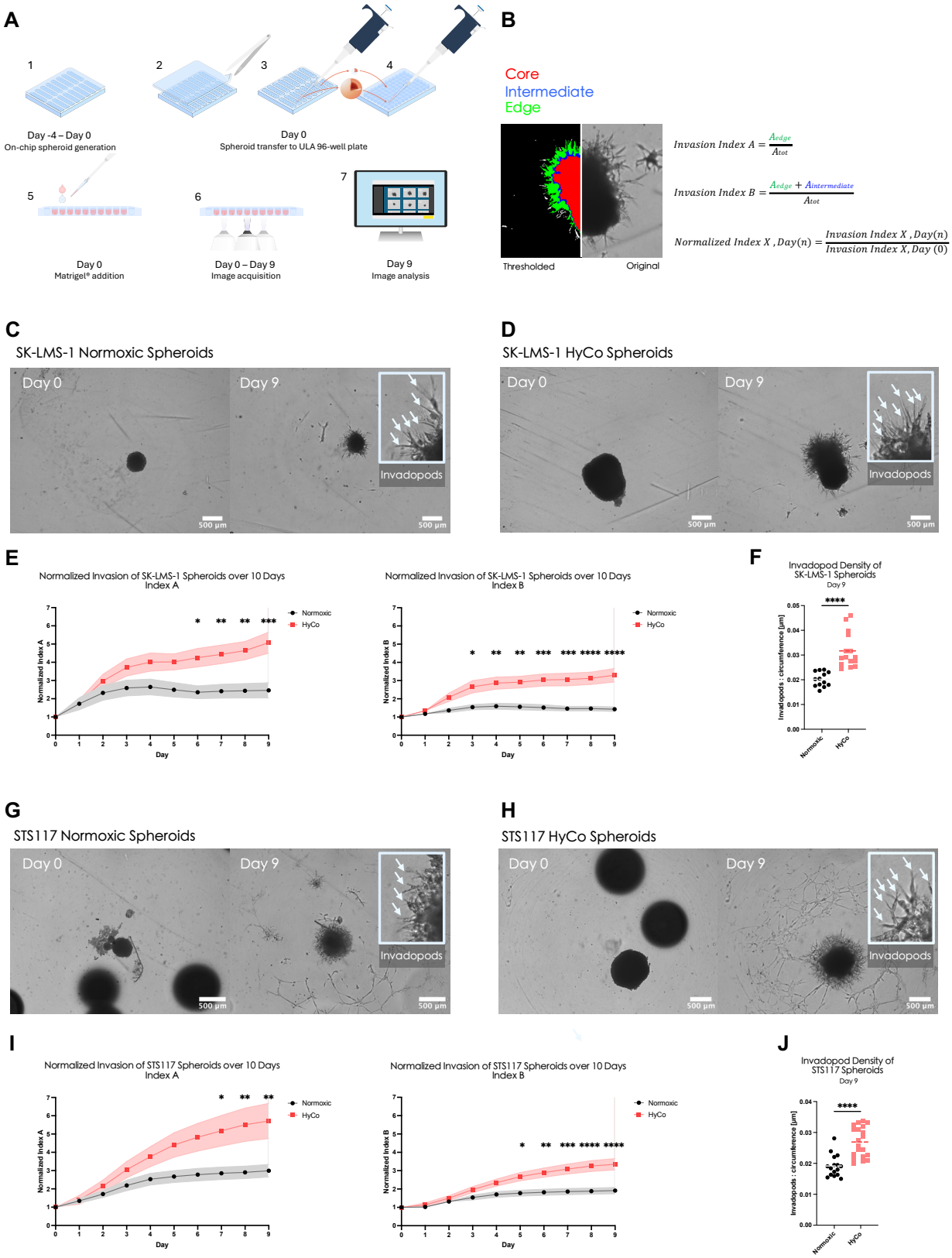

Figure 5-5 HyCo spheroids are more invasive than small normoxic ones.

(A) Schematic of experimental timeline. (B) Example of invasion image analysis pipeline. (C), (D) Brightfield images of SK-LMS-1 normoxic and HyCo spheroids at day 0 and day 9. White arrows indicate invadopods, i.e. cell protrusions into the Matrigel. (E) Normalized invasion indexes A and B for SK-LMS-1 normoxic and HyCo spheroids over 10 days. (F) Invadopod density of SK-LMS-1 normoxic and HyCo spheroids at day 9. (G), (H) Brightfield images of STS117 normoxic and HyCo spheroids at day 0 and day 9. White arrows indicate invadopods, i.e. cell protrusions into the Matrigel. (I) Normalized invasion indexes A and B for STS117 normoxic and HyCo spheroids over 10 days. (J) Invadopod density of SK-LMS-1 normoxic and HyCo spheroids at day 9. All invasion indexes data are presented as mean ± SEM, (*) : adjusted p-value < 0.05, (**) : adjusted p-value < 0.01, (***) : adjusted p-value < 0.001, (****) : adjusted p-value < 0.0001, N = 4 independent experiments, n = 5 normoxic spheroids and n= 5 HyCo spheroids per experiments, 2way ANOVA, Šidák's multiple comparisons test. Invadopod density data are presented as a scatter plot with mean value, p-value < 0.001, (****), N = 4 independent experiments, n = 5 normoxic spheroids and n= 5 HyCo spheroids per experiments, unpaired t-test.

5.6.4 HyCo spheroids recapitulate clinically-observed hypoxia-induced tumor aggressiveness

Another critical characteristic of hypoxia in cancer is the promotion of an aggressive phenotype, manifesting as increased invasiveness and metastatic progression. To investigate this, we performed an invasion assay on HyCo and normoxic spheroids by following the invasion of spheroids in a Matrigel matrix over 10 days (Fig. 5A). We then analyzed the invasion images using the method described in Fig. 5B, adapted from G. J. Lim et al. [300]. Briefly, invasion index A describes the invading outermost regions of the spheroid, while invasion index B includes the loosely aggregating intermediate region (Fig. 5B)

For both cell lines, normalized invasion indexes A and B were significantly higher for HyCo spheroids compared to normoxic ones (Fig. 5C, D, F). Normalized invasion index A is 1.8-times higher for HyCo spheroids than for normoxic ones on day 7 for SK-LMS-1 (Fig. 5F) and day 6 for STS117 (Fig. 5I) (adjusted p-value < 0.05). On the other hand, normalized invasion index B is 1.7-times higher on day 5 for SK-LMS-1 (Fig. 5F) (adjusted p-value < 0.05) and 1.5-times on day 3 for STS117 (Fig. 5I) (adjusted p-value < 0.05) HyCo spheroids compared to normoxic ones. Furthermore, both normalized indexes remain significantly higher for HyCo spheroids for the remainder of the experiment. It is also worth noting that normalized invasion indexes of HyCo spheroids of both cell lines continuously increase overtime while normalized invasion indexes of normoxic spheroids plateaued starting day 4.

In addition, invasion assays can provide information on the distribution of the various arms protruding from the spheroids into the surrounding Matrigel, which we have termed “invadopods”. As shown on Fig. 5C, D, I, and J, each spheroid is surrounded by dozens of such protrusions, the amount of which can be normalized to the circumference of the invading area to derive an invadopod density. Here, for both SK-LMS-1 and STS117, invadopod density on day 9 is on average higher in HyCo spheroids by 57 % and 40 % respectively (p-value < 0.0001) (Fig. 5G, L). In other words, the proportionally higher invasiveness of HyCo spheroids is also accompanied by a proportionally higher amount of invadopods.

As a side note, across all repetitions, 6 SK-LMS-1 HyCo spheroids underwent a process we labeled “sprouting”, whereby a secondary spheroid is partially or completely expulsed from the primary one (Fig. S4). This process was only observed for HyCo spheroids of the SK-LMS-1 cell line and was not investigated further.

Overall, our results demonstrate that HyCo spheroids exhibit a more invasive phenotype, in accordance with clinical literature on tumor hypoxia.

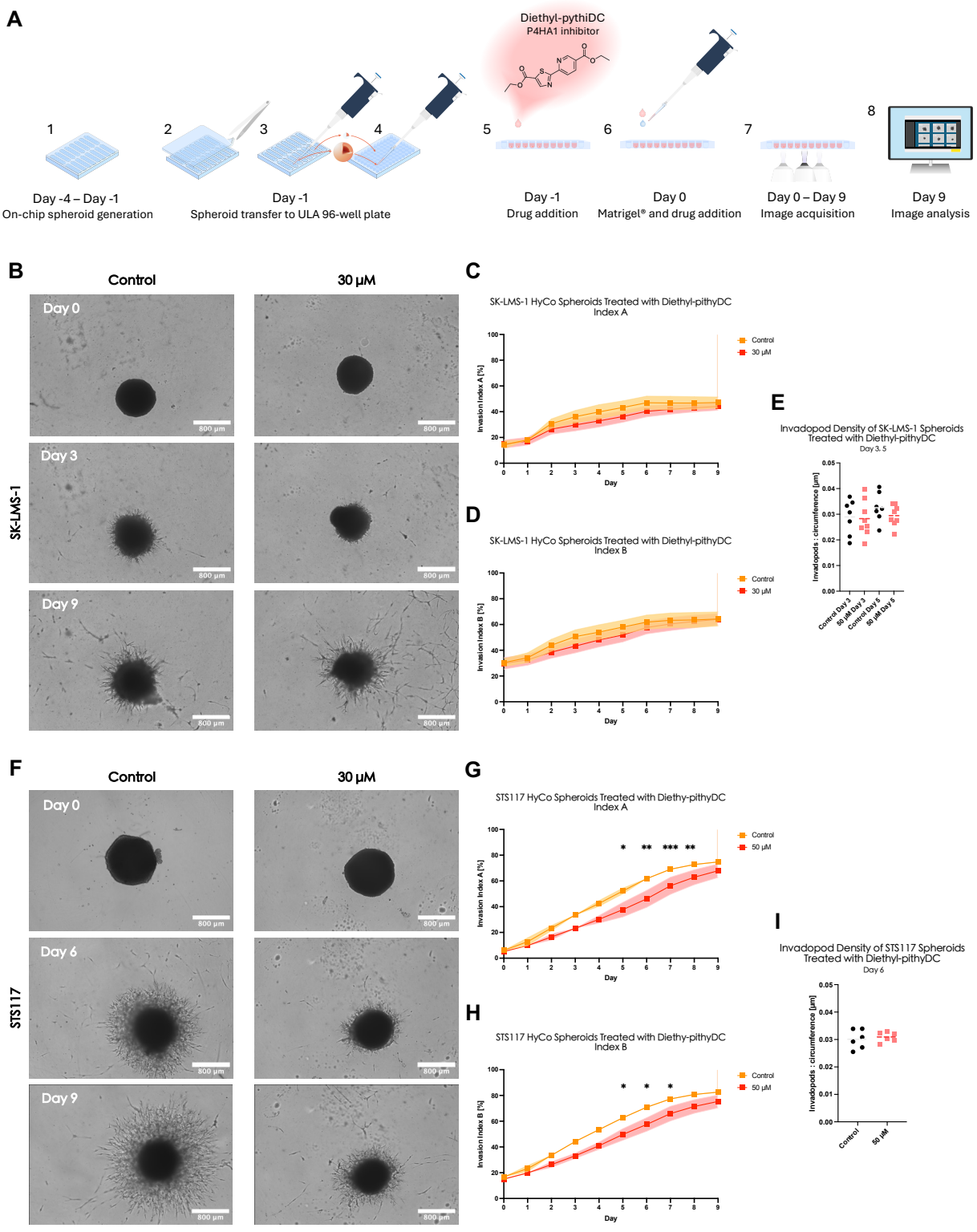

Figure 5-6 HyCo spheroids can provide preclinical information on drug efficacy.

(A) Schematic of experimental timeline. (B) Brightfield images of SK-LMS-1 HyCo spheroids treated with control buffer (left) and diethyl-pythiDC (right) at days 0, 3 and 9. (C),(D) Normalized invasion indexes A and B for SK-LMS-1 control and treated HyCo spheroids over 10 days. (E) Invadopod density of SK-LMS-1 control and treated HyCo spheroids at day 3 and day 5. (F) Brightfield images of STS117 HyCo spheroids treated with control buffer (left) and diethyl-pythiDC (right) at day 0, 6 and 9. (G), (H) Normalized invasion indexes A and B for STS117 control and treated HyCo spheroids over 10 days. (I) Invadopod density of STS117 control and treated HyCo spheroids at day 6. All invasion indexes data are presented as mean ± SEM, (*) : adjusted p-value < 0.05, (**) : adjusted p-value < 0.01, (***) : adjusted p-value < 0.001. N = 4 independent experiments for SK-LMS-1 and N = 3 for STS117. n = 4 HyCo spheroids per experiments (2 control and 2 treated). For SK-LMS-1, a mixed-effects analysis with Šidák's multiple comparisons test was used due to uneven group sizes (1 blurry spheroid in N3 control group). For STS117, 2way ANOVA, Šidák's multiple comparisons test analysis was used.

5.6.5 HyCo spheroids enable data-driven cancer-specific preclinical drug testing

Finally, we sought to demonstrate applications of our HyCo spheroids to drug testing. Based on genes upregulated in both SK-LMS-1 and STS117 (Fig. 3C), availability of such compounds and documented evidence of preclinical efficacy, we selected P4HA1-specific inhibitor diethyl-pythiDC as a drug candidate. Diethyl-pythiDC mode of action relies on directly decreasing tumor ability to infiltrate local microenvironment, and as such has been shown to reduce tumor invasion and metastasis [301]. Given the documented impact of this compound on proliferation and invasion, and given the metastatic nature of STSs, we chose to quantify diethyl-pythiDC efficacy by measuring spheroid invasiveness through invasion assays (Fig. 6A).

We observed no significant effect of diethyl-pythiDC on SK-LMS-1 HyCo spheroids. Still, both indexes were lower compared to control, with the maximum difference between the 2 conditions observed at day 5 and 3 for indexes A (16.3 %) and B (14.7 %) respectively (Fig 6B-D). Furthermore, we report no differences in invadopod density for spheroids at either day 3 or day 5 (Fig. 6E).

On the other hand, diethyl-pythiDC appears effective for STS117 HyCo spheroids, with indexes A and B being significantly lower for HyCo at days 5 to 8 and 5 to 7 respectively (Fig. 6F-H). This difference is the highest at day 6, with indexes A and B being reduced by 25.4 % (61.8 ± 4.1 to 46.1 ± 16.0, adjusted p-value < 0.001) and 18.9 % (70.9 ± 3.1 to 57.5 ± 12.8, adjusted p-value < 0.05) respectively. However, indexes of the control group appear to ultimately catch up to that of the treated group, with no significant difference at day 9 for index A and at day 8 for index B. Finally, there was no difference in invadopod density between treated and untreated spheroids at day 6 (Fig. 6I).

This indicates that the reduced invasiveness is not mediated by reduced number of invadopods but rather by reduced ability of these invadopods to invade, consistent with diethyl-pythiDC mechanism of action.

Overall, these results demonstrate that HyCo spheroids can be efficiently applied to preclinical treatment testing, with their clinically-relevant hypoxia-specific gene signatures being used as guidance for treatment selection.

5.7 Discussion

While tumor hypoxia represents a well-known feature associated with worsened patient survival, there is still no user-friendly platform to study it in laboratory settings. As previously mentioned, hypoxia research requires complex experimental setups such as hypoxic chambers or chemicals (e.g., cobalt chloride), which can introduce biological biases including media acidification and interaction with treatments, assays and outcomes. Conversely, although closer to clinical mechanisms of hypoxia, mice tumor models are heterogeneous in their hypoxic content, both spatially and temporally, thereby increasing the complexity and cost of studying them. Quantification of hypoxia *in vivo* is either post-mortem using immunofluorescence (IF) or immunohistochemistry (IHC) or require methods such as needle-type O_2 electrodes or complex and costly imaging techniques (e.g, PET, fMRI), which are not universally available and demand specialized personnel. Overall, animal models, though biologically relevant, are ill-suited to study hypoxia for the first steps of preclinical studies. In 2022, the FDA Modernization Act 2.0 encouraged the use of “cell-based assays, microphysiological systems, or bioprinted or computer models” as alternatives to animal testing for purposes of drug and biological product development [173]. A proposal to mandate the FDA to update its regulations within 12 months, dubbed FDA Modernization Act 3.0, has been introduced in the US Senate in January of this year [174]. Thus, developing a simple powerful preclinical tool to study hypoxia can contribute to the democratization of scientific research by lowering barriers to entry, encouraging interdisciplinary collaboration, and enabling broader participation in scientific research and hypoxia-related treatment development.

Our microfluidic chips easily produce 240 size-controlled spheroids that naturally harbor both a hypoxic core and a normoxic shell due to oxygen-diffusion limitations, defined as HyCo spheroids. As shown in our previous publication and in Fig.2B and 2C HyCo spheroids reliably feature a hypoxic core comprising 35 - 45% of their total volume [33]. In this study, we further characterize > 900 μm spheroids and demonstrated that they upregulate key hypoxia-response genes such as CAIX, SCL2A1, or VEGFA [37]. As previously stated, HIF1A gene was not upregulated at the gene level despite demonstrable downstream effects of HIF1α protein stabilization, including CAIX expression. Given that most of the volume of HyCo spheroids is in normoxic conditions, it is possible that the signal from hypoxic cells is simply masked by that of normoxic ones [33]. Furthermore, although post-translational regulation of HIF1α activity under hypoxic conditions is well-known, oxygen-independent regulatory mechanisms of HIF1A transcription and translation have also been identified and observed firsthand in our previous publication [33], [299], [302].

Although HyCo spheroids are not entirely hypoxic, their gene expressions recapitulate those observed in clinical STSs hypoxic samples. Transcriptomic profiling showed a clear difference in gene expression between HyCo and normoxic spheroids, which was more evident for SK-LMS-1 than STS117. Indeed, SK-LMS-1 HyCo spheroids have 10-times more significantly upregulated genes than STS117 despite having the same controlled hypoxia content. These differences may stem from STS subtype-specific adaptation to hypoxia or inherent differences between commercially-available and patient-derived cell lines, both of which have been documented [303], [304], [305]. Genes significantly upregulated in both SK-LMS-1 and STS117 included SLC2A1, SRD5A3, IGFBP3, NDRG1, CAIX and ERO1A, all of which are known to be involved in tumor response to hypoxia at various levels and have been shown to correlate with poorer clinical outcomes [1], [19], [42].

Our transcriptomic data and GO analyses support the biological relevance and alignment with known clinically-identified hypoxia-related cancer gene expression profiles, and more specifically with STSs-derived profiles [19], [306]. This solidifies HyCo spheroids as an excellent clinically-relevant in vitro model of STSs hypoxia. Given the heterogeneity of STSs and clinical outcomes, better risk stratification strategies are warranted. Currently, despite the identifications of several prognostic gene signatures, their clinical utility are limited by the lack of efficacious systemic or hypoxia-targeted treatments that could alter patient outcomes [19], [306].

As HyCo spheroids can be generated from both commercially available and patient-derived cell lines, our chip-based strategy offers a versatile platform for identifying cancer-specific hypoxia biomarker and testing treatment response.

To further validate the functional relevance of our HyCo spheroids, we treated the spheroid on-chip with both CT and EBRT to demonstrate hypoxia related chemo- and radioresistance. We selected cisplatin as it is a widely-used alkylating chemotherapeutic agent, with a 10% clinical response rate in STSs compared to the 20% response rate of doxorubicin, the first-line treatment for STSs [17]. Like RT, cisplatin cytotoxicity relies on DNA-damage induction which is an oxygen-dependent process, lessened under hypoxic conditions. In addition, evidence of a variety of hypoxia-related mechanisms of cisplatin resistance (e.g., increased drug efflux, cisplatin detoxification, etc.) have been reported [307]. HyCo spheroids recapitulate this phenomenon, exhibiting less apoptosis than their normoxic counter parts when treated with cisplatin. Our results indicate that both normoxic and hypoxic regions of HyCo spheroids display resistance to cisplatin, although the difference between each region and normoxic spheroids is not statistically significant (Fig. S3). This suggests not only a hypoxia-driven chemoresistance in hypoxic cells but also a hypoxia-driven paracrine mechanism of resistance in normoxic cells, both of which have been documented [285], [307]. Of note SK-LMS-1 were overall more sensitive to cisplatin than STS117. Increased sensitivity to cisplatin can be attributed to a variety of pathways, including the significant downregulation of MYC in SK-LMS-1 HyCo spheroids [308]. Additionally, it has been reported that commercial cell lines do not adequately reproduce drug sensitivity in cancer patients, highlighting the value of including patient-derived models in non-clinical drug testing [303], [305].

Hypoxia-induced resistance to RT has been widely documented, both in vitro and clinically, and is based on reduced oxygen-dependent fixation of DNA damage [1]. The clonogenic assay is the gold-standard for RT efficacy, based on the ability of individual cells to successfully undergo multiple rounds of mitosis after irradiation [309]. Here, HyCo spheroids recapitulate the expected radioresistance conferred by hypoxia, as HyCo spheroids have consistently higher clonogenic survival compared to normoxic spheroids. In addition, differential response between SK-LMS-1 and STS117 in both normoxic and HyCo conditions points toward treatment resistance being a function of both oxygen status of the cell as well as sarcoma subtype-dependent factors.

As both normoxic and hypoxic cells co-exist within our samples in a controlled manner, performing the clonogenic assay on the whole spheroid can be seen as analogous to evaluating the response of a whole tumor. Once again however, with more than half of the volume of HyCo spheroids in normoxia, the contribution of hypoxic cells to clonogenic survival is significantly diluted. Importantly, unlike hypoxia chambers, our system allows straightforward on-chip irradiation due to its water equivalence and radiocompatibility, enhancing its utility for translational radiotherapy research [33], [54], [55], [197]. This further illustrates the usefulness of chip-based approaches for *in vitro* CT and RT testing, especially in the context of translational cancer research.

The invasion assays provided further support for the aggressive hypoxia phenotypes exhibited by HyCo spheroids with significantly increased and continuously increasing normalized invasion indexes compared to normoxic smaller spheroids. Of interest, sprouting event was only observed in HyCo SK-LMS-1 spheroids and warrant future investigation. Contrary to other assays discussed in this manuscript, invasion assays offer a non-destructive way of evaluating whole spheroids, retaining the three-dimensional architecture and the complex interplay between normoxic and hypoxic cells. Yet, the recency of this methodology makes it prone to potential biases in analysis, and metrics should be carefully selected to mitigate them.

In turn, HyCo spheroids are as such uniquely adapted to perform invasion assays, especially in the context of pre-clinical drug development. To demonstrate this, we applied HyCo spheroids and invasion assays to testing the efficacy of P4HA1-inhibitor diethyl-pythiDC. By inhibiting collagen biosynthesis in tumor cells, diethyl-pythiDC directly limits their ability to remodel neighbouring microenvironment and thus to invade [301]. As such, it has been proven to reduce tumor invasiveness preclinically, but has yet to reach clinical testing [301], [310]. Here, we confirmed the efficacy of diethyl-pythiDC on reducing invasiveness of STS117 HyCo spheroids, but could not do so for SK-LMS-1. Although advantageous, invasion assay must currently be performed off-chip due to Matrigel viscosity and limited on-chip well area. A chip-compatible invasion assay would require less viscous alternative matrix products or extensive chip design modification. Despite that, HyCo spheroids prove to be an adequate model for drug testing that could potentially improve the accuracy and success rate of bringing drugs from *in vitro* to *in vivo* to human trials.

Overall, we have demonstrated that our HyCo spheroids generated on-chip recapitulate clinical hallmarks of tumor hypoxia: gene signature of hypoxic STSs, hypoxia-induced treatment resistance and aggressive metastatic phenotype. Although described here for STSs, our device and methodology are inherently cancer agnostic and can be used with any spheroid-forming cell line of interest. Our ability to produce 15 HyCo spheroids per channel in only a few days, with high reproducibility, demonstrates that this technology can be efficiently used in a research setting. In addition, our microfluidic device is specifically designed to be as user-friendly and versatile as possible, broadening the scope of its possible uses and increasing its chances of adoption by the research community [311], [312], [313], [314]. At the fundamental level, our methodology can be applied to the investigation of response to hypoxia in cancer subtype-specific models, easily generating hypoxic gene expression data. As shown here, this data can in turn be used to find druggable targets, for which compounds can easily be tested on the very same clinically-relevant models using a variety of bioassays. By being complex enough yet easily-produced, HyCo spheroids demonstrate themselves to be a suitable *in vitro* model for researchers to investigate whether their findings can be converted into actionable targets, as well as model the downstream effects on phenotype before moving to *in vivo* studies. In addition, the radiocompatibility and broader user-friendliness of our microfluidic platform allows for easy investigation of treatment combinations, further increasing the potential of our technology and of our HyCo spheroids to bridge the gap between bench and benchmark in drug development.

5.8 Materials and Methods

5.8.1 Experimental design

The objectives of the study were as follows: on-chip generation of normoxic and HyCo spheroids from two human STSs cell lines, validation of hypoxia-specific gene expression in HyCo spheroids, validation of hypoxia-induced radioresistance and chemoresistance in HyCo spheroids, validation of increased invasiveness of HyCo spheroids, application of HyCo spheroids to drug testing based on RNAseq data. The following sub-sections describe the various methodologies associated to each of these objectives.

5.8.2 Microfluidic chip

Negative molds of the top and bottom layers of the microfluidic chip were machined PMMA by computer numerical control Modela MDX-40A 3D milling machine (Roland, USA) using the chip design from our previously published paper. A mix of polydimethylsiloxane (PDMS) Dow SYLGARD 184 Silicon Elastomer Clear with a 1:10 ratio of Dow SYLGARD 184 curing agent (Ellsworth Adhesive, Canada) was used to cast the top and bottom layers of the chips. After a 15 min desiccation step, PDMS-filled molds were cured at 80 °C for 30 min in a Precision Compact oven (Thermo Fisher Scientific, Canada). The top and bottom layers of the chip were unmolded using tweezers, with inlets and outlets punctured using a 3 mm biopsy punch. Devices were then assembled manually after a 30 s exposure of each layer to atmospheric plasma using Enercon plasma gun (Enercon Industries Corporation, USA).

5.8.3 Cell culture

SK-LMS-1 human leiomyosarcoma cell line was purchased from American Type Culture Collection (HTB-88, ATCC, USA). STS117 cell line was kindly provided by Dr. R. Gladdy (Mount Sinai Hospital, Canada). STS117 is a human STS primary cell line harboring a loss of function mutation of TP53, derived from patients' primary extremity STS diagnosed as an undifferentiated pleomorphic sarcoma. SK-LMS-1 were cultured in Eagle's minimum essential medium (EMEM, 320-005-CL, Wisent, Canada), supplemented with 10% fetal bovine serum (FBS, 12483-020, lot: 2567894RP, Gibco, ThermoFisher, Canada) and 1% penicillin-streptomycin mix (450-201-EL, Wisent, Canada).

STS117 were cultured in Dulbecco's modified Eagle medium/nutrient mixture F12 (DMEM/F12, 319-075-CL, Wisent, Canada), supplemented with 10% FBS and 1% penicillin–streptomycin solution. Both cell lines were maintained by subculturing at 80% of confluency for a maximum of 30 passages. Briefly, after the culture medium was aspirated, cells were washed with D-PBS and subsequently trypsinized with 0.25% trypsin EDTA (325-043-EL, Wisent Inc., Canada) for 3–5 min at 37 °C. Once detached, the enzymatic reaction was stopped by adding appropriately supplemented culture medium, and cells were passaged 1:4 in a new cell culture flask.

5.8.4 Microfluidic Chip Preparation

Plastic inlets and outlets were connected to the microfluidic chips and assembled chips were placed in an empty pipet tips box for autoclave sterilization. Channels were first filled with 4 °C cold isopropanol to remove air bubbles. Beyond this step, the channels must remain filled with fluids to prevent air bubble formation. Then, the channels are washed three times with 200 µL 4 °C cold D-PBS (311-425-CL, Wisent, Canada), and three times with 4 °C cold PEG–PPG–PEG, Pluronic® F-108 solution (Sigma-Aldrich Canada Co, Canada). To prevent cell adhesion, Pluronic-filled devices were left to incubate overnight in 37 °C, 5% CO_2 incubator. Prior to cell seeding, the channels are rinsed three times with 200 µL 37°C D-PBS and another three times with 200 µL of 37°C appropriately culture media.

5.8.5 Spheroid Formation

To prepare cells for cell seeding, culture medium was aspirated, cells were washed with 5 mL of D-PBS and were trypsinized with 3 mL of 0.25 % trypsin 2.21 mM EDTA (325-043-EL, Wisent, Canada) and incubated for 3–5 min at 37 °C. Once detached, the enzymatic reaction was stopped by adding 7 mL of appropriately supplemented culture medium. The cell suspension was then collected in 50 mL Falcon tubes (Sarstedt Inc., Canada) and centrifuged for 5 min at 1500 rpm. The cell pellet is then resuspended in an appropriate volume to reach the final concentrations described in table 1. In prepared microfluidic devices, 200 µL of culture medium was aspirated from the outlet and 200 µL of cell suspension was added to the inlet. This step was performed three times and another three times starting from the outlet to the inlet, to ensure homogeneous distribution of the cell suspension. Culture medium is then changed every 24 hours until spheroids are formed.

Table 5-1 Cell suspension concentration for on-chip generation of HyCo and normoxic spheroids.

Spheroid type	Concentration (cells/mL)
Hypoxic-Core (HyCo) spheroids	4×10^6
Normoxic spheroids	2.5×10^6

5.8.6 RNA extraction

Three days after seeding, 15 spheroids (1 channel) were washed on-chip by pipetting three times 200 µL of 37°C D-PBS (ref, Wisent, Canada), then, washed three times with 200 µL of RNAlater stabilization solution (AM7020, Invitrogen, ThermoFisher Scientific, Canada) directly on-chip. RNAlater stabilization solution was used to stabilize and protect cellular RNA of spheroids to avoid RNA degradation and to allow long-term storage of samples. Spheroids were retrieved from the chip in 800 µL of RNAlater, transferred in a 1.5 mL DNA LoBind Eppendorf tube (022431021, Eppendorf), 200 µL of PBS were added and tubes were kept overnight at 4°C. 600 µL of RNAlater-PBS buffer was removed, 400 µL of ice-cold PBS was added and sample were centrifuged at 4000 min^{-1}.g for 3 min. The remaining 400 µL were removed, 600 µL of RLT buffer (Qiagen RNeasy® Plus Mini Kit, Cat. 74134, Qiagen, Canada) were added and tube was vortexed for 10 s. After, tubes were sonicated (xl-2000 Misonix, Canada) 3 times at level 6 for 1 s with 30 s rest on ice between each pulse. Lysates were centrifuge at 13000 min^{-1}.g for 3 min. Supernatants were then transferred in gDNA eliminator spin columns placed in a 2 mL collection tubes. Next, samples were processed following Qiagen Purification of Total RNA from Animal Tissues protocol using Qiagen RNeasy® Plus Mini Kit. Of note, no β-mercaptoethanol was added to RLT buffer as RNAlater was already used to prevent RNA degradation. Finally, RNA concentration was measured using nano drop spectrophotometers (DS-11 FX, DeNovix, USA).

5.8.7 RTPCR and qPCR

Reverse transcriptase (RT) PCR was performed using SuperScript IV VILO Master Mix with ezDNase enzyme kit (11766050, Invitrogen, Thermofisher, Canada) according to the manufacturer protocol. Mixture was gently homogenized, incubated at 37 °C for 2 min, briefly centrifuged and placed on ice. 4 µL of SuperScript IV VILO Master Mix and 6 µL of DNase-free water were added and gently mixed with the solution. Following steps were performed according to the manufacturer protocol. The resulting cDNAs were diluted 5-times in nuclease-free water and stored at -80°C until qPCR. PowerTrack SYBR green master mix kit (A46109, Applied Biosystems, ThermoFisher, Canada) was used for qPCR and samples were processed following the provided protocol. Samples were then placed in qPCR machine (Applied Biosystems™ StepOnePlus™ Real-Time PCR System). Expression of human GAPDH and Actin mRNA were used as endogenous control in the comparative cycle threshold method (2-δδCt) with the listed primers (PrimerBank, USA) [315], [316], [317].

Table 5-2 Primer sequences used for qPCR

GENE	FORWARD PRIMER	REVERSE PRIMER
ACTIN	CATGTACGTTGCTATCCAGGC	CTCCTTAATGTCACGCACGAT
GAPDH	GGAGCGAGATCCCTCCAAAAT	GGCTGTTGTCATACTTCTCATGG
CAIX	GGATCTACCTACTGTTGAGGCT	CATAGCGCCAATGACTCTGGT
CD47	AGAAGGTGAAACGATCATCGAGC	CTCATCCATACCACCGGATCT
CD73	CCAGTACCAGGGCACTATCTG	TGGCTCGATCAGTCCTTCCA
CXCL12	ATTCTCAACACTCCAAACTGTGC	ACTTTAGCTTCGGGTCAATGC
HIF1A	GAACGTCGAAAAGAAAAGTCTCG	CCTTATCAAGATGCGAACTCACA
LOX	GCCGACCAAGATATTCCTGGG	GCAGGTCATAGTGGCTAAACTC
PGK1	TGGACGTTAAAGGGAAGCGG	GCTCATAAGGACTACCGACTTGG
SLC2A1	GGCCAAGAGTGTGCTAAAGAA	ACAGCGTTGATGCCAGACAG
VEGFA	AGGGCAGAATCATCACGAAGT	AGGGTCTCGATTGGATGGCA
VIM	AGTCCACTGAGTACCGGAGAC	CATTTCACGCATCTGGCGTTC

5.8.8 Bulk RNA Sequencing

Upon RNA extraction, samples were sent for sequencing at McGill Genome Center, Victor Phillip Dahdaleh Institute of Genomic Medicine at McGill. The following protocols were followed:

Table 5-3 Bulk RNA sequencing protocol

QC, RNA, TapeStation
Library preparation RNAseq, NEBNextUltra II Directional RNA
Sequencing, Illumina NovaSeq6000 Sprime v1.5, PE100 (depth of ~400M reads per samples)
QC, Library for Illumina sequencing

All samples had RNA integrity (RIN) measured with RNA TapeStation. All samples had RIN values between 6.9 and 9.4.

5.8.9 RNA Sequencing Analysis

Unmapped paired-end sequences from an Illumina NovaSeq6000 sequencer were tested by FastQC v0.11.5 using a variety of metrics. Sequence adapters were removed and reads trimmed using Trimmomatic v0.39. The reads were mapped against the reference human genome (version hg38) using Burrows-Wheeler Aligner v0.7.17. Counts per gene were calculated with featureCounts v2.0.8 using annotation from Ensembl. Normalization and differential expression were calculated with DESeq2 (v1.46.0). Genes up- and down-regulated were identified with DESeq2 (p-value < 10e-6 and ≥ 2 fold change on pre-$\log_2$ transformed expression). Gene ontology terms enriched with protein-coding genes consistently induced by hypoxia in multiple cell lines were identified using WebGestalt 2024 (Benjamini corrected FDR < 0.05) [318].

5.8.10 Radiotherapy treatment

Conventional EBRT was used for on-chip irradiation of HyCo and normoxic spheroids. Briefly, culture medium was replaced before whole-chip single dose irradiation using a Gammacell 3000 irradiator (Best Theratronics, Canada) at 4 or 8 Gy. Clonogenic assay was then performed immediately after irradiation following the previously described protocol.

5.8.11 Drug treatment

5.8.11.1 Cisplatin

Cisplatin (1 mg/mL, DIN02355183, Accord Healthcare Inc., Canada) was obtained from the University of Montreal Hospital Center (CHUM) pharmacy and directly diluted in appropriate media at a final concentration of 5 µM (control: D-PBS). Treatment with cisplatin was performed 3 days after seeding by pipetting 3 x 200 µL in each channel. Then devices were incubated for 16 h at 37°C 5% CO_2 incubator.

5.8.11.2 Treatment for invasion assays

Table 5-4 Drug, buffer, concentration and control buffer concentration

Drug	Buffer	Concentration	Buffer Concentration (control)
Diethyl-pythiDC	DMSO	50 µM	1:2000

Diethyl-pythiDC was obtained from MedChemExpress (HY-103068, USA) and resuspended in DMSO (MedChemExpress, USA) (Table 2). Treatment with diethyl-pythiDC was performed off-chip. Spheroids were retrieved and plated as previously described in the Invasion Assay section. Then, 90 µL of treatment-media solution was added on top of each spheroid and the plate was incubated overnight at 37°C 5% CO_2 incubator. The next day, Invasion Assay protocol was performed, and plate was put inside the Incucyte S3 for image acquisition.

5.8.12 Immnunofluorescence Assay

For cisplatin treatment experiments, CellEvent Caspase-3/7 Green Ready Probe reagent was added to the culture medium of treated and untreated spheroids. 16 h after treatment, spheroids were washed three times with PBS directly in the device and fixed with Formalin 10% (Fisher Scientific Company, Toronto, ON, Canada) and 0.03 g/mL of sucrose (Invitrogen, USA) for 45 min. Then, spheroids were washed five times with PBS (Wisent Inc., Saint Jean-Baptiste, QC, Canada) and the top layer of the chip was peeled off. 15 spheroids per condition were retrieved using a cut-up 1000 µL pipet tip and pipetted directly into a histopathological cassette filled with optical cutting temperature (OCT) compound (Leica, Buffalo Grove, IL, USA). Included samples were left to sediment overnight, subsequently frozen on dry ice and stored at −80 °C. Frozen samples were sectioned using a Leica Cryostat (Leica, USA) with a 8 µm thickness and mounted onto glass slides. Sections were incubated for 1 h at room temperature with blocking buffer (PBS 1×, 3% IgG-free, Protease-free BSA, 0.5% Triton 100 10×). Sections were then incubated in a solution of blocking buffer with rabbit anti-CAIX (1:1000) (PA1-16592, ThermoFisher Scientific, USA) overnight at 4 °C. After washing three times with PBS, sections were then incubated in secondary antibody buffer (PBS 1×, 3% BSA) with AlexaFluor-647 antibody (1:750) (A31573, Invitrogen, USA) for 1 h at room temperature. Then, sections were stained with DAPI (1:5000 from 5 mg/mL stock solution) (D3571, Invitrogen, USA) to localize cell nuclei. Finally, sections were mounted using ProLong™ Gold Antifade Mountant (P36934, Invitrogen, ThermoFisher Scientific, USA). Fluorescence images were obtained on a Zeiss fluorescence microscope with ZEN microscopy software (Carl Zeiss AG, Germany).

5.8.13 Clonogenic Assay

For each condition, after channels were washed with warm D-PBS, 5 HyCo spheroids and 21 normoxic spheroids were pipetted in a 15 mL Falcon tube. The spheroids were then centrifuged for 2 min at 1500 rpm, and D-PBS was aspirated. 300 µL of trypsin were added and left to incubate for 8 and 5 min respectively. Afterwards, a total of twenty ups and downs were performed with the pipette to ensure complete dissociation, and 700 µL of warm culture medium were added to block enzymatic reaction. 10 µL of cell suspension is then mixed to 10 µL of trypan blue in a 96-well plate, and 10 µL of this solution is pipetted in a cell counting slide to perform cell counting using a TC 20^{TM} Automated cell counter (BioRad, Canada).

The cells are then centrifuged for 5 min at 1500 rpm, and the pellet is resuspended in appropriate volume to obtain a 1×10^5 cells per mL solution. Then, the appropriate number of cells were seeded in triplicate in 6-well plates (3516, Corning Inc, Canada), of appropriate culture medium. Plates were kept in a 37°C 5% CO_2 incubator with medium being changed every 3 days. After 10 days, wells were rinsed with 1 mL of D-PBS, and 2 mL 70% methanol solution containing 0.5% crystal violet (Sigma-Aldrich, Canada) was added to fix the colonies. After rinsing them with water, plates were imaged with Chemidoc (Bio-Rad, Canada). Colonies were manually counted using ImageJ software and normalized to the number of cells seeded to calculate clonogenic survival, which was in turn normalized to the control condition [319].

5.8.14 Invasion Assay

Each microfluidic chip was placed in a petri dish to prevent spillage. The top layer was carefully peeled off using a pair of sterile tweezers, leaving the well layer containing the spheroids exposed. Then, 400 µL of appropriate culture media were added on top, and spheroids were harvested using a cut-up 1000 µL pipet tip to avoid damaging them. Spheroids are then individually pipetted in 90 µL of appropriate culture media into an ultra-low-attachment round bottom 96 well-plate (7007, Corning, USA). Media is then removed and 90 µL of media-drug mixture is added and spheroids are incubated at 37 °C 5% CO_2 for 24h. The next day, the plate was cooled over ice using a cooling plate in a cool box until it reached approximately 4°C, at which point 90 µL of phenol-red free Matrigel (356237, Corning, USA) were added. The plate was then centrifuged at 300 rpm for 1 min at 4°C. Then, the plate was incubated for 30 min in a 37 °C 5% CO_2 until the Matrigel polymerized. Finally, 50 µL of media alone or media-drug mixture were added, and the plate was placed in Incucyte S3 (Sartorius AG, Germany) for image acquisition over 10 days. Brightfield images were analyzed using custom ImageJ software analysis pipeline, by intensity thresholding to delimit three regions of interest (ROI) : edge, intermediate and core (Fig. 4.B) [319]. Invasion indexes A and B were calculated using the following formulas. When comparing small normoxic and HyCo spheroids, invasion indexes A and B were normalized to their values at day 0 to account for size-induced biases. For each spheroid, invadopods were manually counted on the day where the difference in invasion indexes between conditions was the highest. Invadopod count is then normalized to the circumference of the edge ROI, estimated from the total invasion area, on the same day.

5.8.15 Statistical analysis

Statistical analysis was conducted using GraphPad Prism (Version 9.0.1, GraphPad, USA). For spheroid size distribution, diameters were analyzed for significance using an unpaired t-test. For RNAseq, gene expressions were analyzed for significance using DESeq2 built-in statistical analysis. For gene ontology analysis, False Discovery Rate (FDR) correction is applied using Benjamini-Hochberg (BH) method. For clonogenic assay, clonogenic survival of spheroids were analyzed for significance using Holm-Šídák's multiple unpaired t-test. For IF, caspase 3/7 signal was analyzed for significance using a two-way ANOVA with Šídák's multiple comparisons test. For invasion assays, invasion indexes and invadopod densities were compared using a two-way ANOVA with Šídák's multiple comparisons test and unpaired t-test, respectively. For invasion assay of treated spheroids, a mixed-effects analysis with Šidák’s multiple comparisons test was used due to uneven group sizes for SK-LMS-1.

5.9 Acknowledgments, Fundings and Contributions

We thank Dr. Audrey Glory for her support and advice. We also thank Guillaume Cardin, Isabelle Clément, and Dr. Nicolas Malaquin for their help with EBRT irradiation. Finally, we thank Liliane Meunier and Véronique Barrès, of the CRCHUM's molecular pathology core facility, for performing the cryo-sectioning and slide mounting steps.

Funding: This research was conducted as part of the activities of the TransMedTech Institute, thanks in part to the financial support of the Apogee Canada First Research Excellence Fund. T. G. acknowledges funding from the Natural Science and Engineering Research Council of Canada (NSERC, RGPIN – 2020 – 06838). We also acknowledge funding from Fonds de recherche du Québec – Nature et technologies (FRQNT), Institut du Cancer de Montreal and Bourse Canderel.

Author contributions:

Conceptualization: ERM, PW, TG
Methodology: ERM, RC, JL, DY
Software: ERM, DY
Validation: ERM, RC, PW, TG
Formal Analysis: ERM, RC, DY
Investigation: ERM, RC
Resources: PW, TG
Data Curation: ERM, DY
Project administration: ERM, PW, TG
Visualization: ERM
Supervision: TG, PW
Funding acquisition: ERM, PW, TG
Writing—original draft: ERM, RC
Writing—review & editing: ERM, RC, JL, TG, PW

All authors have read and agreed to the published version of the manuscript.

Competing interests:

P. W. and T. G. are co-founders and shareholders of MISO Chip Inc. a spin-off company dedicated to on-chip 3D biology. The funders had no role in the design of the research, in the collection, analyses, or interpretation of data, in the writing of the manuscript, or in the decision to publish it. All other authors declare they have no competing interests.

Data and materials availability:

The data presented in this study are available on request from the corresponding author.

5.10 Supplementary Materials

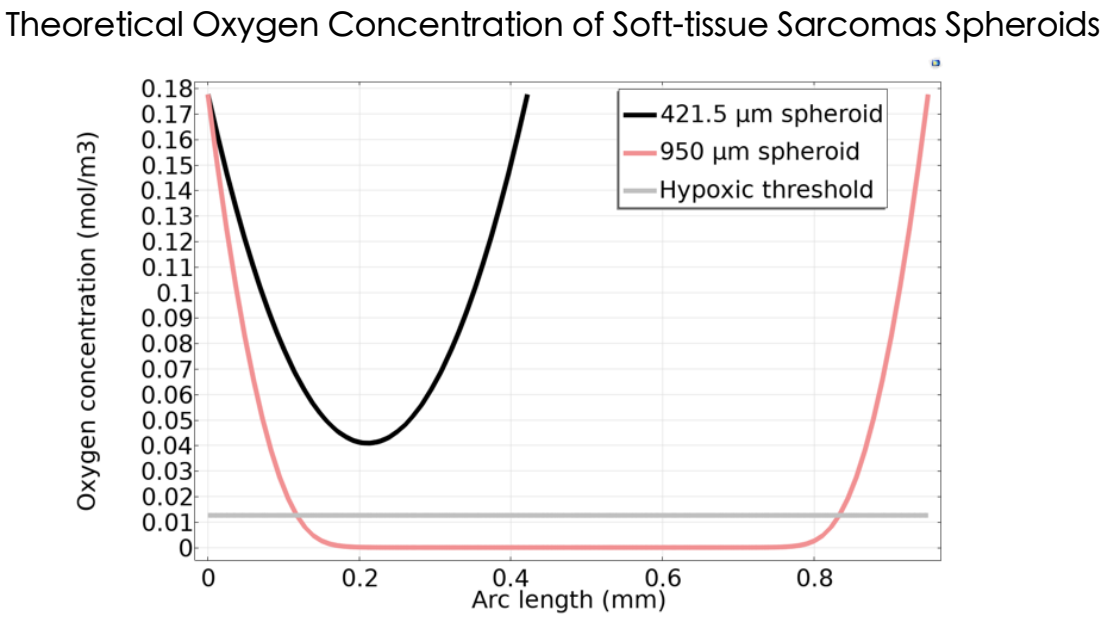

Figure 5-7 In silico model of the oxygen concentration in an on-chip soft-tissue sarcoma spheroid, depending on its diameter.

HyCo spheroid diameter was set at 950 µm, and based on previous results normoxic spheroid diameter was set at 421.5 µm. Hypoxic threshold is set at 10 mmHg, i.e. the threshold for CAIX expression.

Figure 5-8 Volcano Plot of combined SK-LMS-1 and STS117 HyCo spheroids compared to normoxic spheroids. All data comes from N = 3 to 4 independent experiments.

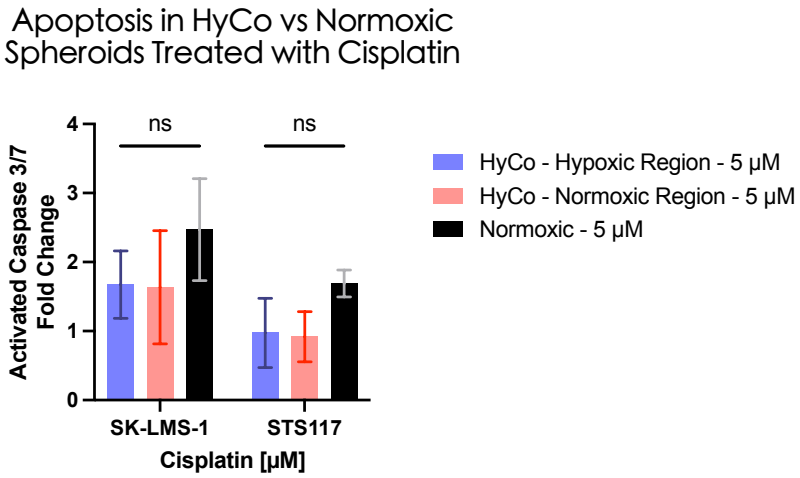

Figure 5-9 Quantification of apoptosis signal (activated caspase 3/7) after overnight exposure to 5µM of cisplatin in SK-LMS-1 and STS117 HyCo and normoxic spheroids.

Data are presented as mean ± SD, (ns) : non-significant, N=3 independent experiments, n = 2 to 8 spheroids, 2way ANOVA, Šidák's multiple comparisons test.

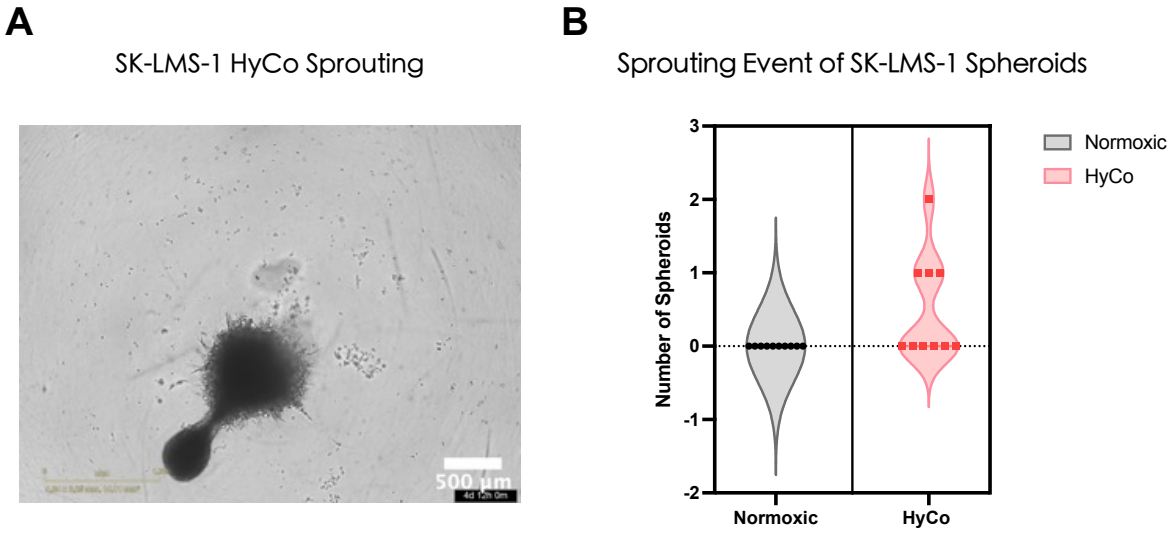

Figure 5-10 Sprouting Event in SK-LMS-1 HyCo Spheroids

(A) Brightfield image of sprouting spheroid. (B) Quantification of sprouting event in SK-LMS-1 normoxic and HyCo spheroids over 10 days.

CHAPTER 6 DISCUSSION

This project started as my M.Sc. A. project with a simple question: how big can a spheroid be while remaining alive without any vasculature or perfusion? To this simple question asked by Prof. Thomas Gervais, my co-director Dr. Philip Wong added: “It would very interesting if the spheroid would be big enough to exhibit hypoxia”. From that initial exchange with my supervisors, what would ultimately become my Ph.D project was born: hypoxic spheroids on-chip.

As I have presented in the literature review, the more I delved into the field of cancer research and hypoxia the more I realized how and why hypoxia was often left aside. Hypoxia was often being referred to in the discussion sections to explain potential observed effects or as future work, rather than being the object of a research hypothesis within the papers themselves. I observed this firsthand at the Montreal Cancer Institute, where no one was including hypoxia to their research hypothesis at the time of the beginning of my project despite its relevance for many of their research fields and hypotheses.

However, this is no fault of their own and it is easily understandable given the complex setups needed and the many constraints of working with hypoxia. Therefore, I wanted to facilitate the integration of hypoxia to cancer research hypotheses by engineering a better *in vitro* preclinical tool, using the advantages of microfluidics. To address this unmet need, this tool must be compact, simple, user-friendly and compatible with the generation, treatment and bioanalysis of clinically-relevant hypoxic 3D tumor models.

6.1 The Quest for the Biggest Spheroid on-Chip

My first objective was to generate the largest spheroid on-chip possible, and to assess if it was hypoxic. Based on previously-published microfluidic chips from our group, I designed multiple iterations of small microfluidic chips, progressively increasing the diameter of the spheroids I was able to produce. I designed, 3D-printed and manufactured multiple versions of the chip based on the design of Patra et al. (2019). Patra's chip has a straightforward design consisting of 2 layers: the "channel layer" containing the culture channel(s) and the "well layer" containing the spheroid culture wells. The channel layer consists of two 70 x 4 mm rectangular channels, with a total volume of ~ 200 µL each. Below each channel, the wells are arranged as 5 groups of 3 x 8 grids of 0.5 x 0.5 x 0.5 mm^3 square wells. Using this chip, our team was able to produce spheroids of ~ 250 µm of diameter. My initial approach was to simply incrementally scale-up the size of the wells until it reached 1 x 1 x 1 mm^3 as shown in figure 5-1. Each increment was accompanied by an optimization of cell seeding density to yield, every time, a larger spheroid than the last iteration.

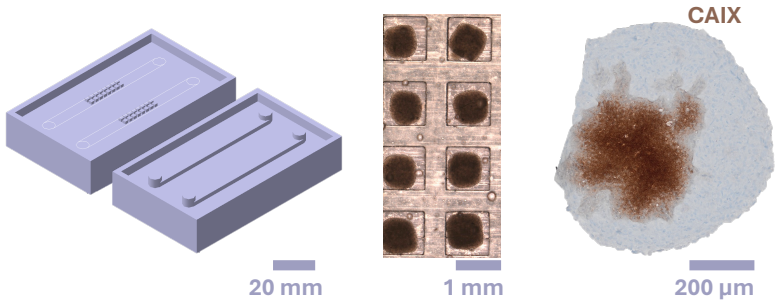

Figure 6-1 CAD of well and channel layers molds of Patra's adapted chip (1 mm^3 well). STS117 spheroids 2 days post seeding. CAIX immunostaining

Using what would be the last iteration of this chip, and after optimizing cell seeding density, I generated the largest spheroids produced in our lab: 800 µm of diameter STS117 spheroids (figure 5-1). I decided to leave the race of the largest spheroid once I reached the 800 µm cap. As a 400 µm spheroid should have a few cells under hypoxia, a spheroid twice the size should harbor a substantial hypoxic core. Thus, I performed an immunostaining to assess the presence of hypoxia by staining for CAIX using the paraffin embedding method developed by Simeone et al. (2019) in collaboration with our lab (figure 5-1). After confirming that I was able to produce large spheroids with a positive signal of CAIX, I wanted to improve the chip design.

Indeed, the designs of chips used in our lab are at times inefficient, with a relatively high footprint compared to their size and their throughput with only 2 distinct conditions (i.e., 2 channels), and are not compatible with multipipettes. This high footprint extends to their molds, with only 2 devices (4 channels) being fabricated each time, requiring 2 separate steps of plasma bonding. As each fabrication requires roughly an hour, the chip fabrication rate is of a mere 4 channels per hour. As everyone knows, working in biology is already time consuming without much room for optimization, and finding ways to save time when doable can go a long way. Therefore, I wanted to optimize my chip to produce a maximum number of channels in the minimum amount of time. Initially, chips were manufactured at Polytechnique, and all the biology was achieved at the CRCHUM, a 45 min trip between the 2 institutions, also explaining why I wanted to increase chips production rate. Since then, a chip fabrication station has been made available at the newly launched Microfluidics Core Facility at the CRCHUM.

Taking inspiration from the honeycomb structure of bee hives and their high compacity, I changed the design of the well to hexagons. Compared to squares, this also increases the well volume per spheroid, and helps with their sphericity. It increases the compactness of the device. Well area over total area is maximized in hexagonal arrays compared to face centered square arrays. Finally, it also preserves a three-fold symmetry around each well which can be exploited in certain applications, such as brachytherapy, where the distance between wells is important. This modification allows to produce a chip no larger than a glass slide, containing 3 channels with only 8 wells in each, enabling the production of 24 large spheroids (figure 5-2, left schematic). Again, I confirmed that I could generate 800 µm spheroids harboring a hypoxic core. However, this chip was just a test design before the production of an even larger chip.

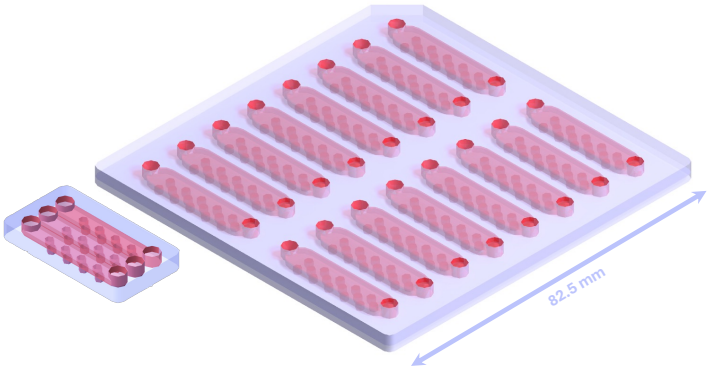

Figure 6-2 Schematic of the antepenultimate and ultimate versions of my chip

Upon confirmation of the channels and well designs, spheroid generation and CAIX content, I developed the final and last version of my chip: 16 channels, 15 well each for a total of 240, no larger than a 96 well plate and compatible with an 8-channel multipipettes (figure 5-2, right schematic). My thought process was to engineer a chip design that could ultimately be compatible with the pipetting robots used by pharmaceutical companies. With this new design, I was able to produce 16 channels per hour, a 4-times higher yield than what was previously implemented. This chip is assembled using only one plasma bonding step, and can then be cut into smaller chips with an unspecified number of channels depending on experimental requirements. This design is more efficient, easier to manufacture and more versatile, making it more user-friendly altogether. On a side note, the initial design by Patra et al. was ultimately modified within our lab to slightly increase the spheroid size closer to that of MDTs, but still yielded spheroids smaller than the threshold for hypoxia. As such, I used this modified design to generate all of my negative (and positive) controls for both of my publications.

This work completed the first objective of my thesis: I produced, at that time, the largest spheroid on-chip. Since then, 3 publications have reported larger on-chip spheroids: one from our group (Chermat et al., 2024 [55]), one from Pires' group (Pyne et al., 2024 [207]) and another one from myself. As such, my next objective was to characterize the large spheroids produced on my chip.

6.2 The Trials of Hypoxia Validation

The characterization of my hypoxic-core spheroids, initially referred to as "jumbo spheroids" in my 1st publication, was essential to convince biologists that the hypoxia they contained was similar to *in vivo* hypoxia.

The step 0 was to compare my data with both a negative and a positive control. I used small spheroids (diameter < 450 µm) as a negative control as they should not exhibit any hypoxia, which was confirmed by an immunostaining of CAIX. However, the challenge was to find a suitable positive control. The easiest way was to artificially induce hypoxia in HyCo spheroids 24 h post seeding, not dense enough to express hypoxia yet. To do so, I placed the chip inside an Acrylonitrile "engineered pouch" (i.e., a nitrile glove), removed the air using the biohood vacuum and incubated this setup for 2 h and 6 h and stained for CAIX signal. I also needed a control for these hypoxia-induced spheroids to compare if expression of CAIX in the cell lines I used was truly positive.

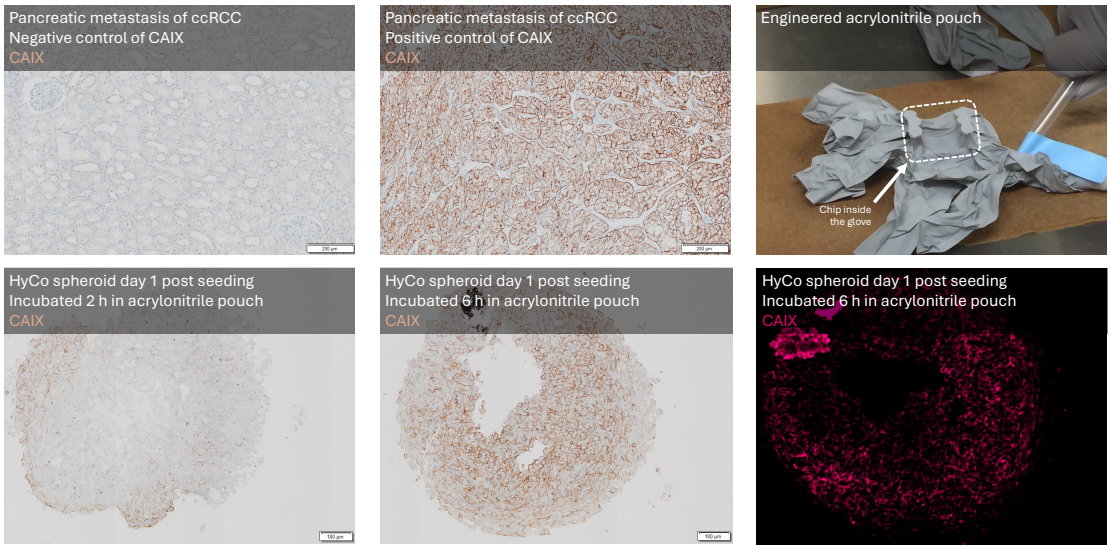

Figure 6-3 Control of hypoxia. CAIX stainings and hypoxia induction setup

For this, I compared my positive controls to 2 pancreatic metastases from clear cell renal cell carcinoma (ccRCC) tumor biopsy slides kindly provided by Mame-Kany Diop from Dominique Trudel's research group, one positive and one negative for hypoxia. Staining results demonstrate that I was able to artificially induce hypoxia with a signal comparable to the biopsy slide of ccRCC metastasis positive for CAIX as shown in figure 6-3.

Of note, still with the goal of streamlining the experimental processes as much as possible, the 3 days/20 steps paraffin-embedding and processing of spheroids was quickly replaced by a 1 day/5 steps OCT inclusion protocol.

Nevertheless, as the engineered pouch was not a standard method of inducing hypoxia and thanks to the availability of an oxygen-controlled incubator from Francis Rodier's lab, I decided to use this incubator to artificially induce hypoxia in small normoxic spheroids. As such, I was confronted to all the problems rising from the use of an oxygen-controlled incubator, among which the need to work extremely fast to compensate for reoxygenation and protein degradation.

After finding a way to have both positive and negative controls for my HyCo spheroids, I performed a Western-Blot and IF to assess the expression of HIF-1α and its downstream target CAIX. Again, this first experiment was extremely challenging regarding the positive control. As stated in the literature review, as soon as the door of the oxygen-controlled incubator is opened, samples reoxygenate. As such, due to HIF-1α short half-life (8-10 min), I had to process my samples extremely fast [320]. To put it simply, all positive control experiments for my first paper required a lot of running around to limit reoxygenation. The fact that my HyCo spheroids were substantially easier to generate and manipulate for experimental purposes than any positive control was not lost on me. It proved early-on a strong point of this thesis: that *in vitro* study of hypoxia is a tedious process that must be refined to potentiate pre-clinical research.

Another question arose from these first experiments: how to compare my hypoxic-core spheroid to an imperfect standard? Indeed, if we go back to the literature review, the discrepancies between induction of hypoxia and *in vivo* hypoxia are well-known and range from differences in gene expression to treatment response. Should I expect my HyCo to have similar protein levels as hypoxia-induced small spheroids? Should I expect that they do not and if so, how would I justify using them as positive controls? Positive controls of what exactly? In fine, these "positive controls" were considered more as another set of samples rather than true positive controls. Their role was as much to provide a reference point for *in vitro* hypoxia as to showcase their inadequacies.

With this consideration in mind, my first publication showcased that HyCo spheroids express gold-standard hypoxic protein CAIX in their core only, but HIF-1α protein expression was trickier to observe. Indeed, I only observed significant level of HIF-1α in positive controls for both SK-LMS-1 and STS117, but only in STS117 for HyCo spheroid.

One possible explanation was the altered MYC pathway leading to a dysregulation of HIF-1α expression. This was further confirmed in my second publication by the RNAseq data, as MYC was indeed significantly downregulated in SK-LMS-1 HyCo spheroids. In addition, even if the role of HIF-3α in the hypoxia-response pathways is still not fully understood, its upregulation in HyCo SK-LMS-1 spheroids could also play a role in the low level of HIF-1α observed. Surprisingly, IF staining of HIF-1α was unsuccessful even in positive controls, contradicting the Western-Blot results. Indeed, no signal was observed in positive controls despite antibody concentrations as high as 1:50 (recommended concentration by the manufacturer was 1:500). This can be explained by the increased duration of preparation steps, namely the 35 min fixation, giving ample time for HIF-1α degradation. Overall, this also confirms the difficulty of working with hypoxia given the short half-life of hypoxia-related molecules and the non-negligeable risk of reoxygenation.

Following consultation with the other authors of the 1st manuscript, I decided to no longer use the so-called positive controls again: they are disproportionally hard to work with, are incompatible with some of my experiments and are a poor representation of the *in vivo* hypoxia I was trying to emulate.

To further confirm that HyCo spheroids responded as *in vivo* hypoxic tumors, I treated them with the known hypoxia activated prodrug (HAP) tirapazamine (TPZ), and radiotherapy (RT). My hypothesis was: if HyCo spheroids are sensitive to TPZ and resistant to RT, then their hypoxia will have value for preclinical studies. I demonstrated that 35 µM of TPZ was preferentially cytotoxic to the hypoxic core rather than to the normoxic region of the same spheroid. Unexpectedly, there was no difference in response to RT between the hypoxic and normoxic regions, i.e. no hypoxia-induced radioresistance, despite an evident dose-response to RT. However, this might be explained by the choice of assay and timepoints I used to assess response to RT. Standard methods for evaluating RT efficacy consist of either staining for reporters of DSBs (γH2AX, 53BP1) 30 - 45 min after irradiation or performing a clonogenic assay. The γH2AX protein is the first step in recruiting and localizing DNA repair proteins following the formation of a DNA double-strand break (DSBs) due to endogenous or exogenous stimuli (e.g., ionizing radiation). γH2AX appears as foci within cell nuclei representing the DSBs in a 1:1 manner, making it a highly sensitive biomarker for DNA damages. Like γH2AX, 53BP1 (i.e. p53-binding protein 1) is also recruited at the site of DNA damages to recruit other DNA repair proteins, and appears as foci [2].

The 30 - 45 min post-RT is generally chosen, as it corresponds to the peak of recruitment of DSB reporters [2], [321]. Another option is the clonogenic assay, which allows the observation of the overall survival, accounting for all types of cell death resulting from mitotic catastrophe for up to two weeks after treatment. As an in-between, I chose to quantify DSBs by staining for γH2AX 24 h after RT, this timepoint having been shown to correlate with clonogenic survival [277]. However, as this correlation was established on 2D cell cultures and xenografts using FACS analysis, translating it to my newly validated HyCo spheroids using IF was quite a gamble. In hindsight, performing both assays separately would have probably enabled me to observe the radioresistance in terms of both decreased induction of DNA damages and increased clonogenic survival, which was ultimately observed in another publication from our group and in my second paper [55]. The efficacy of TPZ + RT was also assessed by staining for γH2AX 24 h after treatment, with the combination appearing to have additive effects in both hypoxic and normoxic regions. Once again, the use of other assays and time point of interest might have yielded different results. As previously mentioned, γH2Ax appears as foci within the nucleus, and contrary to 2D models, cell nuclei cannot be individually segmented in our 3D spheroids. In addition, cells and their nuclei might intersect with the 2D slice at different heights, therefore only appearing as fractions of the total cell/nuclei. As such we elected to quantify foci per mm^2 of nuclei, a method that cannot be easily compared to measurement of hypoxia gradient within the spheroid. Although any number of small regions of varying oxygen levels could have been defined, we ultimately elected to only discriminate between hypoxic and normoxic nuclei area by CAIX expression.

Finally, as other students in our lab wanted to use the hypoxic-core spheroid and as one of the Gervais' lab expertise is designing in silico model, Rodin Chermat and I elaborated a finite element model of oxygen consumption as a function of spheroid size. Based on hypoxic content of HyCo spheroids derived from our CAIX IF staining data and on the methodology described by Grimes et al., this model correctly predicted that, solely based on their size, our small spheroids would indeed be normoxic [47]. Since then, the hypoxic content of all spheroids generated in our lab match with this model, regardless of their size, with slight variations attributable to cell line-specific differences (e.g., smaller cells, denser spheroids, higher metabolic rate).

With this, I had demonstrated that my HyCo spheroids were indeed hypoxic and seemed to respond to treatments as hypoxic tumors would, but there was still a long way to go if I wanted to convince biologists to adopt this model and methodology. This became the focus of my second publication: do my HyCo spheroids recapitulate clinical hallmarks of hypoxia?

6.3 "If it looks like clinical hypoxia and behaves like clinical hypoxia …"

Following the adage "if it quacks like a duck and walks like a duck …", my goal was to show that since HyCo spheroids recapitulate hallmarks of clinical hypoxia, they are close enough to *in vivo* hypoxic tumors to have value at the fundamental and preclinical levels. My goal was to convince potential users by showing them not only the CAIX core but also the quantifiable downstream effects of hypoxia on gene expression, treatment resistance and invasiveness.

I delved deeper in the characterization of the HyCo spheroid on-chip, progressively adding building blocks to the work I have done.

Characterizing gene expression was a necessary step to convince biologists, and was the obvious next step of my thesis, therefore I assessed the relative expression of a selection of 11 hypoxia-related genes by RTqPCR. In addition, this first experiment was conducted to de-risk a potential future bulk RNAseq. Indeed, as a reminder for the members of the jury, only 30 % of the volume of HyCo spheroid is hypoxic and I was at the time unsure if this hypoxic content would be enough to counterbalance the gene expression of the normoxic region. As RTqPCR results were conclusive, meaning that almost all hypoxia-related genes had an increased relative expression compared to small normoxic spheroid, I followed through with the whole genome bulk RNAseq.

Unequivocally, RNAseq provided clearly distinct gene expression profiles between small normoxic and HyCo spheroids. It is worth noting here that since only 30 – 45 % of the total volume of the HyCo spheroid is hypoxic, the gene expression changes induced by hypoxia are diluted by a similar factor. Still, all upregulated genes in HyCo spheroids were associated with hypoxia and was further confirmed by the gene ontology analysis. Indeed, upregulated pathways were associated with response to hypoxia and metabolic changes in accordance with what was found by Yang et al, who also studied hypoxia in STS patients [19].

However, RNAseq results of STS117 were not as clear as that of SK-LMS-1. This difference highlights the importance of using various patient-derived or commercial cell lines to better represent the many STSs subtypes. Thanks to our versatile methodology, many spheroid forming cell lines can be tested, be they subtypes of STSs or different cancer types altogether. These results completed the validation of the 1st hallmark: hypoxia-specific gene expression profile.

As I was not able to demonstrate the RT resistance of the HyCo spheroids in my 1st paper, and as another student from our group had been able to do so in the meantime, I wanted to showcase in my 2nd paper that they were resistant to both RT and CT [55].

Therefore, I repeated the previous experiment, treating both normoxic and HyCo spheroids with 4 Gy and 8 Gy of RT, this time assessing RT efficacy using clonogenic assay. Results showcased a higher clonogenic survival of HyCo spheroid after RT, proving their inherent hypoxia-related radio-resistance. In addition, I treated spheroids with cisplatin, a common CT. Although cisplatin is not used in the context of STS patients, hypoxia-related cisplatin resistance and its mechanisms are widely known and recapitulating them would be convincing to many. Again, I was able to demonstrate that HyCo spheroids were less sensitive to cisplatin compared to their smaller normoxic counterparts. These results confirmed a 2nd hallmark: hypoxia-related treatment resistance.

Finaly I was interested in the increased metastasis potential attributed to hypoxia. The spheroid invasion assay is a newly validated method correlating with metastasis progression [322], [323]. Briefly, it simply consists of placing individual spheroids in a ULA 96-well plate, embedding them in Matrigel and following their growth and invasion overtime using brightfield microscopy. For once, this method does not require dissociation or fixation of spheroids, HyCo spheroids can be kept intact and alive for the duration of the experiment. This preserves the oxygen gradient and cross-talk between hypoxic and normoxic regions, essential to the metastatic cascade. With this method, I was able to observe an increased invasion potential in HyCo spheroids compared to small normoxic ones, demonstrating their more aggressive phenotype. As such, HyCo spheroids recapitulate yet another hallmark of hypoxic tumors: hypoxia-related aggressive phenotype.

With the last figure of my 2nd paper, I wanted to showcase possible applications of HyCo spheroids, such as a RNAseq-based drug screening using invasion assays. Invasion assays are indeed compatible with treatment screening on whole spheroids, again retaining the coexistence of hypoxic and normoxic cells found *in vivo*. Spheroid invasion in Matrigel can be thought of as analogous to tumor burden, with each spheroid being a microtumor, without requiring animal models. However, invasion assays must still be performed off-chip and do not take full advantage of the microfluidic format. Indeed, I was not able to inject Matrigel® inside the chip due to its high viscosity.

Overall, “if it looks like clinical hypoxia and behaves like clinical hypoxia …” then it must be sufficiently close to it. HyCo spheroids recapitulate key hallmarks found in hypoxic solid tumors and can thus be used as preclinical models of said hypoxia in translational cancer research.

6.4 Limitations

This body of work demonstrated that on-chip HyCo spheroids have many advantages for the fundamental and preclinical study of hypoxia and its effects on phenotype and treatment response, both my microfluidic device and on-chip spheroid models have a number of limitations hindering their potential. These current limitations must be addressed to improve the chances of the broader adoption of my device and HyCo spheroids by other translational cancer researchers, be they in my lab, at the Montreal Cancer Institute or in other research centers.

First, despite being versatile and user-friendly, all bioassays have to be performed off-chip apart from treatments. For example, the chip is not compatible with the Incucyte® imaging system, being one reason for spheroids transfer into a ULA plate for invasion assay. While rinsing, fixation or RNA stabilization can be done on-chip in an efficient cost-effective and streamlined manner, spheroids have to be extracted from the chip to perform most bioanalysis protocols (RNA extraction, clonogenic assay, OCT embedding). This limitation is not specific to the microfluidic format however, as spheroids must also be removed from a 96-well plate for bioanalysis. Conversely, whole spheroid imaging techniques are physically-limited by the size of the sample regardless of whether the spheroid has been generated on-chip or off-chip. Still, despite the transparency of PDMS, imaging of on-chip spheroids cannot provide information on its internal structure, viability or protein expression. These limitations are as much a limitation of chips themselves, among which my own, as of spheroid-based assays altogether. The development and validation of non-destructive biomarker-based assays (e.g., cfDNA, soluble biomarkers) has been gaining interest *in vivo* and clinically, and could be easily translated to spheroid models. Uniquely, by concentrating 15 spheroids in a 250 µL channels my design is advantageous for culture medium-based assays compared to 96-well plates, as any biomarker of interest will also be more concentrated and thus easier to detect. The exploration of this research avenue is the topic of Maryam Ziaee's ongoing PhD project in Prof. Gervais and Dr. Wong's labs, with my chip being used to generate spheroids and quantify soluble biomarkers of interest.

Second, HyCo spheroids can only be generated from spheroid-forming cell lines. Although in appearance self-evident, this means that potential cell lines of interest must be able to coalesce into a dense spherical aggregate using our on-chip method to be compatible with my methodology. Although I was able to generate HyCo spheroids from all STSs cell lines available in our lab (SK-LMS-1, SW684, SW872, MCA205, STS117, STS93), users of my device and/or protocol were not always as lucky. While head and neck carcinoma (FaDu), colon carcinoma (HCT116), lung adenocarcinoma (A549) and breast cancer (HCC1954, Hs578T, MCF7, MDA-MB-361) cell lines prove successful, no prostate cancer cell line has yet been able to yield a HyCo spheroid. Plate-based spheroid generation generally consists of plating a small number of cells and waiting for them to proliferate into a spheroid. Our on-chip method bypasses this growing phase by directly seeding a high number of cells, extremely high in the case of HyCo. As such, on-chip spheroid formation ability is probably linked to the ability and propensity of cells to aggregate and to the speed at which they do (or do not). However, it should be possible to adapt the plate-based method to the chip which will be further investigated by other students.

Although addition of compounds promoting spheroid formation (Matrigel, collagen, chitosan) could be considered in well-plates, it is made challenging on-chip due to their high viscosity. Indeed, the injection of these compounds to a microfluidic channel systematically results in a large quantity of bubbles, i.e. the microfluidicist's archenemy, preventing the filling of the wells around the cell aggregate.

Third, my model is made from cancer cells only, while tumors are comprised of a mix of multiple cell types (fibroblasts, endothelial cells, immune cells). This could limit the translational potential of the HyCo spheroid. For example, one hallmark of hypoxia that was not addressed in my thesis, is its impact on immune cells. While being one of my research objectives at the beginning of my thesis, it quickly became evident that it was beyond the scope of this work. However, Aliya Ortaaslan, an undergrad student in Dr Wong's lab, demonstrated the feasibility of harvesting peripheral blood mononuclear cells (PBMC) from mice spleen and to put them in contact with spheroid on-chip. Similarly, impact of hypoxia on cancer-associated fibroblasts is well-known. Rodin Chermat, PhD student in Prof. Thomas Gervais' and Dr. Philip Wong's labs, is currently validating HyCo co-culture spheroids comprised of both colon carcinoma and colon fibroblast cell lines.

Finally, integration of vasculature to on-chip spheroids has been demonstrated in other research groups and could be applied to HyCo spheroids following slights modification of the chip design [324], [325].

Overall, although my HyCo spheroid and my microfluidic chips are not without limitations, most of these can and hopefully will be addressed in future work.

CHAPTER 7 CONCLUSION AND RECOMMENDATIONS OF HYPOXIA AND CHIPS

As I have discussed throughout this document, hypoxia has a major impact on cancer and cancer treatment efficacy. Hypoxia is one of the culprits behind chemoresistance, radioresistance, and immunoresistance, increased tumor growth, increased metastasis potential and overall poor patient prognosis. As such, its integration at the fundamental and preclinical level is of paramount importance for the identification of biomarkers, the understanding of its underlying mechanisms and the development of better treatment modalities. However, all preclinical methods for the study of hypoxia are either cumbersome, limited, and are poor representations of clinical hypoxia.

The purpose of my PhD project was to design a microfluidic chip for the generation of tumor spheroids that naturally express a hypoxic-core, characterize their multi-layered structure, validate hallmarks of clinical hypoxia and study its impact on treatment efficacy. My overarching goal was to finally provide a user-friendly tool to study hypoxia at the fundamental and preclinical level for translational cancer research.

As described in my thesis and my two publications: my HyCo spheroids are hypoxic, and this hypoxia is akin to clinical hypoxia. As a biomedical engineer, I have provided researchers with a user-friendly tool to study hypoxia at the fundamental and preclinical level for translational cancer research.

In my own research group, 2 students, Maryam Ziaee and Sara Ghasemi, are using my chip for their Ph.D projects. Maryam is working on validating cell-free DNA as a biomarker of hypoxia and treatment response in STS and colorectal cancer, while Sara focuses on the role of hypoxia-related G3PP protein in castration resistant prostate cancer. Dr. David Roberge, head of the radio-oncology department at the CHUM, and his M.Sc. student Dr. Kevin Pehr will also be using my chip to generate preclinical data on efficacy of FLASH RT modality in non-melanoma skin cancer to justify a clinical trial. Dr. Clara Fallone, medical physicist at the University of Calgary, and her team are currently using my chip to demonstrate that MRI can be tuned to quantify hypoxic content of tumors. France Coulet, Ph.D student at the Université de Bretagne Occidentale in France in Prof.

Hymery's lab, is using my device to investigate the effect of mycotoxins on liver organoids. Following my first publication, Rodin Chermat (Ph.D student in our group) adapted my chip design for brachytherapy irradiation of my HyCo spheroids, further demonstrating the use of my methodology. In addition, 2 students under his supervision will be using his chip and by extension my HyCo spheroids model to elucidate the mechanisms of FLASH RT efficacy.

While resulting in more complex *in vitro* tumor models, the challenges of spheroid culture still prevent their broad adoption to the field of cancer research. Taking the Institut du Cancer de Montréal as an example, most groups and researchers still prefer 2D culture or *in vivo* models. By showcasing the potential of microfluidics for user-friendly culture of hypoxic 3D tumors models, I hope that more will use chip-based approaches to ease their transition to 3D culture and will progressively adopt my methodology or similar on-chip approaches to incorporate hypoxia to their research hypothesis. As Gerardo Ferbeyre (Chairholder of CIBC Chaire en Recherche sur les Causes du Cancer du Sein de l'Université de Montréal and full professor at the Université de Montréal) told me during the 2025 Institut du Cancer de Montréal Research Day: "You want to put hypoxic chamber companies out of business!". My answer was an emphatic yes.

As I have stated in the "limitations" subsection, all bioassays for HyCo spheroids unfortunately still must be performed off-chip. Thus, developing on-chip bioassays or chip-compatible methodologies would improve the chances of adoption of the HyCo spheroid microfluidic chip. As previously mentioned, Maryam Ziaee is currently using my device to develop an on-chip assay taking advantage of the highly concentrated secreted molecules in the culture medium. Similarly, slightly adapting the design for on-chip invasion assay could also benefit the adoption of the chip.

More broadly, adding a channel emulating the vasculature system would be of interest, specifically regarding hypoxia. Understanding the mechanisms by which tumor cells escape the primary tumor/spheroid would benefit the development of anti-cancer treatment for highly metastatic cancer such as STSs.

By definition, the role of an engineer is to provide fit for purpose tools, but a tool is only as useful as you make it. When I reflect on my 5 years of B. Eng and 6 years as a biomedical engineer graduate student and on all the engineering meetings I attended, I realize that engineers mostly like to invent "stuff" other engineers will find cool. They lose themselves in the engineering of it, and at times forget the purpose of what they are developing.

Even if I understand the importance of doing science for the sake of science, I think it is always important and useful to think of potential future applications of what we develop, be they 10 or 100 years from now. Looking back at recent MicroTAS meetings (International Conference on Miniaturized Systems for Chemistry and Life Sciences - Micro-Total Analysis Systems) I understand better why microfluidic technologies are perceived the way they are, and why most biologists are reluctant to use any of them. The majority of the setups are complex, bordering on the incomprehensible, without clear advantages compared to standard methods, as if no one ever consulted a potential user. As the heart of the field of biomedical engineering is to provide tools for clinicians and biologists, to cultivate a transdisciplinary research environment is of the utmost importance.

The engineer must adjust the technology to the need of our users, while proving them that the innovative aspects are worth it and valuable. It is a fine balance of innovation, simplicity, user-friendliness. The goal is to meet the unmet-need and it often involves changing mindset and taking disruptive approaches to do so. The proposed solution must neither be broad to the point of having no obvious application nor a hyper-specific single use device. The relative quick adoption of my technologies within the CRCHUM and beyond testifies of the standard I strove to achieve in bioengineering design: "*Always strive to consult potential users, to attend meetings related to the field of application of the technology you develop. Always keep an open mind: you never know when you'll meet someone interested or interesting.*"

REFERENCES

[1] Ian F. Tannock, Richard P. Hill, Robert G. Bristow, and Lea Harrington, *The Basic Science of Oncology*, 4th ed. United States: McGraw-Hill Medical Publishing Division, 2005.

[2] M. Joiner and A. van der Kogel, Eds., *Basic clinical radiobiology*, Fifth edition. Boca Raton, FL: CRC Press/Taylor & Francis Group, 2018.

[3] L. H. Gray, A. D. Conger, M. Ebert, S. Hornsey, and O. C. A. Scott, "The Concentration of Oxygen Dissolved in Tissues at the Time of Irradiation as a Factor in Radiotherapy," *British Journal of Radiology*, vol. 26, no. 312, pp. 638–648, Dec. 1953, doi: 10.1259/0007-1285-26-312-638.

[4] R. H. Thomlinson and L. H. Gray, "The Histological Structure of Some Human Lung Cancers and the Possible Implications for Radiotherapy," *Br J Cancer*, vol. 9, no. 4, pp. 539–549, Dec. 1955, doi: 10.1038/bjc.1955.55.

[5] A. L. Harris, "Hypoxia--a key regulatory factor in tumour growth," *Nat Rev Cancer*, vol. 2, no. 1, pp. 38–47, Jan. 2002, doi: 10.1038/nrc704.

[6] Y. Mi *et al.*, "Hypoxic colorectal cancer cells promote metastasis of normoxic cancer cells depending on IL-8/p65 signaling pathway," *Cell Death Dis*, vol. 11, no. 7, p. 610, Jul. 2020, doi: 10.1038/s41419-020-02797-z.

[7] J. Druker, J. W. Wilson, F. Child, D. Shakir, T. Fasanya, and S. Rocha, "Role of Hypoxia in the Control of the Cell Cycle," *Int J Mol Sci*, vol. 22, no. 9, p. 4874, May 2021, doi: 10.3390/ijms22094874.

[8] W. R. Wilson and M. P. Hay, "Targeting hypoxia in cancer therapy," *Nat Rev Cancer*, vol. 11, no. 6, pp. 393–410, Jun. 2011, doi: 10.1038/nrc3064.

[9] J. M. Brown and W. R. Wilson, "Exploiting tumour hypoxia in cancer treatment," *Nat Rev Cancer*, vol. 4, no. 6, pp. 437–447, Jun. 2004, doi: 10.1038/nrc1367.

[10] J. M. Brown, "Tumor Hypoxia in Cancer Therapy," in *Methods in Enzymology*, vol. 435, Elsevier, 2007, pp. 295–321. doi: 10.1016/S0076-6879(07)35015-5.

[11] N. Devarajan, R. Manjunathan, and S. K. Ganesan, "Tumor hypoxia: The major culprit behind cisplatin resistance in cancer patients," *Critical Reviews in Oncology/Hematology*, vol. 162, p. 103327, Jun. 2021, doi: 10.1016/j.critrevonc.2021.103327.

[12] S. K. Daniel, K. M. Sullivan, K. P. Labadie, and V. G. Pillarisetty, "Hypoxia as a barrier to immunotherapy in pancreatic adenocarcinoma," *Clin Transl Med*, vol. 8, no. 1, p. 10, Apr. 2019, doi: 10.1186/s40169-019-0226-9.

[13] Z. Burningham, M. Hashibe, L. Spector, and J. D. Schiffman, "The Epidemiology of Sarcoma," *Clin Sarcoma Res*, vol. 2, p. 14, Oct. 2012, doi: 10.1186/2045-3329-2-14.

[14] P. Wong *et al.*, "Combining Targeted Agents With Modern Radiotherapy in Soft Tissue Sarcomas," *JNCI Journal of the National Cancer Institute*, vol. 106, no. 11, pp. dju329–dju329, Oct. 2014, doi: 10.1093/jnci/dju329.

[15] M. von Mehren *et al.*, “Soft Tissue Sarcoma, Version 2.2018, NCCN Clinical Practice Guidelines in Oncology,” *J Natl Compr Canc Netw*, vol. 16, no. 5, pp. 536–563, May 2018, doi: 10.6004/jnccn.2018.0025.

[16] “Soft Tissue Sarcoma Treatment (PDQ®) - NCI.” Accessed: Feb. 28, 2025. [Online]. Available: https://www.cancer.gov/types/soft-tissue-sarcoma/hp/adult-soft-tissue-treatment-pdq

[17] Z. Tian and W. Yao, “Chemotherapeutic drugs for soft tissue sarcomas: a review,” *Front. Pharmacol.*, vol. 14, Aug. 2023, doi: 10.3389/fphar.2023.1199292.

[18] C. C. S. / S. canadienne du cancer, “Survival statistics for soft tissue sarcoma,” Canadian Cancer Society. Accessed: Mar. 19, 2025. [Online]. Available: https://cancer.ca/en/cancer-information/cancer-types/soft-tissue-sarcoma/prognosis-and-survival/survival-statistics

[19] L. Yang, L. Forker, J. J. Irlam, N. Pillay, A. Choudhury, and C. M. L. West, “Validation of a hypoxia related gene signature in multiple soft tissue sarcoma cohorts,” *Oncotarget*, vol. 9, no. 3, pp. 3946–3955, Dec. 2017, doi: 10.18632/oncotarget.23280.

[20] J. C. Walsh, A. Lebedev, E. Aten, K. Madsen, L. Marciano, and H. C. Kolb, “The Clinical Importance of Assessing Tumor Hypoxia: Relationship of Tumor Hypoxia to Prognosis and Therapeutic Opportunities,” *Antioxid Redox Signal*, vol. 21, no. 10, pp. 1516–1554, Oct. 2014, doi: 10.1089/ars.2013.5378.

[21] A. Yuen and B. Díaz, “The impact of hypoxia in pancreatic cancer invasion and metastasis,” *Hypoxia (Auckl)*, vol. 2, pp. 91–106, Jul. 2014, doi: 10.2147/HP.S52636.

[22] A. Datta, C. West, J. P. B. O’Connor, A. Choudhury, and P. Hoskin, “Impact of hypoxia on cervical cancer outcomes,” *International Journal of Gynecological Cancer*, vol. 31, no. 11, pp. 1459–1470, Nov. 2021, doi: 10.1136/ijgc-2021-002806.

[23] J. Z. Li, W. Gao, J. Y.-W. Chan, W.-K. Ho, and T.-S. Wong, “Hypoxia in head and neck squamous cell carcinoma,” *ISRN Otolaryngol*, vol. 2012, p. 708974, 2012, doi: 10.5402/2012/708974.

[24] A. R. Monteiro, R. Hill, G. J. Pilkington, and P. A. Madureira, “The Role of Hypoxia in Glioblastoma Invasion,” *Cells*, vol. 6, no. 4, p. 45, Nov. 2017, doi: 10.3390/cells6040045.

[25] M. Nordsmark *et al.*, “Hypoxia in human soft tissue sarcomas: Adverse impact on survival and no association with p53 mutations,” *Br J Cancer*, vol. 84, no. 8, pp. 1070–1075, Apr. 2001, doi: 10.1054/bjoc.2001.1728.

[26] L. J. Forker *et al.*, “Technical development and validation of a clinically applicable microenvironment classifier as a biomarker of tumour hypoxia for soft tissue sarcoma,” *Br J Cancer*, vol. 128, no. 12, pp. 2307–2317, Jun. 2023, doi: 10.1038/s41416-023-02265-3.

[27] S. Pasquali *et al.*, “Preclinical models of soft tissue sarcomas – generation and applications to enhance translational research,” *Critical Reviews in Oncology/Hematology*, vol. 207, p. 104621, Mar. 2025, doi: 10.1016/j.critrevonc.2025.104621.

[28] A. Hajitou *et al.*, “A preclinical model for predicting drug response in soft-tissue sarcoma with targeted AAVP molecular imaging,” *Proceedings of the National Academy of Sciences*, vol. 105, no. 11, pp. 4471–4476, Mar. 2008, doi: 10.1073/pnas.0712184105.

[29] T. K. Choueiri *et al.*, “Inhibition of hypoxia-inducible factor-2α in renal cell carcinoma with belzutifan: a phase 1 trial and biomarker analysis,” *Nat Med*, vol. 27, no. 5, pp. 802–805, May 2021, doi: 10.1038/s41591-021-01324-7.

[30] Y. Li, L. Zhao, and X.-F. Li, “Targeting Hypoxia: Hypoxia-Activated Prodrugs in Cancer Therapy,” *Front Oncol*, vol. 11, p. 700407, Jul. 2021, doi: 10.3389/fonc.2021.700407.

[31] J. Brown, “SR 4233 (Tirapazamine): a new anticancer drug exploiting hypoxia in solid tumours,” *Br J Cancer*, vol. 67, no. 6, pp. 1163–1170, Jun. 1993, doi: 10.1038/bjc.1993.220.

[32] L. Marcu and I. Olver, “Tirapazamine: From Bench to Clinical Trials,” *CCP*, vol. 1, no. 1, pp. 71–79, Jan. 2006, doi: 10.2174/157488406775268192.

[33] E. Refet-Mollof *et al.*, “Hypoxic Jumbo Spheroids On-A-Chip (HOnAChip): Insights into Treatment Efficacy,” *Cancers*, vol. 13, no. 16, Art. no. 16, Jan. 2021, doi: 10.3390/cancers13164046.

[34] Z. Luo *et al.*, “Hypoxia signaling in human health and diseases: implications and prospects for therapeutics,” *Sig Transduct Target Ther*, vol. 7, no. 1, pp. 1–30, Jul. 2022, doi: 10.1038/s41392-022-01080-1.

[35] R. Leek, D. R. Grimes, A. L. Harris, and A. McIntyre, “Methods: Using Three-Dimensional Culture (Spheroids) as an In Vitro Model of Tumour Hypoxia,” in *Tumor Microenvironment*, vol. 899, C. Koumenis, L. M. Coussens, A. Giaccia, and E. Hammond, Eds., in Advances in Experimental Medicine and Biology, vol. 899. , Cham: Springer International Publishing, 2016, pp. 167–196. doi: 10.1007/978-3-319-26666-4_10.

[36] K. Graham and E. Unger, “Overcoming tumor hypoxia as a barrier to radiotherapy, chemotherapy and immunotherapy in cancer treatment,” *Int J Nanomedicine*, vol. 13, pp. 6049–6058, Oct. 2018, doi: 10.2147/IJN.S140462.

[37] M. D. Giovannantonio *et al.*, “Defining hypoxia in cancer: A landmark evaluation of hypoxia gene expression signatures,” *Cell Genomics*, vol. 5, no. 2, Feb. 2025, doi: 10.1016/j.xgen.2025.100764.

[38] G. Calvo-Anguiano *et al.*, “Comparison of specific expression profile in two in vitro hypoxia models,” *Experimental and Therapeutic Medicine*, vol. 15, no. 6, pp. 4777–4784, Jun. 2018, doi: 10.3892/etm.2018.6048.

[39] D. Wu and P. Yotnda, “Induction and Testing of Hypoxia in Cell Culture,” *J Vis Exp*, no. 54, Aug. 2011, doi: 10.3791/2899.

[40] J. Michl, K. C. Park, and P. Swietach, “Evidence-based guidelines for controlling pH in mammalian live-cell culture systems,” *Communications Biology*, vol. 2, no. 1, Art. no. 1, Apr. 2019, doi: 10.1038/s42003-019-0393-7.

[41] F. Hirschhaeuser, H. Menne, C. Dittfeld, J. West, W. Mueller-Klieser, and L. A. Kunz-Schughart, “Multicellular tumor spheroids: An underestimated tool is catching up again,” *Journal of Biotechnology*, vol. 148, no. 1, pp. 3–15, Jul. 2010, doi: 10.1016/j.jbiotec.2010.01.012.

[42] U. Lendahl, K. L. Lee, H. Yang, and L. Poellinger, “Generating specificity and diversity in the transcriptional response to hypoxia,” *Nat Rev Genet*, vol. 10, no. 12, pp. 821–832, Dec. 2009, doi: 10.1038/nrg2665.

[43] P. Workman *et al.*, "Guidelines for the welfare and use of animals in cancer research," *Br J Cancer*, vol. 102, no. 11, pp. 1555–1577, May 2010, doi: 10.1038/sj.bjc.6605642.

[44] V. Mirabello, F. Cortezon-Tamarit, and S. I. Pascu, "Oxygen Sensing, Hypoxia Tracing and in Vivo Imaging with Functional Metalloprobes for the Early Detection of Non-communicable Diseases," *Front Chem*, vol. 6, Feb. 2018, doi: 10.3389/fchem.2018.00027.

[45] C. Jensen and Y. Teng, "Is It Time to Start Transitioning From 2D to 3D Cell Culture?," *Front Mol Biosci*, vol. 7, p. 33, Mar. 2020, doi: 10.3389/fmolb.2020.00033.

[46] M. Astolfi *et al.*, "Micro-dissected tumor tissues on chip: an ex vivo method for drug testing and personalized therapy," *Lab Chip*, vol. 16, no. 2, pp. 312–325, Jan. 2016, doi: 10.1039/C5LC01108F.

[47] D. R. Grimes, C. Kelly, K. Bloch, and M. Partridge, "A method for estimating the oxygen consumption rate in multicellular tumour spheroids," *J R Soc Interface*, vol. 11, no. 92, p. 20131124, Mar. 2014, doi: 10.1098/rsif.2013.1124.

[48] S. Gunti, A. T. K. Hoke, K. P. Vu, and N. R. London, "Organoid and Spheroid Tumor Models: Techniques and Applications," *Cancers (Basel)*, vol. 13, no. 4, p. 874, Feb. 2021, doi: 10.3390/cancers13040874.

[49] S. J. Han, S. Kwon, and K. S. Kim, "Challenges of applying multicellular tumor spheroids in preclinical phase," *Cancer Cell International*, vol. 21, no. 1, p. 152, Mar. 2021, doi: 10.1186/s12935-021-01853-8.

[50] Y. Long, B. Xie, H. C. Shen, and D. Wen, "Translation Potential and Challenges of In Vitro and Murine Models in Cancer Clinic," *Cells*, vol. 11, no. 23, p. 3868, Nov. 2022, doi: 10.3390/cells11233868.

[51] P. K. Chaudhuri, M. E. Warkiani, T. Jing, Kenry, and C. T. Lim, "Microfluidics for research and applications in oncology," *Analyst*, vol. 141, no. 2, pp. 504–524, Jan. 2016, doi: 10.1039/C5AN00382B.

[52] C. G. Uhl and Y. Liu, "Microfluidic device for expedited tumor growth towards drug evaluation," *Lab Chip*, vol. 19, no. 8, pp. 1458–1470, Apr. 2019, doi: 10.1039/C8LC01250D.

[53] B. Patra *et al.*, "On-chip combined radiotherapy and chemotherapy testing on soft-tissue sarcoma spheroids to study cell death using flow cytometry and clonogenic assay," *Scientific Reports*, vol. 9, no. 1, Art. no. 1, Feb. 2019, doi: 10.1038/s41598-019-38666-9.

[54] R. Chermat *et al.*, "Radiotherapy on-chip: microfluidics for translational radiation oncology," *Lab Chip*, vol. 22, no. 11, pp. 2065–2079, May 2022, doi: 10.1039/D2LC00177B.

[55] R. Chermat, E. Refet-Mollof, Y. Kamio, J.-F. Carrier, P. Wong, and T. Gervais, "Brachytherapy on-a-chip: a clinically-relevant approach for radiotherapy testing in 3d biology," *Lab Chip*, vol. 24, no. 8, pp. 2335–2346, Apr. 2024, doi: 10.1039/D4LC00032C.

[56] N. Bhattacharjee, A. Urrios, S. Kang, and A. Folch, "The upcoming 3D-printing revolution in microfluidics," *Lab Chip*, vol. 16, no. 10, pp. 1720–1742, May 2016, doi: 10.1039/c6lc00163g.

[57] D. J. Guckenberger, T. E. de Groot, A. M. D. Wan, D. J. Beebe, and E. W. K. Young, "Micromilling: a method for ultra-rapid prototyping of plastic microfluidic devices," *Lab Chip*, vol. 15, no. 11, pp. 2364–2378, Jun. 2015, doi: 10.1039/c5lc00234f.

[58] S. R. McKeown, "Defining normoxia, physoxia and hypoxia in tumours—implications for treatment response," *Br J Radiol*, vol. 87, no. 1035, Mar. 2014, doi: 10.1259/bjr.20130676.

[59] P. Vaupel, M. Höckel, and A. Mayer, "Detection and characterization of tumor hypoxia using pO2 histography," *Antioxid Redox Signal*, vol. 9, no. 8, pp. 1221–1235, Aug. 2007, doi: 10.1089/ars.2007.1628.

[60] B. R. Walker, N. R. Colledge, S. Ralston, I. D. Penman, and R. Britton, Eds., *Davidson's principles and practice of medicine*, 22nd edition. Edinburgh ; New York: Churchill Livingstone/Elsevier, 2014.

[61] Kamby Gilany, Mohtaram Vafakhah, "Hypoxia: a Review," *JPS*, vol. 1, no. 2, pp. 43–60, 2010.

[62] R. G. Bristow and R. P. Hill, "Hypoxia, DNA repair and genetic instability," *Nat Rev Cancer*, vol. 8, no. 3, pp. 180–192, Mar. 2008, doi: 10.1038/nrc2344.

[63] Z. Chen, F. Han, Y. Du, H. Shi, and W. Zhou, "Hypoxic microenvironment in cancer: molecular mechanisms and therapeutic interventions," *Sig Transduct Target Ther*, vol. 8, no. 1, pp. 1–23, Feb. 2023, doi: 10.1038/s41392-023-01332-8.

[64] "Nobel Prize in Physiology or Medicine 2019," NobelPrize.org. Accessed: Mar. 11, 2025. [Online]. Available: https://www.nobelprize.org/prizes/medicine/2019/summary/

[65] B. G. Wouters and M. Koritzinsky, "Hypoxia signalling through mTOR and the unfolded protein response in cancer," *Nat Rev Cancer*, vol. 8, no. 11, pp. 851–864, Nov. 2008, doi: 10.1038/nrc2501.

[66] M. Y. Koh, T. R. Spivak-Kroizman, and G. Powis, "HIF-1 regulation: not so easy come, easy go," *Trends in Biochemical Sciences*, vol. 33, no. 11, pp. 526–534, Nov. 2008, doi: 10.1016/j.tibs.2008.08.002.

[67] G. L. Semenza, "HIF-1 mediates metabolic responses to intratumoral hypoxia and oncogenic mutations," *J Clin Invest*, vol. 123, no. 9, pp. 3664–3671, Sep. 2013, doi: 10.1172/JCI67230.

[68] J. M. Berg, J. L. Tymoczko, and L. Stryer, *Biochemistry, 5th edition*, 5th ed. New York: W. H. Freeman and Company, 2002. Accessed: Apr. 28, 2020. [Online]. Available: https://www.ncbi.nlm.nih.gov/books/NBK21208/

[69] Z. Chen, F. Han, Y. Du, H. Shi, and W. Zhou, "Hypoxic microenvironment in cancer: molecular mechanisms and therapeutic interventions," *Sig Transduct Target Ther*, vol. 8, no. 1, pp. 1–23, Feb. 2023, doi: 10.1038/s41392-023-01332-8.

[70] B. H. Jiang, G. L. Semenza, C. Bauer, and H. H. Marti, "Hypoxia-inducible factor 1 levels vary exponentially over a physiologically relevant range of O2 tension," *American Journal of Physiology-Cell Physiology*, vol. 271, no. 4, pp. C1172–C1180, Oct. 1996, doi: 10.1152/ajpcell.1996.271.4.C1172.

[71] K. M. Rouschop *et al.*, "PERK/eIF2α signaling protects therapy resistant hypoxic cells through induction of glutathione synthesis and protection against ROS," *Proc. Natl. Acad. Sci. U.S.A.*, vol. 110, no. 12, pp. 4622–4627, Mar. 2013, doi: 10.1073/pnas.1210633110.

[72] C. Koumenis *et al.*, "Regulation of Protein Synthesis by Hypoxia via Activation of the Endoplasmic Reticulum Kinase PERK and Phosphorylation of the Translation Initiation Factor eIF2α," *Mol Cell Biol*, vol. 22, no. 21, pp. 7405–7416, Nov. 2002, doi: 10.1128/MCB.22.21.7405-7416.2002.

[73] H. Cam, J. B. Easton, A. High, and P. J. Houghton, "mTORC1 signaling under hypoxic conditions is controlled by ATM-dependent phosphorylation of HIF-1α," *Mol Cell*, vol. 40, no. 4, pp. 509–520, Nov. 2010, doi: 10.1016/j.molcel.2010.10.030.

[74] G. L. Semenza, "Defining the Role of Hypoxia-Inducible Factor 1 in Cancer Biology and Therapeutics," *Oncogene*, vol. 29, no. 5, pp. 625–634, Feb. 2010, doi: 10.1038/onc.2009.441.

[75] J. A. Bertout, S. A. Patel, and M. C. Simon, "The impact of O2 availability on human cancer," *Nat Rev Cancer*, vol. 8, no. 12, pp. 967–975, Dec. 2008, doi: 10.1038/nrc2540.

[76] W. G. Kaelin and P. J. Ratcliffe, "Oxygen Sensing by Metazoans: The Central Role of the HIF Hydroxylase Pathway," *Molecular Cell*, vol. 30, no. 4, pp. 393–402, May 2008, doi: 10.1016/j.molcel.2008.04.009.

[77] A. J. Majmundar, W. J. Wong, and M. C. Simon, "Hypoxia-Inducible Factors and the Response to Hypoxic Stress," *Molecular Cell*, vol. 40, no. 2, pp. 294–309, Oct. 2010, doi: 10.1016/j.molcel.2010.09.022.

[78] E. L. Bell, T. A. Klimova, J. Eisenbart, P. T. Schumacker, and N. S. Chandel, "Mitochondrial Reactive Oxygen Species Trigger Hypoxia-Inducible Factor-Dependent Extension of the Replicative Life Span during Hypoxia," *Molecular and Cellular Biology*, vol. 27, no. 16, pp. 5737–5745, Aug. 2007, doi: 10.1128/MCB.02265-06.

[79] Y. Z. Gu, S. M. Moran, J. B. Hogenesch, L. Wartman, and C. A. Bradfield, "Molecular characterization and chromosomal localization of a third alpha-class hypoxia inducible factor subunit, HIF3alpha," *Gene Expr*, vol. 7, no. 3, pp. 205–213, 1998.

[80] S.-L. Yang, C. Wu, Z.-F. Xiong, and X. Fang, "Progress on hypoxia-inducible factor-3: Its structure, gene regulation and biological function (Review)," *Molecular Medicine Reports*, vol. 12, no. 2, pp. 2411–2416, Aug. 2015, doi: 10.3892/mmr.2015.3689.

[81] B. Keith, R. S. Johnson, and M. C. Simon, "HIF1α and HIF2α: sibling rivalry in hypoxic tumour growth and progression," *Nat Rev Cancer*, vol. 12, no. 1, pp. 9–22, Jan. 2012, doi: 10.1038/nrc3183.

[82] N. L. Downes, N. Laham-Karam, M. U. Kaikkonen, and S. Ylä-Herttuala, "Differential but Complementary HIF1α and HIF2α Transcriptional Regulation," *Molecular Therapy*, vol. 26, no. 7, pp. 1735–1745, Jul. 2018, doi: 10.1016/j.ymthe.2018.05.004.

[83] P. Zhang, Q. Yao, L. Lu, Y. Li, P.-J. Chen, and C. Duan, "Hypoxia-inducible factor 3 is an oxygen-dependent transcription activator and regulates a distinct transcriptional response to hypoxia," *Cell Rep*, vol. 6, no. 6, pp. 1110–1121, Mar. 2014, doi: 10.1016/j.celrep.2014.02.011.

[84] D. D. Vadysirisack and L. W. Ellisen, "mTOR Activity Under Hypoxia," *Methods Mol Biol*, vol. 821, pp. 45–58, 2012, doi: 10.1007/978-1-61779-430-8_4.

[85] Y. C. Tsai and A. M. Weissman, “The Unfolded Protein Response, Degradation from the Endoplasmic Reticulum, and Cancer,” *Genes & Cancer*, vol. 1, no. 7, pp. 764–778, Jul. 2010, doi: 10.1177/1947601910383011.

[86] S. Bartoszewska and J. F. Collawn, “Unfolded protein response (UPR) integrated signaling networks determine cell fate during hypoxia,” *Cell Mol Biol Lett*, vol. 25, no. 1, p. 18, Mar. 2020, doi: 10.1186/s11658-020-00212-1.

[87] C. Hetz, “The unfolded protein response: controlling cell fate decisions under ER stress and beyond,” *Nat Rev Mol Cell Biol*, vol. 13, no. 2, pp. 89–102, Feb. 2012, doi: 10.1038/nrm3270.

[88] D. T. Rutkowski and R. J. Kaufman, “All Roads Lead to ATF4,” *Developmental Cell*, vol. 4, no. 4, pp. 442–444, Apr. 2003, doi: 10.1016/S1534-5807(03)00100-X.

[89] I. Novoa, H. Zeng, H. P. Harding, and D. Ron, “Feedback Inhibition of the Unfolded Protein Response by GADD34-Mediated Dephosphorylation of eIF2α,” *Journal of Cell Biology*, vol. 153, no. 5, pp. 1011–1022, May 2001, doi: 10.1083/jcb.153.5.1011.

[90] C. C. Hudson *et al.*, “Regulation of hypoxia-inducible factor 1alpha expression and function by the mammalian target of rapamycin,” *Mol Cell Biol*, vol. 22, no. 20, pp. 7004–7014, Oct. 2002, doi: 10.1128/MCB.22.20.7004-7014.2002.

[91] G. L. Semenza, “Targeting HIF-1 for cancer therapy,” *Nat Rev Cancer*, vol. 3, no. 10, pp. 721–732, Dec. 2003, doi: 10.1038/nrc1187.

[92] M. C. Bosco *et al.*, “Hypoxia Modifies the Transcriptome of Primary Human Monocytes: Modulation of Novel Immune-Related Genes and Identification Of CC-Chemokine Ligand 20 as a New Hypoxia-Inducible Gene1,” *The Journal of Immunology*, vol. 177, no. 3, pp. 1941–1955, Aug. 2006, doi: 10.4049/jimmunol.177.3.1941.

[93] Y. Benita, H. Kikuchi, A. D. Smith, M. Q. Zhang, D. C. Chung, and R. J. Xavier, “An integrative genomics approach identifies Hypoxia Inducible Factor-1 (HIF-1)-target genes that form the core response to hypoxia,” *Nucleic Acids Research*, vol. 37, no. 14, pp. 4587–4602, Aug. 2009, doi: 10.1093/nar/gkp425.

[94] A. Yfantis *et al.*, “Transcriptional Response to Hypoxia: The Role of HIF-1-Associated Co-Regulators,” *Cells*, vol. 12, no. 5, p. 798, Mar. 2023, doi: 10.3390/cells12050798.

[95] V. L. Dengler, M. Galbraith, and J. M. Espinosa, “Transcriptional Regulation by Hypoxia Inducible Factors,” *Crit Rev Biochem Mol Biol*, vol. 49, no. 1, pp. 1–15, 2014, doi: 10.3109/10409238.2013.838205.

[96] PubChem, “VEGFA - vascular endothelial growth factor A (human).” Accessed: Mar. 11, 2025. [Online]. Available: https://pubchem.ncbi.nlm.nih.gov/gene/VEGFA/human

[97] L. Szablewski, “Expression of glucose transporters in cancers,” *Biochimica et Biophysica Acta (BBA) - Reviews on Cancer*, vol. 1835, no. 2, pp. 164–169, Apr. 2013, doi: 10.1016/j.bbcan.2012.12.004.

[98] S. J. Kierans and C. T. Taylor, “Regulation of glycolysis by the hypoxia-inducible factor (HIF): implications for cellular physiology,” *The Journal of Physiology*, vol. 599, no. 1, pp. 23–37, 2021, doi: 10.1113/JP280572.

[99] I. Papandreou, R. A. Cairns, L. Fontana, A. L. Lim, and N. C. Denko, “HIF-1 mediates adaptation to hypoxia by actively downregulating mitochondrial oxygen consumption,” *Cell Metabolism*, vol. 3, no. 3, pp. 187–197, Mar. 2006, doi: 10.1016/j.cmet.2006.01.012.

[100] P. C. McDonald and S. Dedhar, “Carbonic Anhydrase IX (CAIX) as a Mediator of Hypoxia-Induced Stress Response in Cancer Cells,” in *Carbonic Anhydrase: Mechanism, Regulation, Links to Disease, and Industrial Applications*, vol. 75, S. C. Frost and R. McKenna, Eds., in Subcellular Biochemistry, vol. 75. , Dordrecht: Springer Netherlands, 2014, pp. 255–269. doi: 10.1007/978-94-007-7359-2_13.

[101] M. Hosonuma and K. Yoshimura, “Association between pH regulation of the tumor microenvironment and immunological state,” *Front Oncol*, vol. 13, p. 1175563, Jul. 2023, doi: 10.3389/fonc.2023.1175563.

[102] M. Meyenberg Cunha-de Padua *et al.*, “Hypoxia protects against the cell death triggered by oxovanadium–galactomannan complexes in HepG2 cells,” *Cellular & Molecular Biology Letters*, vol. 24, no. 1, p. 18, Mar. 2019, doi: 10.1186/s11658-019-0135-3.

[103] G. Bellot *et al.*, “Hypoxia-Induced Autophagy Is Mediated through Hypoxia-Inducible Factor Induction of BNIP3 and BNIP3L via Their BH3 Domains,” *Molecular and Cellular Biology*, vol. 29, no. 10, pp. 2570–2581, May 2009, doi: 10.1128/MCB.00166-09.

[104] T. Shang *et al.*, “Unraveling the triad of hypoxia, cancer cell stemness, and drug resistance,” *Journal of Hematology & Oncology*, vol. 18, no. 1, p. 32, Mar. 2025, doi: 10.1186/s13045-025-01684-4.

[105] Q. Zhang, Z.-Y. An, W. Jiang, W.-L. Jin, and X.-Y. He, “Collagen code in tumor microenvironment: Functions, molecular mechanisms, and therapeutic implications,” *Biomedicine & Pharmacotherapy*, vol. 166, p. 115390, Oct. 2023, doi: 10.1016/j.biopha.2023.115390.

[106] A. Datta *et al.*, “Cytoskeletal Dynamics in Epithelial-Mesenchymal Transition: Insights into Therapeutic Targets for Cancer Metastasis,” *Cancers (Basel)*, vol. 13, no. 8, p. 1882, Apr. 2021, doi: 10.3390/cancers13081882.

[107] R. A. Battaglia, S. Delic, H. Herrmann, and N. T. Snider, “Vimentin on the move: new developments in cell migration,” Nov. 15, 2018, *F1000Research*: 7:1796. doi: 10.12688/f1000research.15967.1.

[108] G. Xiong *et al.*, “Collagen prolyl 4-hydroxylase 1 is essential for HIF-1α stabilization and TNBC chemoresistance,” *Nat Commun*, vol. 9, no. 1, p. 4456, Oct. 2018, doi: 10.1038/s41467-018-06893-9.

[109] C. Han, L. Jin, Y. Mei, and M. Wu, “Endoplasmic reticulum stress inhibits cell cycle progression via induction of p27 in melanoma cells,” *Cell Signal*, vol. 25, no. 1, pp. 144–149, Jan. 2013, doi: 10.1016/j.cellsig.2012.09.023.

[110] M. E. Hubbi and G. L. Semenza, “Regulation of cell proliferation by hypoxia-inducible factors,” *American Journal of Physiology-Cell Physiology*, vol. 309, no. 12, pp. C775–C782, Dec. 2015, doi: 10.1152/ajpcell.00279.2015.

[111] M. Koshiji, Y. Kageyama, E. A. Pete, I. Horikawa, J. C. Barrett, and L. E. Huang, "HIF-1α induces cell cycle arrest by functionally counteracting Myc," *The EMBO Journal*, vol. 23, no. 9, pp. 1949–1956, May 2004, doi: 10.1038/sj.emboj.7600196.

[112] J. M. Low, M. Skwarski, R. Macpherson, G. S. Higgins, and D. R. McGowan, "Potential Link between Hypoxic Status of Tumors and Surgical Outcomes in NSCLC Patients," *International Journal of Radiation Oncology*Biology*Physics*, vol. 120, no. 2, Supplement, pp. e42–e43, Oct. 2024, doi: 10.1016/j.ijrobp.2024.07.1872.

[113] H. Gelband, P. Jha, R. Sankaranarayanan, and S. Horton, Eds., *Cancer: Disease Control Priorities, Third Edition (Volume 3)*. Washington (DC): The International Bank for Reconstruction and Development / The World Bank, 2015. Accessed: Nov. 29, 2021. [Online]. Available: http://www.ncbi.nlm.nih.gov/books/NBK343628/

[114] G. Delaney, S. Jacob, C. Featherstone, and M. Barton, "The role of radiotherapy in cancer treatment: estimating optimal utilization from a review of evidence-based clinical guidelines," *Cancer*, vol. 104, no. 6, pp. 1129–1137, Sep. 2005, doi: 10.1002/cncr.21324.

[115] M. B. Barton, M. Frommer, and J. Shafiq, "Role of radiotherapy in cancer control in low-income and middle-income countries," *Lancet Oncol*, vol. 7, no. 7, pp. 584–595, Jul. 2006, doi: 10.1016/S1470-2045(06)70759-8.

[116] M. B. Barton *et al.*, "Estimating the demand for radiotherapy from the evidence: A review of changes from 2003 to 2012," *Radiotherapy and Oncology*, vol. 112, no. 1, pp. 140–144, Jul. 2014, doi: 10.1016/j.radonc.2014.03.024.

[117] S. Tyldesley, G. Delaney, F. Foroudi, L. Barbera, M. Kerba, and W. Mackillop, "Estimating the need for radiotherapy for patients with prostate, breast, and lung cancers: verification of model estimates of need with radiotherapy utilization data from British Columbia," *Int J Radiat Oncol Biol Phys*, vol. 79, no. 5, pp. 1507–1515, Apr. 2011, doi: 10.1016/j.ijrobp.2009.12.070.

[118] B. G. Wouters and J. M. Brown, "Cells at Intermediate Oxygen Levels Can Be More Important Than the 'Hypoxic Fraction' in Determining Tumor Response to Fractionated Radiotherapy," *Radiation Research*, vol. 147, no. 5, p. 541, May 1997, doi: 10.2307/3579620.

[119] C. Beckers, M. Pruschy, and I. Vetrugno, "Tumor hypoxia and radiotherapy: A major driver of resistance even for novel radiotherapy modalities," *Semin Cancer Biol*, vol. 98, pp. 19–30, Jan. 2024, doi: 10.1016/j.semcancer.2023.11.006.

[120] D. Sprong, H. L. Janssen, C. Vens, and A. C. Begg, "Resistance of hypoxic cells to ionizing radiation is influenced by homologous recombination status," *International Journal of Radiation Oncology*Biology*Physics*, vol. 64, no. 2, pp. 562–572, Feb. 2006, doi: 10.1016/j.ijrobp.2005.09.031.

[121] M. T. Amjad, A. Chidharla, and A. Kasi, "Cancer Chemotherapy," in *StatPearls*, Treasure Island (FL): StatPearls Publishing, 2025. Accessed: Mar. 12, 2025. [Online]. Available: http://www.ncbi.nlm.nih.gov/books/NBK564367/

[122] "Doxorubicin." Accessed: Mar. 12, 2025. [Online]. Available: https://go.drugbank.com/drugs/DB00997

[123] “Paclitaxel.” Accessed: Mar. 12, 2025. [Online]. Available: https://go.drugbank.com/drugs/DB01229

[124] “Fluorouracil.” Accessed: Mar. 12, 2025. [Online]. Available: https://go.drugbank.com/drugs/DB00544

[125] C. W. Taylor, W. S. Dalton, K. Mosley, R. T. Dorr, and S. E. Salmon, “Combination chemotherapy with cyclophosphamide, vincristine, adriamycin, and dexamethasone (CVAD) plus oral quinine and verapamil in patients with advanced breast cancer,” *Breast Cancer Res Treat*, vol. 42, no. 1, pp. 7–14, Jan. 1997, doi: 10.1023/A:1005716214718.

[126] R. V. Smalley, J. Carpenter, A. Bartolucci, C. Vogel, and S. Krauss, “A comparison of cyclophosphamide, adriamycin, 5-fluorouracil (CAF) and cyclophosphamide, methotrexate, 5-fluorouracil, vincristine, prednisone (CMFVP) in patients with metastatic breast cancer. A southeastern cancer study group project,” *Cancer*, vol. 40, no. 2, pp. 625–632, 1977, doi: 10.1002/1097-0142(197708)40:2<625::AID-CNCR2820400206>3.0.CO;2-M.

[127] B. P. Mahoney, N. Raghunand, B. Baggett, and R. J. Gillies, “Tumor acidity, ion trapping and chemotherapeutics: I. Acid pH affects the distribution of chemotherapeutic agents in vitro,” *Biochemical Pharmacology*, vol. 66, no. 7, pp. 1207–1218, Oct. 2003, doi: 10.1016/S0006-2952(03)00467-2.

[128] R. Shi, C. Liao, and Q. Zhang, “Hypoxia-Driven Effects in Cancer: Characterization, Mechanisms, and Therapeutic Implications,” *Cells*, vol. 10, no. 3, p. 678, Mar. 2021, doi: 10.3390/cells10030678.

[129] S. Yoshiba, D. Ito, T. Nagumo, T. Shirota, M. Hatori, and S. Shintani, “Hypoxia induces resistance to 5-fluorouracil in oral cancer cells via G(1) phase cell cycle arrest,” *Oral Oncol*, vol. 45, no. 2, pp. 109–115, Feb. 2009, doi: 10.1016/j.oraloncology.2008.04.002.

[130] B. Muz, P. de la Puente, F. Azab, and A. K. Azab, “The role of hypoxia in cancer progression, angiogenesis, metastasis, and resistance to therapy,” *HP*, p. 83, Dec. 2015, doi: 10.2147/HP.S93413.

[131] X. Song *et al.*, “Hypoxia-induced resistance to cisplatin and doxorubicin in non-small cell lung cancer is inhibited by silencing of HIF-1alpha gene,” *Cancer Chemother Pharmacol*, vol. 58, no. 6, pp. 776–784, Dec. 2006, doi: 10.1007/s00280-006-0224-7.

[132] M. Osada-Oka *et al.*, “Suppression of the doxorubicin response by hypoxia-inducible factor-1α is strictly dependent on oxygen concentrations under hypoxic conditions,” *European Journal of Pharmacology*, vol. 920, p. 174845, Apr. 2022, doi: 10.1016/j.ejphar.2022.174845.

[133] L. Huang *et al.*, “Hypoxia induced paclitaxel resistance in human ovarian cancers via hypoxia-inducible factor 1alpha,” *J Cancer Res Clin Oncol*, vol. 136, no. 3, pp. 447–456, Mar. 2010, doi: 10.1007/s00432-009-0675-4.

[134] L. Marcu and I. Olver, “Tirapazamine: From Bench to Clinical Trials,” *CCP*, vol. 1, no. 1, pp. 71–79, Jan. 2006, doi: 10.2174/157488406775268192.

[135] “Evofosfamide.” Accessed: Mar. 12, 2025. [Online]. Available: https://go.drugbank.com/drugs/DB06091

[136] Sidney Kimmel Comprehensive Cancer Center at Johns Hopkins, “Digoxin as a Novel Inhibitor of Global Hypoxia Inducible Factor-1α (HIF-1α) Expression & Downstream Targets in Breast Cancer: DIG-HIF-1 Pharmacodynamic Trial,” clinicaltrials.gov, Clinical trial registration NCT01763931, Jan. 2020. Accessed: Mar. 12, 2025. [Online]. Available: https://clinicaltrials.gov/study/NCT01763931

[137] C. Wigerup, S. Påhlman, and D. Bexell, “Therapeutic targeting of hypoxia and hypoxia-inducible factors in cancer,” *Pharmacology & Therapeutics*, vol. 164, pp. 152–169, Aug. 2016, doi: 10.1016/j.pharmthera.2016.04.009.

[138] E. M. Dunbar *et al.*, “Phase 1 trial of dichloroacetate (DCA) in adults with recurrent malignant brain tumors,” *Invest New Drugs*, vol. 32, no. 3, pp. 452–464, Jun. 2014, doi: 10.1007/s10637-013-0047-4.

[139] University of Florida, “Phase 1, Open-Label, Single-Arm, Clinical and Metabolomics Study of Dichloroacetate (DCA) in Adults With Recurrent Malignant Brain Tumors,” clinicaltrials.gov, Clinical trial registration NCT01111097, Sep. 2015. Accessed: Mar. 12, 2025. [Online]. Available: https://clinicaltrials.gov/study/NCT01111097

[140] “Everolimus - NCI.” Accessed: Mar. 12, 2025. [Online]. Available: https://www.cancer.gov/about-cancer/treatment/drugs/everolimus

[141] R. Wesolowski, M. Abdel-Rasoul, M. Lustberg, M. Paskell, C. L. Shapiro, and E. R. Macrae, “Treatment-Related Mortality With Everolimus in Cancer Patients,” *Oncologist*, vol. 19, no. 6, pp. 661–668, Jun. 2014, doi: 10.1634/theoncologist.2013-0355.

[142] P. J. Houghton, “Everolimus,” *Clinical Cancer Research*, vol. 16, no. 5, pp. 1368–1372, Feb. 2010, doi: 10.1158/1078-0432.CCR-09-1314.

[143] C. for D. E. and Research, “FDA approves belzutifan for advanced renal cell carcinoma,” *FDA*, Dec. 2023, Accessed: Mar. 12, 2025. [Online]. Available: https://www.fda.gov/drugs/resources-information-approved-drugs/fda-approves-belzutifan-advanced-renal-cell-carcinoma

[144] J. Hu *et al.*, “Tumor heterogeneity in VHL drives metastasis in clear cell renal cell carcinoma,” *Sig Transduct Target Ther*, vol. 8, no. 1, pp. 1–16, Apr. 2023, doi: 10.1038/s41392-023-01362-2.

[145] J. Hu *et al.*, “Tumor heterogeneity in VHL drives metastasis in clear cell renal cell carcinoma,” *Sig Transduct Target Ther*, vol. 8, no. 1, pp. 1–16, Apr. 2023, doi: 10.1038/s41392-023-01362-2.

[146] J. Hu, X. Li, L. Yang, and H. Li, “Hypoxia, a key factor in the immune microenvironment,” *Biomedicine & Pharmacotherapy*, vol. 151, p. 113068, Jul. 2022, doi: 10.1016/j.biopha.2022.113068.

[147] P. D. A. Vignali *et al.*, “Hypoxia drives CD39-dependent suppressor function in exhausted T cells to limit antitumor immunity,” *Nat Immunol*, vol. 24, no. 2, pp. 267–279, Feb. 2023, doi: 10.1038/s41590-022-01379-9.

[148] P. Jayaprakash *et al.*, “Targeted hypoxia reduction restores T cell infiltration and sensitizes prostate cancer to immunotherapy,” *Journal of Clinical Investigation*, vol. 128, no. 11, pp. 5137–5149, Oct. 2018, doi: 10.1172/JCI96268.

[149] A. Brown *et al.*, "A novel approach to neoadjuvant chemoradiation for soft tissue sarcoma using cisplatin and adriamycin.," *JCO*, vol. 37, no. 15_suppl, pp. e22515–e22515, May 2019, doi: 10.1200/JCO.2019.37.15_suppl.e22515.

[150] M. Savina *et al.*, "Patterns of care and outcomes of patients with METAstatic soft tissue SARComa in a real-life setting: the METASARC observational study," *BMC Medicine*, vol. 15, no. 1, p. 78, Apr. 2017, doi: 10.1186/s12916-017-0831-7.

[151] A. M. Frezza, S. Stacchiotti, and A. Gronchi, "Systemic treatment in advanced soft tissue sarcoma: what is standard, what is new," *BMC Medicine*, vol. 15, no. 1, p. 109, Jun. 2017, doi: 10.1186/s12916-017-0872-y.

[152] J. C. Walsh, A. Lebedev, E. Aten, K. Madsen, L. Marciano, and H. C. Kolb, "The Clinical Importance of Assessing Tumor Hypoxia: Relationship of Tumor Hypoxia to Prognosis and Therapeutic Opportunities," *Antioxid Redox Signal*, vol. 21, no. 10, pp. 1516–1554, Oct. 2014, doi: 10.1089/ars.2013.5378.

[153] Z. Fan, C. Chi, Y. Tong, Z. Huang, Y. Song, and S. You, "Score for the Risk and Overall Survival of Lung Metastasis in Patients First Diagnosed With Soft Tissue Sarcoma: A Novel Nomogram-Based Risk Assessment System," *Technol Cancer Res Treat*, vol. 21, p. 15330338211066240, Jan. 2022, doi: 10.1177/15330338211066240.

[154] A. Italiano *et al.*, "Trends in survival for patients with metastatic soft-tissue sarcoma," *Cancer*, vol. 117, no. 5, pp. 1049–1054, 2011, doi: 10.1002/cncr.25538.

[155] M. Nordsmark *et al.*, "Hypoxia in human soft tissue sarcomas: Adverse impact on survival and no association with p53 mutations," *Br J Cancer*, vol. 84, no. 8, pp. 1070–1075, Apr. 2001, doi: 10.1054/bjoc.2001.1728.

[156] L. P. Ferreira, V. M. Gaspar, and J. F. Mano, "Design of spherically structured 3D *in vitro* tumor models -Advances and prospects," *Acta Biomaterialia*, vol. 75, pp. 11–34, Jul. 2018, doi: 10.1016/j.actbio.2018.05.034.

[157] C. Jensen and Y. Teng, "Is It Time to Start Transitioning From 2D to 3D Cell Culture?," *Front Mol Biosci*, vol. 7, p. 33, 2020, doi: 10.3389/fmolb.2020.00033.

[158] K. Białkowska, P. Komorowski, M. Bryszewska, and K. Miłowska, "Spheroids as a Type of Three-Dimensional Cell Cultures—Examples of Methods of Preparation and the Most Important Application," *Int J Mol Sci*, vol. 21, no. 17, p. 6225, Aug. 2020, doi: 10.3390/ijms21176225.

[159] N.-E. Ryu, S.-H. Lee, and H. Park, "Spheroid Culture System Methods and Applications for Mesenchymal Stem Cells," *Cells*, vol. 8, no. 12, p. 1620, Dec. 2019, doi: 10.3390/cells8121620.

[160] R. Foty, "A Simple Hanging Drop Cell Culture Protocol for Generation of 3D Spheroids," *J Vis Exp*, no. 51, p. 2720, May 2011, doi: 10.3791/2720.

[161] S. J. Han, S. Kwon, and K. S. Kim, "Challenges of applying multicellular tumor spheroids in preclinical phase," *Cancer Cell International*, vol. 21, no. 1, p. 152, Mar. 2021, doi: 10.1186/s12935-021-01853-8.

[162] W. H. Abuwatfa, W. G. Pitt, and G. A. Husseini, "Scaffold-based 3D cell culture models in cancer research," *Journal of Biomedical Science*, vol. 31, no. 1, p. 7, Jan. 2024, doi: 10.1186/s12929-024-00994-y.

[163] S. Riffle, R. N. Pandey, M. Albert, and R. S. Hegde, "Linking hypoxia, DNA damage and proliferation in multicellular tumor spheroids," *BMC Cancer*, vol. 17, no. 1, p. 338, May 2017, doi: 10.1186/s12885-017-3319-0.

[164] M. Xavierselvan, B. Bednarke, R. T. Shethia, V. Yang, L. Moses, and S. Mallidi, "Oxygen-releasing nanodroplets relieve intratumoral hypoxia in head and neck cancer spheroids," May 31, 2024, *bioRxiv*. doi: 10.1101/2024.05.26.595914.

[165] D. Dorrigiv *et al.*, "Microdissected Tissue vs Tissue Slices—A Comparative Study of Tumor Explant Models Cultured On-Chip and Off-Chip," *Cancers*, vol. 13, no. 16, Art. no. 16, Jan. 2021, doi: 10.3390/cancers13164208.

[166] J. Rodrigues, M. A. Heinrich, L. M. Teixeira, and J. Prakash, "3D *In Vitro* Model (R)evolution: Unveiling Tumor–Stroma Interactions," *Trends in Cancer*, vol. 7, no. 3, pp. 249–264, Mar. 2021, doi: 10.1016/j.trecan.2020.10.009.

[167] B. Majumder *et al.*, "Predicting clinical response to anticancer drugs using an ex vivo platform that captures tumour heterogeneity," *Nat Commun*, vol. 6, p. 6169, Feb. 2015, doi: 10.1038/ncomms7169.

[168] T. G. Meijer, K. A. Naipal, A. Jager, and D. C. van Gent, "Ex vivo tumor culture systems for functional drug testing and therapy response prediction," *Future Sci OA*, vol. 3, no. 2, p. FSO190, Mar. 2017, doi: 10.4155/fsoa-2017-0003.

[169] H. Clevers, "Modeling Development and Disease with Organoids," *Cell*, vol. 165, no. 7, pp. 1586–1597, Jun. 2016, doi: 10.1016/j.cell.2016.05.082.

[170] K. Simeone *et al.*, "Paraffin-embedding lithography and micro-dissected tissue micro-arrays: tools for biological and pharmacological analysis of ex vivo solid tumors," *Lab Chip*, vol. 19, no. 4, pp. 693–705, 2019, doi: 10.1039/C8LC00982A.

[171] J. Chuprin *et al.*, "Humanized mouse models for immuno-oncology research," *Nat Rev Clin Oncol*, vol. 20, no. 3, pp. 192–206, Mar. 2023, doi: 10.1038/s41571-022-00721-2.

[172] I. Daimiel, "Insights into Hypoxia: Non-invasive Assessment through Imaging Modalities and Its Application in Breast Cancer," *J Breast Cancer*, vol. 22, no. 2, pp. 155–171, May 2019, doi: 10.4048/jbc.2019.22.e26.

[173] "Text - S.5002 - 117th Congress (2021-2022): FDA Modernization Act 2.0 | Congress.gov | Library of Congress." Accessed: Mar. 03, 2025. [Online]. Available: https://www.congress.gov/bill/117th-congress/senate-bill/5002/text

[174] S. Vazquez, "FDAModernization3.0.2025".

[175] "EMA implements new measures to minimise animal testing during medicines development | European Medicines Agency (EMA)." Accessed: Apr. 02, 2025. [Online]. Available: https://www.ema.europa.eu/en/news/ema-implements-new-measures-minimise-animal-testing-during-medicines-development

[176] M. Di Mattia *et al.*, "Hypoxia-Mimetic CoCl2 Agent Enhances Pro-Angiogenic Activities in Ovine Amniotic Epithelial Cells-Derived Conditioned Medium," *Cells*, vol. 11, no. 3, p. 461, Jan. 2022, doi: 10.3390/cells11030461.

[177] J. Muñoz-Sánchez and M. E. Chánez-Cárdenas, "The use of cobalt chloride as a chemical hypoxia model," *Journal of Applied Toxicology*, vol. 39, no. 4, pp. 556–570, 2019, doi: 10.1002/jat.3749.

[178] D. Wu and P. Yotnda, "Induction and Testing of Hypoxia in Cell Culture," *J Vis Exp*, no. 54, p. 2899, Aug. 2011, doi: 10.3791/2899.

[179] N. Zhigalova, A. Artemov, A. Mazur, and E. Prokhortchouk, "Transcriptome sequencing revealed differences in the response of renal cancer cells to hypoxia and CoCl 2 treatment," *F1000Res*, vol. 4, p. 1518, 2015, doi: 10.12688/f1000research.7571.1.

[180] M. H. Kim, S. D. Green, C. Lin, and H. Konig, "Engineering Tools for Regulating Hypoxia in Tumour Models," *J Cell Mol Med*, vol. 25, no. 16, pp. 7581–7592, Aug. 2021, doi: 10.1111/jcmm.16759.

[181] S. Barmaki, D. Obermaier, E. Kankuri, J. Vuola, S. Franssila, and V. Jokinen, "A Microfluidic Chip Architecture Enabling a Hypoxic Microenvironment and Nitric Oxide Delivery in Cell Culture," *Micromachines*, vol. 11, no. 11, Art. no. 11, Nov. 2020, doi: 10.3390/mi11110979.

[182] J. A. Hickman *et al.*, "Three-dimensional models of cancer for pharmacology and cancer cell biology: Capturing tumor complexity in vitro/ex vivo," *Biotechnology Journal*, vol. 9, no. 9, pp. 1115–1128, 2014, doi: 10.1002/biot.201300492.

[183] D. Rodenhizer, T. Dean, E. D'Arcangelo, and A. P. McGuigan, "The Current Landscape of 3D In Vitro Tumor Models: What Cancer Hallmarks Are Accessible for Drug Discovery?," *Advanced Healthcare Materials*, vol. 7, no. 8, p. 1701174, 2018, doi: 10.1002/adhm.201701174.

[184] J. Friedrich, C. Seidel, R. Ebner, and L. A. Kunz-Schughart, "Spheroid-based drug screen: considerations and practical approach," *Nat Protoc*, vol. 4, no. 3, Art. no. 3, Mar. 2009, doi: 10.1038/nprot.2008.226.

[185] Z. Xu *et al.*, "Application of a microfluidic chip-based 3D co-culture to test drug sensitivity for individualized treatment of lung cancer," *Biomaterials*, vol. 34, no. 16, pp. 4109–4117, May 2013, doi: 10.1016/j.biomaterials.2013.02.045.

[186] N. Gupta, J. R. Liu, B. Patel, D. E. Solomon, B. Vaidya, and V. Gupta, "Microfluidics-based 3D cell culture models: Utility in novel drug discovery and delivery research," *Bioeng Transl Med*, vol. 1, no. 1, pp. 63–81, Jul. 2016, doi: 10.1002/btm2.10013.

[187] L. F. Horowitz, A. D. Rodriguez, T. Ray, and A. Folch, "Microfluidics for interrogating live intact tissues," *Microsyst Nanoeng*, vol. 6, no. 1, pp. 1–27, Aug. 2020, doi: 10.1038/s41378-020-0164-0.

[188] R. Edmondson, J. J. Broglie, A. F. Adcock, and L. Yang, "Three-Dimensional Cell Culture Systems and Their Applications in Drug Discovery and Cell-Based Biosensors," *Assay Drug Dev Technol*, vol. 12, no. 4, pp. 207–218, May 2014, doi: 10.1089/adt.2014.573.

[189] A. St-Georges-Robillard *et al.*, “Long-term fluorescence hyperspectral imaging of on-chip treated co-culture tumour spheroids to follow clonal evolution,” *Integrative Biology*, vol. 11, no. 4, pp. 130–141, avril 2019, doi: 10.1093/intbio/zyz012.

[190] Y. Ding *et al.*, “Microfluidic-Enabled Print-to-Screen Platform for High-Throughput Screening of Combinatorial Chemotherapy,” *Anal. Chem.*, vol. 87, no. 20, pp. 10166–10171, Oct. 2015, doi: 10.1021/acs.analchem.5b00826.

[191] X. Cao *et al.*, “A Tumor-on-a-Chip System with Bioprinted Blood and Lymphatic Vessel Pair,” *Advanced Functional Materials*, vol. 29, no. 31, p. 1807173, 2019, doi: 10.1002/adfm.201807173.

[192] J. B. Nielsen, R. L. Hanson, H. M. Almughamsi, C. Pang, T. R. Fish, and A. T. Woolley, “Microfluidics: Innovations in Materials and Their Fabrication and Functionalization,” *Anal Chem*, vol. 92, no. 1, pp. 150–168, Jan. 2020, doi: 10.1021/acs.analchem.9b04986.

[193] S. Aralekallu, R. Boddula, and V. Singh, “Development of glass-based microfluidic devices: A review on its fabrication and biologic applications,” *Materials & Design*, vol. 225, p. 111517, Jan. 2023, doi: 10.1016/j.matdes.2022.111517.

[194] V. Mehta and S. N. Rath, “3D printed microfluidic devices: a review focused on four fundamental manufacturing approaches and implications on the field of healthcare,” *Bio-des. Manuf.*, vol. 4, no. 2, pp. 311–343, Jun. 2021, doi: 10.1007/s42242-020-00112-5.

[195] P. Kim, K. W. Kwon, M. C. Park, S. H. Lee, S. M. Kim, and K. Y. Suh, “Soft lithography for microfluidics: a review,” *BIOCHIP JOURNAL*, vol. 2, no. 1, pp. 1–11, 2008.

[196] M. Kalashnikov *et al.*, “Plasma-assisted building and coating of multi-layered microfluidic devices,” p. 5.

[197] I. Kamal *et al.*, “Evaluation of radiation attenuation properties on a various composition of polydimethylsiloxane (PDMS) for fabrication of kidney phantom,” *Radiation Physics and Chemistry*, vol. 189, p. 109661, Dec. 2021, doi: 10.1016/j.radphyschem.2021.109661.

[198] K. Raj M and S. Chakraborty, “PDMS microfluidics: A mini review,” *Journal of Applied Polymer Science*, vol. 137, no. 27, p. 48958, 2020, doi: 10.1002/app.48958.

[199] K. Moshksayan *et al.*, “Spheroids-on-a-chip: Recent advances and design considerations in microfluidic platforms for spheroid formation and culture,” *Sensors and Actuators B: Chemical*, vol. 263, pp. 151–176, Jun. 2018, doi: 10.1016/j.snb.2018.01.223.

[200] P. Panuška *et al.*, “Advanced Microfluidic Platform for Tumor Spheroid Formation and Cultivation Fabricated from OSTE+ Polymer,” *BioChip J*, vol. 18, no. 3, pp. 393–409, Sep. 2024, doi: 10.1007/s13206-024-00167-x.

[201] K. Simeone *et al.*, “Paraffin-embedding lithography and micro-dissected tissue micro-arrays: tools for biological and pharmacological analysis of ex vivo solid tumors,” *Lab Chip*, vol. 19, no. 4, pp. 693–705, Feb. 2019, doi: 10.1039/C8LC00982A.

[202] D. Dorrigiv, P.-A. Goyette, A. St-Georges-Robillard, A.-M. Mes-Masson, and T. Gervais, “Pixelated Microfluidics for Drug Screening on Tumour Spheroids and Ex Vivo Microdissected Tumour Explants,” *Cancers*, vol. 15, no. 4, Art. no. 4, Jan. 2023, doi: 10.3390/cancers15041060.

[203] R. Cheah, R. Srivastava, N. D. Stafford, A. W. Beavis, V. Green, and J. Greenman, "Measuring the response of human head and neck squamous cell carcinoma to irradiation in a microfluidic model allowing customized therapy," *International Journal of Oncology*, vol. 51, no. 4, pp. 1227–1238, Oct. 2017, doi: 10.3892/ijo.2017.4118.

[204] R. Kennedy *et al.*, "A patient tumour-on-a-chip system for personalised investigation of radiotherapy based treatment regimens," *Sci Rep*, vol. 9, p. 6327, Apr. 2019, doi: 10.1038/s41598-019-42745-2.

[205] S. D. Carr, V. L. Green, N. D. Stafford, and J. Greenman, "Analysis of Radiation-Induced Cell Death in Head and Neck Squamous Cell Carcinoma and Rat Liver Maintained in Microfluidic Devices," *Otolaryngol Head Neck Surg*, vol. 150, no. 1, pp. 73–80, Jan. 2014, doi: 10.1177/0194599813507427.

[206] M. Barisam, F. R. Niavol, M. A. Kinj, M. S. Saidi, H. Ghanbarian, and N. Kashaninejad, "Enrichment of cancer stem-like cells by controlling oxygen, glucose and fluid shear stress in a microfluidic spheroid culture device," *Journal of Science: Advanced Materials and Devices*, vol. 7, no. 2, p. 100439, Jun. 2022, doi: 10.1016/j.jsamd.2022.100439.

[207] E. Pyne *et al.*, "Investigating the impact of the interstitial fluid flow and hypoxia interface on cancer transcriptomes using a spheroid-on-chip perfusion system," *Lab on a Chip*, vol. 24, no. 19, pp. 4609–4622, 2024, doi: 10.1039/D4LC00512K.

[208] M. Geyer, D. Schreyer, L.-M. Gaul, S. Pfeffer, C. Pilarsky, and K. Queiroz, "A microfluidic-based PDAC organoid system reveals the impact of hypoxia in response to treatment," *Cell Death Discov.*, vol. 9, no. 1, pp. 1–8, Jan. 2023, doi: 10.1038/s41420-023-01334-z.

[209] C. Bouquerel, "Hypoxia-on-chip: from technological developments to biological applications".

[210] S. M. Grist *et al.*, "Long-term monitoring in a microfluidic system to study tumour spheroid response to chronic and cycling hypoxia," *Scientific Reports*, vol. 9, no. 1, Art. no. 1, Nov. 2019, doi: 10.1038/s41598-019-54001-8.

[211] I. Berger Fridman, G. S. Ugolini, V. VanDelinder, S. Cohen, and T. Konry, "High throughput microfluidic system with multiple oxygen levels for the study of hypoxia in tumor spheroids," *Biofabrication*, vol. 13, no. 3, p. 035037, Apr. 2021, doi: 10.1088/1758-5090/abdb88.

[212] A. Morshed and P. Dutta, "Hypoxic behavior in cells under controlled microfluidic environment," *Biochimica et Biophysica Acta (BBA) - General Subjects*, vol. 1861, no. 4, pp. 759–771, Apr. 2017, doi: 10.1016/j.bbagen.2017.01.017.

[213] M. Busek *et al.*, "Microfluidic system for in-vitro hypoxia assays," presented at the SPIE BiOS, B. L. Gray and H. Becker, Eds., San Francisco, California, United States, Feb. 2017, p. 1006110. doi: 10.1117/12.2253664.

[214] M. Busek *et al.*, "Microfluidic system for in-vitro hypoxia assays," *Sci Rep*, vol. 13, no. 1, p. 5428, Apr. 2023, doi: 10.1038/s41598-023-32334-9.

[215] K. Funamoto, I. K. Zervantonakis, Y. Liu, C. J. Ochs, C. Kim, and R. D. Kamm, "A novel microfluidic platform for high-resolution imaging of a three-dimensional cell culture under

a controlled hypoxic environment," *Lab Chip*, vol. 12, no. 22, pp. 4855–4863, Oct. 2012, doi: 10.1039/C2LC40306D.

[216] L. Ding *et al.*, "Microfluidic Device with an Oxygen Gradient Generator for Investigating Effects of Specific Hypoxia Conditions on Responses of Tumor Cells," *Langmuir*, vol. 40, no. 37, pp. 19316–19323, Sep. 2024, doi: 10.1021/acs.langmuir.4c00714.

[217] J. M. Oh, H. M. Begum, Y. L. Liu, Y. Ren, and K. Shen, "Recapitulating Tumor Hypoxia in a Cleanroom-Free, Liquid-Pinning-Based Microfluidic Tumor Model," *ACS Biomater. Sci. Eng.*, vol. 8, no. 7, pp. 3107–3121, Jul. 2022, doi: 10.1021/acsbiomaterials.2c00207.

[218] M. D. Brennan, M. L. Rexius-Hall, L. J. Elgass, and D. T. Eddington, "Oxygen control with microfluidics," *Lab Chip*, vol. 14, no. 22, pp. 4305–4318, Oct. 2014, doi: 10.1039/C4LC00853G.

[219] S. M. Kirsh, S. A. Pascetta, and J. Uniacke, "Spheroids as a 3D Model of the Hypoxic Tumor Microenvironment," in *The Tumor Microenvironment: Methods and Protocols*, J. Ursini-Siegel, Ed., New York, NY: Springer US, 2023, pp. 273–285. doi: 10.1007/978-1-0716-2914-7_17.

[220] M. Busek *et al.*, "Microfluidic system for in-vitro hypoxia assays," in *Microfluidics, BioMEMS, and Medical Microsystems XV*, SPIE, Feb. 2017, pp. 173–182. doi: 10.1117/12.2253664.

[221] N. Takahashi *et al.*, "Microfluidic platform for the reproduction of hypoxic vascular microenvironments," *Sci Rep*, vol. 13, no. 1, p. 5428, Apr. 2023, doi: 10.1038/s41598-023-32334-9.

[222] T.-E. Park *et al.*, "Hypoxia-enhanced Blood-Brain Barrier Chip recapitulates human barrier function and shuttling of drugs and antibodies," *Nat Commun*, vol. 10, no. 1, p. 2621, Jun. 2019, doi: 10.1038/s41467-019-10588-0.

[223] Y. B. (Abraham) Kang, J. Eo, B. Bulutoglu, M. L. Yarmush, and O. B. Usta, "Progressive Hypoxia-on-a-Chip: An In Vitro Oxygen Gradient Model for Capturing the Effects of Hypoxia on Primary Hepatocytes in Health and Disease," *Biotechnol Bioeng*, vol. 117, no. 3, pp. 763–775, Mar. 2020, doi: 10.1002/bit.27225.

[224] H.-S. Kim *et al.*, "O2 variant chip to simulate site-specific skeletogenesis from hypoxic bone marrow," *Science Advances*, vol. 9, no. 12, p. eadd4210, Mar. 2023, doi: 10.1126/sciadv.add4210.

[225] S. Ghafoory *et al.*, "Oxygen Gradient Induced in Microfluidic Chips Can Be Used as a Model for Liver Zonation," *Cells*, vol. 11, no. 23, Art. no. 23, Jan. 2022, doi: 10.3390/cells11233734.

[226] D. Dorrigiv *et al.*, "Microdissected Tissue vs. Tissue Slices—A Comparative Study of Tumor Explant Models Cultured On-Chip and Off-Chip," *Cancers (Basel)*, vol. 13, no. 16, p. 4208, Aug. 2021, doi: 10.3390/cancers13164208.

[227] N. Rousset, F. Monet, and T. Gervais, "Simulation-assisted design of microfluidic sample traps for optimal trapping and culture of non-adherent single cells, tissues, and spheroids," *Sci Rep*, vol. 7, no. 1, p. 245, Dec. 2017, doi: 10.1038/s41598-017-00229-1.

[228] L. F. Horowitz *et al.*, "Microdissected 'cuboids' for microfluidic drug testing of intact tissues," *Lab Chip*, vol. 21, no. 1, pp. 122–142, Jan. 2021, doi: 10.1039/d0lc00801j.

[229] L. F. Horowitz *et al.*, "Multiplexed drug testing of tumor slices using a microfluidic platform," *npj Precis. Onc.*, vol. 4, no. 1, pp. 1–15, May 2020, doi: 10.1038/s41698-020-0117-y.

[230] L. F. Horowitz *et al.*, "Microdissected tumor cuboids: a microscale cancer model for large-scale testing that retains a complex tumor microenvironment," *bioRxiv*, p. 2024.03.22.586189, Nov. 2024, doi: 10.1101/2024.03.22.586189.

[231] T. C. Chang, A. M. Mikheev, W. Huynh, R. J. Monnat, R. C. Rostomily, and A. Folch, "Parallel microfluidic chemosensitivity testing on individual slice cultures," *Lab Chip*, vol. 14, no. 23, pp. 4540–4551, Dec. 2014, doi: 10.1039/c4lc00642a.

[232] G. Mehta, A. Y. Hsiao, M. Ingram, G. D. Luker, and S. Takayama, "Opportunities and challenges for use of tumor spheroids as models to test drug delivery and efficacy," *Journal of Controlled Release*, vol. 164, no. 2, pp. 192–204, Dec. 2012, doi: 10.1016/j.jconrel.2012.04.045.

[233] R. H. Wenger, V. Kurtcuoglu, C. C. Scholz, H. H. Marti, and D. Hoogewijs, "Frequently asked questions in hypoxia research," *Hypoxia (Auckl)*, vol. 3, pp. 35–43, Sep. 2015, doi: 10.2147/HP.S92198.

[234] E. B. Rankin and A. J. Giaccia, "Hypoxic control of metastasis," *Science*, vol. 352, no. 6282, pp. 175–180, Apr. 2016, doi: 10.1126/science.aaf4405.

[235] D. M. Gilkes, G. L. Semenza, and D. Wirtz, "Hypoxia and the extracellular matrix: drivers of tumour metastasis," *Nat Rev Cancer*, vol. 14, no. 6, pp. 430–439, Jun. 2014, doi: 10.1038/nrc3726.

[236] S. P. Chawla *et al.*, "Phase II Study of the Safety and Antitumor Activity of the Hypoxia-Activated Prodrug TH-302 in Combination With Doxorubicin in Patients With Advanced Soft Tissue Sarcoma," *JCO*, vol. 32, no. 29, pp. 3299–3306, Oct. 2014, doi: 10.1200/JCO.2013.54.3660.

[237] C. Bernauer, Y. K. S. Man, J. C. Chisholm, E. Y. Lepicard, S. P. Robinson, and J. M. Shipley, "Hypoxia and its therapeutic possibilities in paediatric cancers," *Br J Cancer*, vol. 124, no. 3, pp. 539–551, Feb. 2021, doi: 10.1038/s41416-020-01107-w.

[238] G. L. Semenza, "Oxygen Sensing, Hypoxia-Inducible Factors, and Disease Pathophysiology," *Annual Review of Pathology: Mechanisms of Disease*, vol. 9, no. 1, pp. 47–71, 2014, doi: 10.1146/annurev-pathol-012513-104720.

[239] K. Måseide *et al.*, "Carbonic Anhydrase IX as a Marker for Poor Prognosis in Soft Tissue Sarcoma," *Clin Cancer Res*, vol. 10, no. 13, pp. 4464–4471, Jul. 2004, doi: 10.1158/1078-0432.CCR-03-0541.

[240] S. J. A. van Kuijk, A. Yaromina, R. Houben, R. Niemans, P. Lambin, and L. J. Dubois, "Prognostic Significance of Carbonic Anhydrase IX Expression in Cancer Patients: A Meta-Analysis," *Front. Oncol.*, vol. 0, 2016, doi: 10.3389/fonc.2016.00069.

[241] G. Venkateswaran and S. Dedhar, “Interplay of Carbonic Anhydrase IX With Amino Acid and Acid/Base Transporters in the Hypoxic Tumor Microenvironment,” *Front. Cell Dev. Biol.*, vol. 0, 2020, doi: 10.3389/fcell.2020.602668.

[242] M. W. Dewhirst, Y. Cao, and B. Moeller, “Cycling hypoxia and free radicals regulate angiogenesis and radiotherapy response,” *Nat Rev Cancer*, vol. 8, no. 6, pp. 425–437, Jun. 2008, doi: 10.1038/nrc2397.

[243] A. Lequeux *et al.*, “Impact of hypoxic tumor microenvironment and tumor cell plasticity on the expression of immune checkpoints,” *Cancer Lett*, vol. 458, pp. 13–20, Aug. 2019, doi: 10.1016/j.canlet.2019.05.021.

[244] M. Z. Noman *et al.*, “Improving Cancer Immunotherapy by Targeting the Hypoxic Tumor Microenvironment: New Opportunities and Challenges,” *Cells*, vol. 8, no. 9, Sep. 2019, doi: 10.3390/cells8091083.

[245] B. Wang *et al.*, “Targeting hypoxia in the tumor microenvironment: a potential strategy to improve cancer immunotherapy,” *Journal of Experimental & Clinical Cancer Research*, vol. 40, no. 1, p. 24, Jan. 2021, doi: 10.1186/s13046-020-01820-7.

[246] K. B. Peters and J. M. Brown, “Tirapazamine: A Hypoxia-activated Topoisomerase II Poison,” *Cancer Res.*, vol. 62, no. 18, pp. 1916–1930, Sep. 2002.

[247] S. H. Lin *et al.*, “Opportunities and Challenges in the Era of Molecularly Targeted Agents and Radiation Therapy,” *JNCI: Journal of the National Cancer Institute*, vol. 105, no. 10, pp. 686–693, May 2013, doi: 10.1093/jnci/djt055.

[248] M. Bavoux *et al.*, “X-ray on chip: Quantifying therapeutic synergies between radiotherapy and anticancer drugs using soft tissue sarcoma tumor spheroids,” *Radiotherapy and Oncology*, vol. 157, pp. 175–181, Apr. 2021, doi: 10.1016/j.radonc.2021.01.018.

[249] J. A. Hickman *et al.*, “Three-dimensional models of cancer for pharmacology and cancer cell biology: Capturing tumor complexity in vitro/ex vivo,” *Biotechnology Journal*, vol. 9, no. 9, pp. 1115–1128, Sep. 2014, doi: 10.1002/biot.201300492.

[250] M. Marimuthu *et al.*, “Multi-size spheroid formation using microfluidic funnels,” *Lab Chip*, vol. 18, no. 2, pp. 304–314, 2018, doi: 10.1039/C7LC00970D.

[251] J. Lafontaine, G. B. Cardin, N. Malaquin, J.-S. Boisvert, F. Rodier, and P. Wong, “Senolytic Targeting of Bcl-2 Anti-Apoptotic Family Increases Cell Death in Irradiated Sarcoma Cells,” *Cancers*, vol. 13, no. 3, Art. no. 3, Jan. 2021, doi: 10.3390/cancers13030386.

[252] J. Friedrich, C. Seidel, R. Ebner, and L. A. Kunz-Schughart, “Spheroid-based drug screen: considerations and practical approach,” *Nat Protoc*, vol. 4, no. 3, pp. 309–324, Mar. 2009, doi: 10.1038/nprot.2008.226.

[253] “T47D Cell Line Spheroid Generation and Characterization for HT Assays | Thermo Fisher Scientific - CA.” Accessed: Apr. 28, 2021. [Online]. Available: https://www.thermofisher.com/ca/en/home/references/protocols/cell-culture/3-d-cell-culture-protocol/t47d-cell-line-spheroid-generation.html

[254] J. M. Brown, “The Hypoxic Cell: A Target for Selective Cancer Therapy—Eighteenth Bruce F. Cain Memorial Award Lecture,” *Cancer Res.*, vol. 59, no. 23, pp. 5863–5870, Dec. 1999.

[255] D. Vordermark and J. M. Brown, “Endogenous Markers of TumorHypoxia,” *Strahlenther Onkol*, vol. 179, no. 12, pp. 801–811, Dec. 2003, doi: 10.1007/s00066-003-1150-9.

[256] Y.-J. Kim *et al.*, “Overcoming evasive resistance from vascular endothelial growth factor a inhibition in sarcomas by genetic or pharmacologic targeting of hypoxia-inducible factor 1α,” *Int J Cancer*, vol. 132, no. 1, pp. 29–41, Jan. 2013, doi: 10.1002/ijc.27666.

[257] M. R. Doe, J. Ascano, M. Kaur, and M. D. Cole, “Myc post-transcriptionally induces HIF1 protein and target gene expression in normal and cancer cells,” *Cancer Res*, vol. 72, no. 4, pp. 949–957, Feb. 2012, doi: 10.1158/0008-5472.CAN-11-2371.

[258] J. Gao *et al.*, “Integrative Analysis of Complex Cancer Genomics and Clinical Profiles Using the cBioPortal,” *Sci Signal*, vol. 6, no. 269, p. pl1, Apr. 2013, doi: 10.1126/scisignal.2004088.

[259] E. Cerami *et al.*, “The cBio Cancer Genomics Portal: An Open Platform for Exploring Multidimensional Cancer Genomics Data,” *Cancer Discov*, vol. 2, no. 5, pp. 401–404, May 2012, doi: 10.1158/2159-8290.CD-12-0095.

[260] K. Han *et al.*, “CRISPR screens in cancer spheroids identify 3D growth-specific vulnerabilities,” *Nature*, vol. 580, no. 7801, Art. no. 7801, Apr. 2020, doi: 10.1038/s41586-020-2099-x.

[261] S. Kaluz, M. Kaluzová, S.-Y. Liao, M. Lerman, and E. J. Stanbridge, “Transcriptional control of the tumor- and hypoxia-marker carbonic anhydrase 9: a one transcription factor (HIF-1) show?,” *Biochim Biophys Acta*, vol. 1795, no. 2, pp. 162–172, Apr. 2009, doi: 10.1016/j.bbcan.2009.01.001.

[262] A. McIntyre *et al.*, “Carbonic anhydrase IX promotes tumour growth and necrosis in vivo and inhibition enhances anti-VEGF therapy,” *Clin Cancer Res*, vol. 18, no. 11, pp. 3100–3111, Jun. 2012, doi: 10.1158/1078-0432.CCR-11-1877.

[263] P. L. Olive *et al.*, “Carbonic anhydrase 9 as an endogenous marker for hypoxic cells in cervical cancer,” *Cancer Res*, vol. 61, no. 24, pp. 8924–8929, Dec. 2001.

[264] C. Ward, J. Meehan, M. Gray, I. H. Kunkler, S. P. Langdon, and D. J. Argyle, “Carbonic Anhydrase IX (CAIX), Cancer, and Radiation Responsiveness,” *Metabolites*, vol. 8, no. 1, Art. no. 1, Mar. 2018, doi: 10.3390/metabo8010013.

[265] C. Muriel López *et al.*, “Prognostic Factors in Patients With Advanced Renal Cell Carcinoma,” *Clinical Genitourinary Cancer*, vol. 10, no. 4, pp. 262–270, Dec. 2012, doi: 10.1016/j.clgc.2012.06.005.

[266] N. K. Tafreshi *et al.*, “Evaluation of CAIX and CAXII Expression in Breast Cancer at Varied O2 Levels: CAIX is the Superior Surrogate Imaging Biomarker of Tumor Hypoxia,” *Mol Imaging Biol*, vol. 18, no. 2, pp. 219–231, Apr. 2016, doi: 10.1007/s11307-015-0885-x.

[267] H. Yoo *et al.*, “Expression of the Hypoxia Marker Carbonic Anhydrase 9 Is Associated with Anaplastic Phenotypes in Meningiomas,” *Clin Cancer Res*, vol. 13, no. 1, pp. 68–75, Jan. 2007, doi: 10.1158/1078-0432.CCR-06-1377.

[268] K. H. Shin *et al.*, “Detecting changes in tumor hypoxia with carbonic anhydrase IX and pimonidazole,” *Cancer Biol Ther*, vol. 6, no. 1, pp. 70–75, Jan. 2007, doi: 10.4161/cbt.6.1.3550.

[269] E. A. Sheta, H. Trout, J. J. Gildea, M. A. Harding, and D. Theodorescu, "Cell density mediated pericellular hypoxia leads to induction of HIF-1α via nitric oxide and Ras/MAP kinase mediated signaling pathways," *Oncogene*, vol. 20, no. 52, Art. no. 52, Nov. 2001, doi: 10.1038/sj.onc.1204972.

[270] F. He *et al.*, "Noninvasive Molecular Imaging of Hypoxia in Human Xenografts: Comparing Hypoxia-Induced Gene Expression with Endogenous and Exogenous Hypoxia Markers," *Cancer Res*, vol. 68, no. 20, pp. 8597–8606, Oct. 2008, doi: 10.1158/0008-5472.CAN-08-0677.

[271] B. S. Sørensen *et al.*, "Influence of oxygen concentration and pH on expression of hypoxia induced genes," *Radiotherapy and Oncology*, vol. 76, no. 2, pp. 187–193, Aug. 2005, doi: 10.1016/j.radonc.2005.06.037.

[272] D. G. Buerk, "Measuring Tissue PO2 with Microelectrodes," in *Methods in Enzymology*, vol. 381, in Oxygen Sensing, vol. 381. , Academic Press, 2004, pp. 665–690. doi: 10.1016/S0076-6879(04)81043-7.

[273] W. A. Denny and W. R. Wilson, "Tirapazamine: a bioreductive anticancer drug that exploits tumour hypoxia," *Expert Opinion on Investigational Drugs*, vol. 9, no. 12, pp. 2889–2901, Dec. 2000, doi: 10.1517/13543784.9.12.2889.

[274] S. B. Reddy and S. K. Williamson, "Tirapazamine: a novel agent targeting hypoxic tumor cells," *Expert Opinion on Investigational Drugs*, vol. 18, no. 1, pp. 77–87, Jan. 2009, doi: 10.1517/13543780802567250.

[275] F. W. Hunter, B. G. Wouters, and W. R. Wilson, "Hypoxia-activated prodrugs: paths forward in the era of personalised medicine," *Br J Cancer*, vol. 114, no. 10, pp. 1071–1077, May 2016, doi: 10.1038/bjc.2016.79.

[276] K. R. Luoto, R. Kumareswaran, and R. G. Bristow, "Tumor hypoxia as a driving force in genetic instability," *Genome Integr*, vol. 4, p. 5, Oct. 2013, doi: 10.1186/2041-9414-4-5.

[277] P. L. Olive, J. P. Banáth, and L. T. Sinnott, "Phosphorylated Histone H2AX in Spheroids, Tumors, and Tissues of Mice Exposed to Etoposide and 3-Amino-1,2,4-Benzotriazine-1,3-Dioxide," *Cancer Res*, vol. 64, no. 15, pp. 5363–5369, Aug. 2004, doi: 10.1158/0008-5472.CAN-04-0729.

[278] R. Kumareswaran, O. Ludkovski, A. Meng, J. Sykes, M. Pintilie, and R. G. Bristow, "Chronic hypoxia compromises repair of DNA double-strand breaks to drive genetic instability," *J Cell Sci*, vol. 125, no. Pt 1, pp. 189–199, Jan. 2012, doi: 10.1242/jcs.092262.

[279] P. Wardman, "Chemical Radiosensitizers for Use in Radiotherapy," *Clinical Oncology*, vol. 19, no. 6, pp. 397–417, Aug. 2007, doi: 10.1016/j.clon.2007.03.010.

[280] I. N. Mistry, M. Thomas, E. D. D. Calder, S. J. Conway, and E. M. Hammond, "Clinical Advances of Hypoxia-Activated Prodrugs in Combination With Radiation Therapy," *International Journal of Radiation Oncology*Biology*Physics*, vol. 98, no. 5, pp. 1183–1196, Aug. 2017, doi: 10.1016/j.ijrobp.2017.03.024.

[281] P. Vaupel and A. Mayer, "Hypoxia in cancer: significance and impact on clinical outcome," *Cancer Metastasis Rev*, vol. 26, no. 2, pp. 225–239, Jun. 2007, doi: 10.1007/s10555-007-9055-1.

[282] C. Brahimi-Horn and J. Pouysségur, “The role of the hypoxia-inducible factor in tumor metabolism growth and invasion,” *Bull Cancer*, vol. 93, no. 8, pp. E73-80, Aug. 2006.

[283] M. C. Brahimi-Horn, J. Chiche, and J. Pouysségur, “Hypoxia and cancer,” *J Mol Med (Berl)*, vol. 85, no. 12, pp. 1301–1307, Dec. 2007, doi: 10.1007/s00109-007-0281-3.

[284] M. Hockel and P. Vaupel, “Tumor Hypoxia: Definitions and Current Clinical, Biologic, and Molecular Aspects,” *JNCI Journal of the National Cancer Institute*, vol. 93, no. 4, pp. 266–276, Feb. 2001, doi: 10.1093/jnci/93.4.266.

[285] H. Niizeki *et al.*, “Hypoxia enhances the expression of autocrine motility factor and the motility of human pancreatic cancer cells,” *Br J Cancer*, vol. 86, no. 12, pp. 1914–1919, Jun. 2002, doi: 10.1038/sj.bjc.6600331.

[286] A. L. Harris, “Hypoxia — a key regulatory factor in tumour growth,” *Nat Rev Cancer*, vol. 2, no. 1, pp. 38–47, Jan. 2002, doi: 10.1038/nrc704.

[287] B. Muz, P. de la Puente, F. Azab, and A. K. Azab, “The role of hypoxia in cancer progression, angiogenesis, metastasis, and resistance to therapy,” *Hypoxia (Auckl)*, vol. 3, pp. 83–92, Dec. 2015, doi: 10.2147/HP.S93413.

[288] Z. Chen, F. Han, Y. Du, H. Shi, and W. Zhou, “Hypoxic microenvironment in cancer: molecular mechanisms and therapeutic interventions,” *Sig Transduct Target Ther*, vol. 8, no. 1, pp. 1–23, Feb. 2023, doi: 10.1038/s41392-023-01332-8.

[289] H. E. Barker, J. T. E. Paget, A. A. Khan, and K. J. Harrington, “The tumour microenvironment after radiotherapy: mechanisms of resistance and recurrence,” *Nat Rev Cancer*, vol. 15, no. 7, Art. no. 7, Jul. 2015, doi: 10.1038/nrc3958.

[290] N. Devarajan, R. Manjunathan, and S. K. Ganesan, “Tumor hypoxia: The major culprit behind cisplatin resistance in cancer patients,” *Critical Reviews in Oncology/Hematology*, vol. 162, p. 103327, Jun. 2021, doi: 10.1016/j.critrevonc.2021.103327.

[291] E.-J. Yun *et al.*, “The network of DAB2IP-miR-138 in regulating drug resistance of renal cell carcinoma associated with stem-like phenotypes,” *Oncotarget*, vol. 8, no. 40, pp. 66975–66986, May 2017, doi: 10.18632/oncotarget.17756.

[292] S. P. C. Cole, “Multidrug Resistance Protein 1 (MRP1, ABCC1), a ‘Multitasking’ ATP-binding Cassette (ABC) Transporter,” *J Biol Chem*, vol. 289, no. 45, pp. 30880–30888, Nov. 2014, doi: 10.1074/jbc.R114.609248.

[293] R. Ratan and S. R. Patel, “Chemotherapy for soft tissue sarcoma,” *Cancer*, vol. 122, no. 19, pp. 2952–2960, 2016, doi: 10.1002/cncr.30191.

[294] D. M. Brizel *et al.*, “Tumor Oxygenation Predicts for the Likelihood of Distant Metastases in Human Soft Tissue Sarcoma,” *Cancer Res*, vol. 56, no. 5, pp. 941–943, Mar. 1996.

[295] E. Smeland *et al.*, “Prognostic Impacts of Hypoxic Markers in Soft Tissue Sarcoma,” *Sarcoma*, vol. 2012, p. e541650, Feb. 2012, doi: 10.1155/2012/541650.

[296] I. Godet, S. Doctorman, F. Wu, and D. M. Gilkes, “Detection of Hypoxia in Cancer Models: Significance, Challenges, and Advances,” *Cells*, vol. 11, no. 4, p. 686, Feb. 2022, doi: 10.3390/cells11040686.

[297] S. Bhattacharya, K. Calar, and P. de la Puente, "Mimicking tumor hypoxia and tumor-immune interactions employing three-dimensional in vitro models," *Journal of Experimental & Clinical Cancer Research*, vol. 39, no. 1, p. 75, May 2020, doi: 10.1186/s13046-020-01583-1.

[298] I. Godet, S. Doctorman, F. Wu, and D. M. Gilkes, "Detection of Hypoxia in Cancer Models: Significance, Challenges, and Advances," *Cells*, vol. 11, no. 4, p. 686, Feb. 2022, doi: 10.3390/cells11040686.

[299] M. Yee Koh, T. R. Spivak-Kroizman, and G. Powis, "HIF-1 regulation: not so easy come, easy go," *Trends Biochem Sci*, vol. 33, no. 11, pp. 526–534, Nov. 2008, doi: 10.1016/j.tibs.2008.08.002.

[300] G. J. Lim, S.-J. Kang, and J. Y. Lee, "Novel invasion indices quantify the feed-forward facilitation of tumor invasion by macrophages," *Sci Rep*, vol. 10, no. 1, p. 718, Jan. 2020, doi: 10.1038/s41598-020-57517-6.

[301] A. D. Robinson *et al.*, "Collagen modifying enzyme P4HA1 is overexpressed and plays a role in lung adenocarcinoma," *Translational Oncology*, vol. 14, no. 8, p. 101128, Aug. 2021, doi: 10.1016/j.tranon.2021.101128.

[302] H. Harada, "Hypoxia-inducible factor 1–mediated characteristic features of cancer cells for tumor radioresistance," *Journal of Radiation Research*, vol. 57, no. S1, pp. i99–i105, Aug. 2016, doi: 10.1093/jrr/rrw012.

[303] K. F. Idrisova, H.-U. Simon, and M. O. Gomzikova, "Role of Patient-Derived Models of Cancer in Translational Oncology," *Cancers (Basel)*, vol. 15, no. 1, p. 139, Dec. 2022, doi: 10.3390/cancers15010139.

[304] J.-P. Gillet *et al.*, "Redefining the relevance of established cancer cell lines to the study of mechanisms of clinical anti-cancer drug resistance," *Proceedings of the National Academy of Sciences*, vol. 108, no. 46, pp. 18708–18713, Nov. 2011, doi: 10.1073/pnas.1111840108.

[305] S. Jaeger, M. Duran-Frigola, and P. Aloy, "Drug sensitivity in cancer cell lines is not tissue-specific," *Molecular Cancer*, vol. 14, no. 1, p. 40, Feb. 2015, doi: 10.1186/s12943-015-0312-6.

[306] L. J. Forker *et al.*, "Technical development and validation of a clinically applicable microenvironment classifier as a biomarker of tumour hypoxia for soft tissue sarcoma," *Br J Cancer*, vol. 128, no. 12, pp. 2307–2317, Jun. 2023, doi: 10.1038/s41416-023-02265-3.

[307] N. Devarajan, R. Manjunathan, and S. K. Ganesan, "Tumor hypoxia: The major culprit behind cisplatin resistance in cancer patients," *Critical Reviews in Oncology/Hematology*, vol. 162, p. 103327, Jun. 2021, doi: 10.1016/j.critrevonc.2021.103327.

[308] A. Biroccio, B. Benassi, S. Amodei, C. Gabellini, D. D. Bufalo, and G. Zupi, "C-Myc Down-Regulation Increases Susceptibility to Cisplatin through Reactive Oxygen Species-Mediated Apoptosis in M14 Human Melanoma Cells," *Molecular Pharmacology*, vol. 60, no. 1, pp. 174–182, Jul. 2001, doi: 10.1016/S0026-895X(24)23061-3.

[309] N. A. P. Franken, H. M. Rodermond, J. Stap, J. Haveman, and C. van Bree, "Clonogenic assay of cells in vitro," *Nat Protoc*, vol. 1, no. 5, pp. 2315–2319, Dec. 2006, doi: 10.1038/nprot.2006.339.

[310] J. D. Vasta, K. A. Andersen, K. M. Deck, C. P. Nizzi, R. S. Eisenstein, and R. T. Raines, "Selective Inhibition of Collagen Prolyl 4-Hydroxylase in Human Cells," *ACS Chem Biol*, vol. 11, no. 1, pp. 193–199, Jan. 2016, doi: 10.1021/acschembio.5b00749.

[311] E. K. Sackmann, A. L. Fulton, and D. J. Beebe, "The present and future role of microfluidics in biomedical research," *Nature*, vol. 507, no. 7491, pp. 181–189, Mar. 2014, doi: 10.1038/nature13118.

[312] K. R. Keshari, D. A. Heller, R. Boltyanskiy, H. Hricak, T. Magaldi, and M. Overholtzer, "Engineering focusing on cancer," *Cancer Cell*, vol. 42, no. 7, pp. 1138–1141, Jul. 2024, doi: 10.1016/j.ccell.2024.04.013.

[313] E. R. Flores and W. G. Sawyer, "Engineering cancer's end: An interdisciplinary approach to confront the complexities of cancer," *Cancer Cell*, vol. 42, no. 7, pp. 1133–1137, Jul. 2024, doi: 10.1016/j.ccell.2024.05.017.

[314] M. J. Mitchell, R. K. Jain, and R. Langer, "Engineering and physical sciences in oncology: challenges and opportunities," *Nat Rev Cancer*, vol. 17, no. 11, pp. 659–675, Nov. 2017, doi: 10.1038/nrc.2017.83.

[315] X. Wang and B. Seed, "A PCR primer bank for quantitative gene expression analysis," *Nucleic Acids Res*, vol. 31, no. 24, p. e154, Dec. 2003, doi: 10.1093/nar/gng154.

[316] A. Spandidos, X. Wang, H. Wang, S. Dragnev, T. Thurber, and B. Seed, "A comprehensive collection of experimentally validated primers for Polymerase Chain Reaction quantitation of murine transcript abundance," *BMC Genomics*, vol. 9, no. 1, p. 633, Dec. 2008, doi: 10.1186/1471-2164-9-633.

[317] A. Spandidos, X. Wang, H. Wang, and B. Seed, "PrimerBank: a resource of human and mouse PCR primer pairs for gene expression detection and quantification," *Nucleic Acids Research*, vol. 38, no. suppl_1, pp. D792–D799, Jan. 2010, doi: 10.1093/nar/gkp1005.

[318] J. M. Elizarraras, Y. Liao, Z. Shi, Q. Zhu, A. R. Pico, and B. Zhang, "WebGestalt 2024: faster gene set analysis and new support for metabolomics and multi-omics," *Nucleic Acids Research*, vol. 52, no. W1, pp. W415–W421, Jul. 2024, doi: 10.1093/nar/gkae456.

[319] J. Schindelin *et al.*, "Fiji: an open-source platform for biological-image analysis," *Nat Methods*, vol. 9, no. 7, pp. 676–682, Jul. 2012, doi: 10.1038/nmeth.2019.

[320] S. Salceda and J. Caro, "Hypoxia-inducible Factor 1α (HIF-1α) Protein Is Rapidly Degraded by the Ubiquitin-Proteasome System under Normoxic Conditions: ITS STABILIZATION BY HYPOXIA DEPENDS ON REDOX-INDUCED CHANGES*," *Journal of Biological Chemistry*, vol. 272, no. 36, pp. 22642–22647, Sep. 1997, doi: 10.1074/jbc.272.36.22642.

[321] L.-J. Mah, A. El-Osta, and T. C. Karagiannis, "γH2AX: a sensitive molecular marker of DNA damage and repair," *Leukemia*, vol. 24, no. 4, pp. 679–686, Apr. 2010, doi: 10.1038/leu.2010.6.

[322] N. Pouliot, H. B. Pearson, and A. Burrows, "Investigating Metastasis Using In Vitro Platforms," in *Madame Curie Bioscience Database [Internet]*, Landes Bioscience, 2013. Accessed: Mar. 18, 2025. [Online]. Available: https://www.ncbi.nlm.nih.gov/books/NBK100379/

[323] P. Bouchalova and P. Bouchal, “Current methods for studying metastatic potential of tumor cells,” *Cancer Cell International*, vol. 22, no. 1, p. 394, Dec. 2022, doi: 10.1186/s12935-022-02801-w.

[324] J. Paek *et al.*, “Microphysiological Engineering of Self-Assembled and Perfusable Microvascular Beds for the Production of Vascularized Three-Dimensional Human Microtissues,” *ACS Nano*, vol. 13, no. 7, pp. 7627–7643, Jul. 2019, doi: 10.1021/acsnano.9b00686.

[325] Z. Hu *et al.*, “Vascularized Tumor Spheroid-on-a-Chip Model Verifies Synergistic Vasoprotective and Chemotherapeutic Effects,” *ACS Biomater. Sci. Eng.*, vol. 8, no. 3, pp. 1215–1225, Mar. 2022, doi: 10.1021/acsbiomaterials.1c01099.